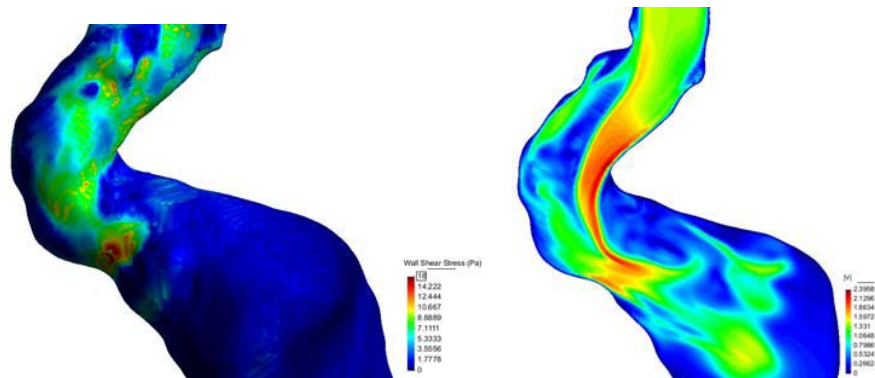


Mechanistic and Pathological Study of the Genesis, Growth, and Rupture of Abdominal Aortic Aneurysms

E. Soudah
M. Bordone
E. N.Y.Kwee
T. H. Loong
C. H. Tan
P. Uei
N. Sriram



Mechanistic and Pathological Study of the Genesis, Growth, and Rupture of Abdominal Aortic Aneurysms



¹ Biomedical Engineering Department, Centre Internacional de Mètodes Numèrics en Enginyeria,

c/ Gran Capità s/, 08034 Barcelona

Register for free at <https://www.scipedia.com> to download the version without the watermark

² School of Mechanical and Aerospace Engineering, Nanyang Technological University, 50 Nanyang Avenue,

Singapore 639798

³ Department of General Surgery, Tan Tock Seng Hospital, 11 Jalan Tan Tock Seng, Singapore 308433



Research project sponsored by the NTU-NHG innovation seed grant project n° ISG/11007

Monograph CIMNE N°-137, April 2013



Register for free at <https://www.scipedia.com> to download the version without the watermark

CENTRO INTERNACIONAL DE MÉTODOS NUMÉRICOS EN INGENIERÍA
Edificio C1, Campus Norte UPC
Gran Capitán s/n
08034 Barcelona, España
www.cimne.com

First edition: April 2013

**MECHANISTIC AND PATHOLOGICAL STUDY OF THE GENESIS, GROWTH, AND RUPTURE OF
ABDOMINAL AORTIC ANEURYSMS**

Monograph CIMNE M137

© Los autores

ISBN: 978-84-941407-7-8

Depósito legal: B-12796-2013

Tabla de contenido

1.	Introduction	6
2.	Methods.....	6
a.	Geometry	6
b.	Computational Fluid Solver	8
3.	Numerical Analysis.....	10
a.	Case S0252869Z	10
i.	Geometry and meshing.....	10
ii.	Results	11
b.	Case S0953163G.....	15
i.	Geometry and meshing.....	15
ii.	Results	16
c.	Case S2530107B	19
i.	Geometry and meshing.....	19
ii.	Results	20
d.	Case S2616541L	22
i.	Geometry and meshing.....	22
ii.	Results	23
e.	Case S0754065E	26
i.	Geometry and meshing.....	26
ii.	Results	27
f.	Case S0042268A	30
i.	Geometry and meshing.....	30
ii.	Results	31
g.	Case S0638600H.....	32
i.	Geometry and meshing.....	33
ii.	Results	38
h.	Case S1184041H.....	35
i.	Geometry and meshing.....	36
ii.	Results	36
i.	Case S1168446G.....	39
i.	Geometry and meshing.....	39
ii.	Results	40
j.	Case S0722132J.....	42
i.	Geometry and meshing.....	42
ii.	Results	43
a.	Case S0942654Z	45
i.	Geometry and meshing.....	45
ii.	Results	46
5.	Conclusions.....	48
6.	References	49
	Annex I: Mesh Quality	51
	Annex II: Paper submitted (under review).....	53

Register for free at <https://www.scipedia.com> to download the version without the watermark

Summary

Background and Objectives.

The aim of this document is to report the study process and the work carried on by CIMNE, in order that NTU and TTSH can validate the AAA results obtained during this analysis. The structure of this numerical analysis will be used for the following cases.

Acronyms

A³: Project Acronyms

AAA: Abdominal Aorta Aneurysm

CFD: Computational Fluid Dynamics

FEM: Finite Elements Method

BC: Boundary Condition

WSS: Wall Shear Stress

ILT: Intraluminal Thrombus

Structure of the document

The structure of the document is as follows:

- **Chapter 1: Summary.** The overview of the document is given. The scope of the document is explained, as well as acronyms used along the document, and contact persons from every implied partner.
- **Chapter 2: Introduction.**
- **Chapter 3: Simulation Data.**
- **Chapter 4: Numerical Analysis.**
- **Chapter 5: Conclusions.**
- **Chapter 6: References.**

Register for free at <https://www.scipedia.com> to download the version without the watermark

Participants: Contact persons

Participant	Contact person	e-mail
CIMNE	Maurizio Bordone	mbordone@cimne.upc.edu
CIMNE	Eduardo Soudah	esoudah@cimne.upc.edu
NTU	Dr. Ng Yin Kwee, Eddie	MYKNG@ntu.edu.sg
TTSH	Dr. Tse Han LOONG	Tse_Han_LOONG@ttsh.com.sg
TTSH	Dr. Cher Heng TAN	Cher_Heng_TAN@ttsh.com.sg
	Dr. Pua Uei	Pua_Uei@ttsh.com.sg
TTSH	Narayanan Sriram	sriram_narayanan@ttsh.com.sg

1. Introduction

Anatomically the aorta is divided in several parts, depending on the zone of the body that the vessel covers. The aorta is first called thoracic aorta as it leaves the heart, ascends, arches, and descends through the chest until it reaches the diaphragm when takes the name of abdominal aorta and continues down the abdomen. The abdominal aorta ends where it splits to form the two iliac arteries that go to the legs. Aorta is subject of aneurysm and it can develop anywhere along the length of the aorta.

The majority, however, are located along the abdominal zone. Most (about 90%) of abdominal aneurysms (AAA) are located below the level of the renal arteries, the vessels that leave the aorta to go to the kidneys. About two-thirds of abdominal aneurysms are not limited to just the aorta but extend from the aorta into one or both of the iliac arteries. Normally aortic aneurysms take a fusiform shape.

Nowadays, it is recognized that current clinical criteria for assessment of the abdominal aortic aneurysm rupture risk can be considered insufficient because they have not a physically theoretical basis [1], despite they are based on a wide empirical evidence. Hence, in last many years, researchers and physicians have had the challenge to identify a more reliable criterion associated with the actual rupture risk of the patient-specific aneurysm. The literature begins to reflect the existence of a consensus that, rather than empirical criteria, the biomechanical approach, based on the material failure, could facilitate a better method to assess the AAA rupture risk. One of these AAA rupture criteria are based on the evaluation of the hemodynamic stresses inside the AAA.

To estimate the AAA rupture risk, from biomechanical point of view (material failure), an aneurysm ruptures when the stresses acting on the arterial wall exceed its failure strength. According to the Laplace's law, the wall stress on an ideal cylinder is directly proportional to its radius and intraluminal pressure. Even though, the AAA is not ideal cylinder, Laplace's law said that with a large diameter, the internal pressure increases, and therefore increases the risk of rupture. Due to the increasing of the internal pressure, against the aortic walls, the AAA diameter grows progressively, and eventually, it could be able to overcome the resistance of the aortic wall with its breakup. In turn, further increase of the AAA diameters produces internal flow recirculation producing ILT formation in the AAA sac. This phenomenon provokes AAA stabilization and starting a vicious circle inside the AAA. It is well documented [1], that the aneurysm shape has a strong influence on flow patterns and consequently on wall stress distribution (peak values and locations). It is reflected by the interaction between the arterial wall structural remodeling and the forces generated by blood flow within the AAA. Therefore, the AAA morphology has a significant influence in its potential rupture.

The study is focused on the behavior of the blood fluid, inside the aneurism and how this illness will change the normal path of the fluid. Vortices and abnormal fluid paths will affect the normal and physiological pressure field and also produce alterations in the Wall Shear Stress (WSS) on the vessel walls.

2. Methods

a. Geometry

Eleven patients with infrarenal aneurysms of the Tan Tock Seng Hospital (Singapore) were included in this study. The patients chosen for this study were selected with different AAAs, in

order to cover the different stages of this pathology. All the patient participated in this trial analysis were volunteered and provided written informed consent of the study. This study was reviewed and approved by the Ethics Committee of the Tan Tock Seng Hospital, Singapore. For the medical image acquisition, a Computed Tomography (CT) Somatom Plus Scanner(AS+) (Siemens Medical Solutions) was used with the following parameters: 512x512x110, pixel spacing: 0.785/0.785 with a resolution of 1.274 pixels per mm and 5-mm slice thickness. CT Scanning was conducted while the volunteer was awake in the head first-supine position using an Endo_leak protocol. The CT covering the entire volume of the abdomen and pelvis and it was performed after the administration of intravenous Omnipaque 350 as IV contrast medium.

To create the computational model, the medical data were sent directly to a personal computer and stored in digital imaging and communications in medicine format (DICOM format). The region of interest (ROI) analyzed was segmented using the three-dimensional computer-aided design system DIPPO software [2]. The segmented area for each patient started at the abdominal aorta (approximately in the infra renal arteries) and extended down to the common iliac arteries. The abdominal images were segmented from CT DICOM images combining two different segmentation procedures thresholding and level set method (based on snakes). Thresholding is a non-linear operation that converts a gray-scale image into a binary image where the two levels are assigned to pixels that are below or above the specified threshold value. The image snake operation creates or modifies an active contour/snake in a grayscale image. The operation iterates to minimize the snake's energy which consists of multiple components including the length of the snake, its curvature and image gradient [3][4].



Figure 1: AAA Segmentation Process

After AAA abdominal segmentation, we get a 3D volume image useful to create a 3D computational model to analyze the blood flow behavior inside the AAA using computational fluid dynamics (CFD). Figure 2 shows an AAA workflow segmentation process. A mesh sensitivity analysis was performed to ensure the accuracy of the simulations using steady test. Depending on the complexity of the AAA model a 3D mesh consisted of 2.000.000–2.500.000 tetrahedral elements. Using the isostuffing algorithm[5] we have obtained a smooth element and an aspect ratio for whole of the meshes upper than 0.9 (ideal ratio=1 for an equilateral triangle). To obtain a good mesh for CFD calculation we must obtain that the elements must be of good quality; in particular there should be no plane or dihedral angle (the angle between two faces) close to 0 or 180 degrees, good results are obtained when angles are $>10^\circ$ and $<170^\circ$. For the whole acquisitions the same medical image protocol, image processing and volume mesh reconstruction were used. Figure 2 shows the 3D segmentation image, 3D computational model and a detail of the elements generated.

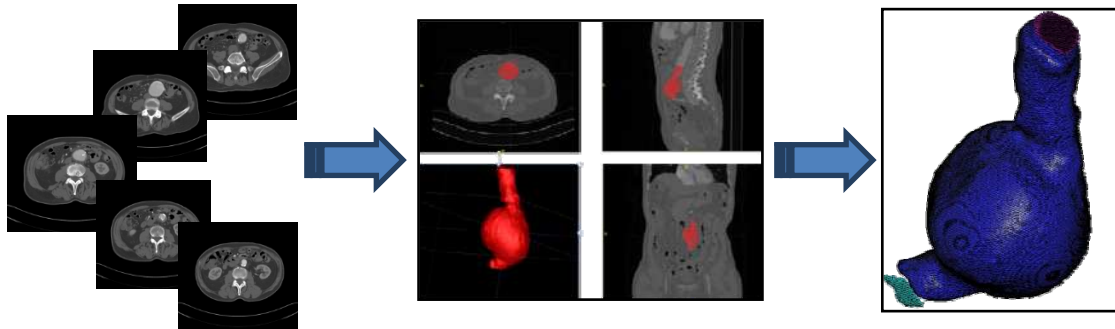


Figure 2: Workflow of the 3D AAA model. Obtaining the CT image of the abdominal aorta, segmentation of the vessel lumen using level set method and 3D model of the AAA.

b. Computational Fluid Solver

CFD analysis was performed using BioDyn, a friendly user-interface based on the commercial software Tdyn [6]. Tdyn is a fluid dynamics and multi-physics simulation environment based on the stabilized Finite Element Method that solved the Navier–Stokes equations. To characterize accurately the blood flow in the AAA, a Reynolds number was calculated for whole cases. Reynolds number is a dimensionless number that determinate the dynamic of the fluid. Reynolds number is defined as $Re = UD/\nu$, where U is the mean velocity, ν is the kinematic viscosity of air and D is the characteristic length given as the hydraulic diameter $D=4A/P$ for the inlet velocity, here A is the cross-sectional area and P is the perimeter of the aorta. Due to the Reynolds numbers in inlet is low (< 1000); we decided to use a CFD solver for laminar flow considering steady, homogeneous, incompressible, adiabatic and Newtonian. Although, three-dimensional flow features such as flow separation and recirculation might trigger a transition to turbulence at lower Reynolds numbers [7]. Based on a preliminary study [8], the effect of the turbulence has been considered to be negligible. Following, we show the Navier-Stokes equations (Equation 1).

Register for free at <https://www.scipedia.com> to download the version without the watermark

$$\left. \begin{aligned} \rho \left(\frac{\partial u}{\partial t} + (u \cdot \nabla) u \right) + \nabla p - \nabla \cdot (\mu \nabla u) &= \rho f \quad \text{in } \Omega \times (0, t) \\ \nabla \cdot u &= 0 \end{aligned} \right\}$$

Equation 1. Navier-Stokes Equation for CFD analysis

where $u=u(x,t)$ denotes the velocity vector, $p=p(x,t)$ the pressure field, the density (ρ) is considered constant with a value of 1050 Kg.m^{-3} and dynamic viscosity (ν), fixed at 0.004 Pa.s and f the volumetric acceleration. The spatial discretization of the Navier-Stokes equations has been done by means of the finite element method(FEM), while for the time discretization an iterative algorithm that can be consider as an implicit two steps "Fractional Step Method" has been used. A new stabilisation method, known as finite increment calculus, has recently been developed [9, 10]. By considering the balance of flux over a finite sized domain, higher order terms naturally appear in the governing equations, which supply the necessary stability for a classical Galerkin finite element discretisation to be used with equal order velocity and pressure interpolations.

The inlet velocity waveform was taken from the literature [11], Figure 3 shows the pulsatile waveforms used. For inlet condition, a transient blood flow was imposed in the abdominal aorta (approximately above the infra renal arteries). The velocity U was calculated for each patient in order to obtain a total fluid volumetric flow rate of 500 ml for an entire cardiac cycle. The outlet boundaries were located at the common iliac arteries where the pressure

follows a pulsatile waveforms as defined in Figure 3(b). It is important to remark that these profiles are not patient-specific data (MR velocity mapping was not performed on these subjects), which can be a limitation of this study. In further studies a patient-specific velocity and pressure profile will be used as boundary conditions

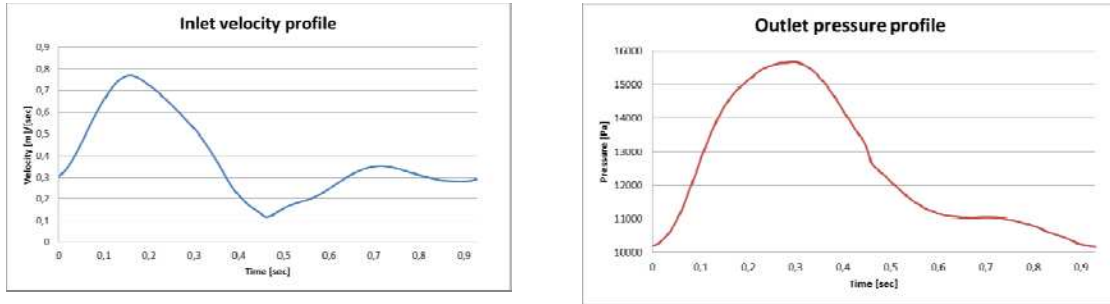


Figure 3.: Boundary conditions for the hemodynamic simulations, adapted from [11]

Mathematically the boundary conditions can be expressed as in equations 2. No-slip condition (vessel rigid wall) was imposed on the surface of the arteries, equation 2a. This choice is motivated by the fact that the physiological parameters characterizing the arterial mechanical behaviour of the AAA wall are not well determinate. This approach however reduces the discretization effort considerably, in particular boundary layer gridding and the computational cost although other approaches consider Fluid Structure Interaction (FSI) models [12]. The inlet velocity is assuming fully developed parabolic profile at the inlet (2b), and time dependent normal traction due to luminal pressure at the outlet (2c).

$$\mathbf{V} = 0|_{\text{wall}} \quad (2a)$$

$$u_z = 2(u(t)) \left(1 - \left(\frac{2r}{d_r} \right)^2 \right); u_r = 0|_{z=0} \quad (2b)$$

$$\tau_{nn} = \mathbf{I} \cdot \mathbf{p}(t) \cdot \mathbf{I} \quad (2c)$$

Equation 2. Boundary condition: mathematical formulation

where d_r is the inner radius of the abdominal aorta, u_r is the Cartesian components of the velocity vector in the 'z' direction, $u(t)$ and $p(t)$ are the time-dependent velocity and pressure waveforms designate in Figure 3. The pressure boundary conditions are given by equation 2c, where τ_{nn} is the normal traction designates at the outlet; \mathbf{I} is the standard identity matrix and \mathbf{n} designates the normal of the respective boundary. Figure 4 shows an example of the AAA reconstructed models and the layers in which our domain is divided in order to impose the boundary conditions.

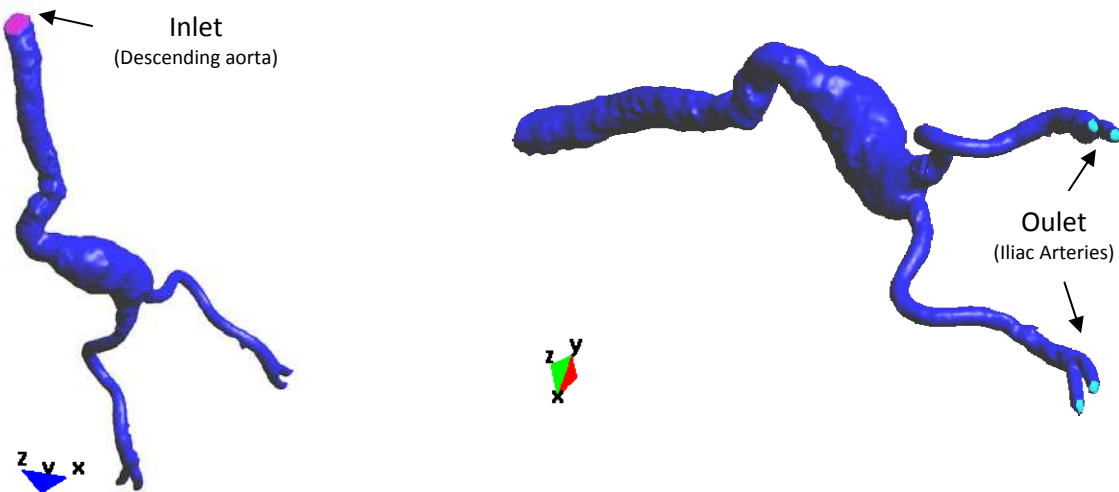


Figure 4. Mesh Surface: different layers are showed: lateral wall (dark blue), Inlet (purple) and outlet sections (light blue)

We start the simulation with 50 initial steps in order to stabilize the initial condition solution. Time integration method chosen was a Backward Euler, using a Bi Conjugate Gradient Non-symmetric solver in order to accelerate the calculation time performance. We used a pressure stabilization of 4th order and automatic velocity advection stabilization [13]. The total CPU time in a Microsoft Windows XP 32-bit PC with 3 GB-RAM using 2 CPU was between 4-6 hours depending of the case.

3. Numerical Analysis

a. Case S0252869Z

i. Geometry and meshing

We take in account the descendent part of thoracic aorta, the abdominal aorta with the aneurysm and the femoral bifurcation. Minor vessels were not segmented in order to improve the performance of the computational analysis in the interested zones and the quality of the mesh. In the next picture we could see the whole 3D geometry. The mesh is composed by tetrahedral elements to describe the volume of the blood flow and triangular elements that describe the inlet, the outlet and the vessel wall. The mesh quality, showed in the next picture is quite good, with more than 2.5 million of elements (figure 5). See Annex 1.

Register for free at <https://www.scipedia.com> to download the version without the watermark

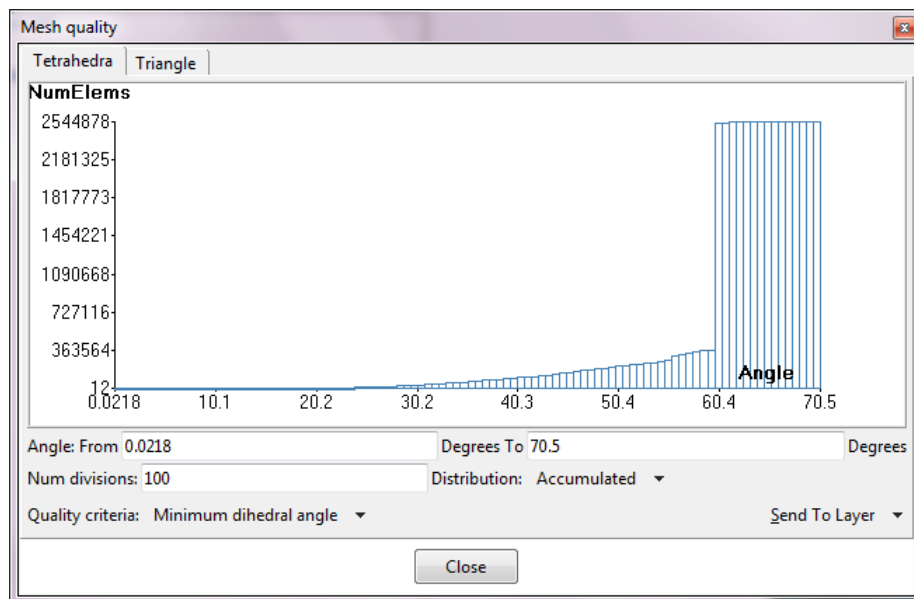
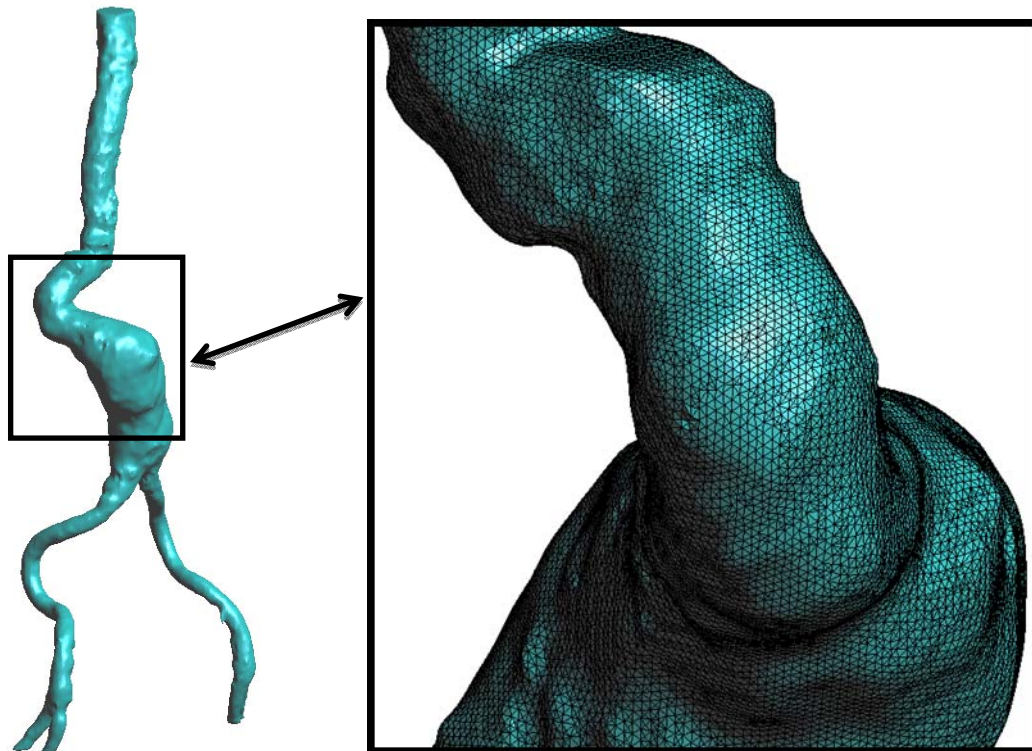


Figure 5. Mesh Volume appearance and detail of the upper part of the aneurysm, and mesh volume quality (good elements are with angle $>10^\circ$).

ii. Results

Preliminary results are focused on the study of the wall shear stress (WSS) and its relationship with the flow behavior inside the vessel.

In the figure 6, WSS on the surface and the velocity field in the moment of maximum velocity of the heartbeat cycle (0.93 sec) are shown.

It is possible to remark that in the elbow created by the aneurysm and its deformation of the aorta, we could appreciate an increment of the values of WSS. In the lower part of the image we could see the velocity flow in a cutting section creating in the middle of the same part analyzed for WSS. It is easy to see that the increment of the WSS is due to an increased velocity field: the blood “hit” against the vessel wall and the central flow, where the velocities are bigger, is moved near the wall. This situation produces a mechanical stress on the arterial wall, increasing the deformation and the alteration of the normal and physiological behavior of the aorta.

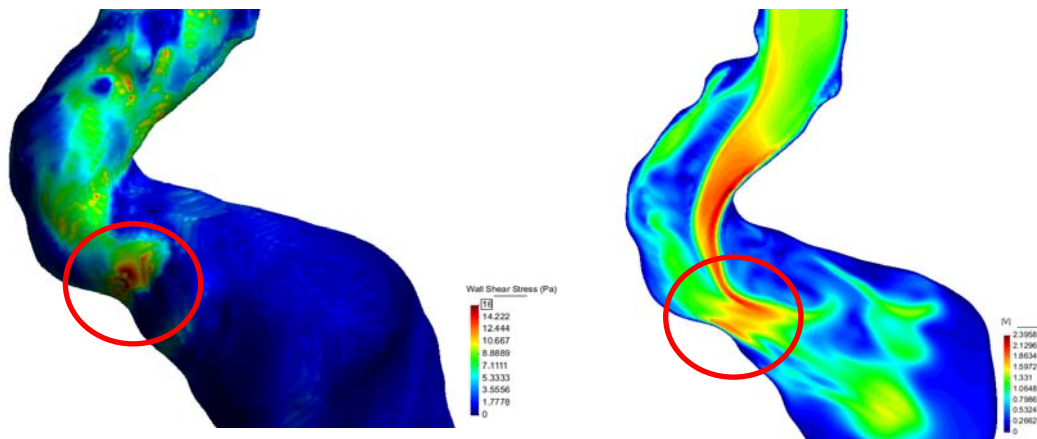


Figure 6. WSS on the surface and velocity field (m/s) in the middle section of the superior part of the aneurysm. The value belongs to the moment of maximum velocity of the heart beat.

Next figure (figure 7) shows the bottom part of the aneurysm. In this part the WSS is increased in the initial part of the bifurcation. This fact could bring to think that the aneurysm could move down along these stressed zones. More accurate analysis and clinician support will improve the diagnosis using FEM simulations.

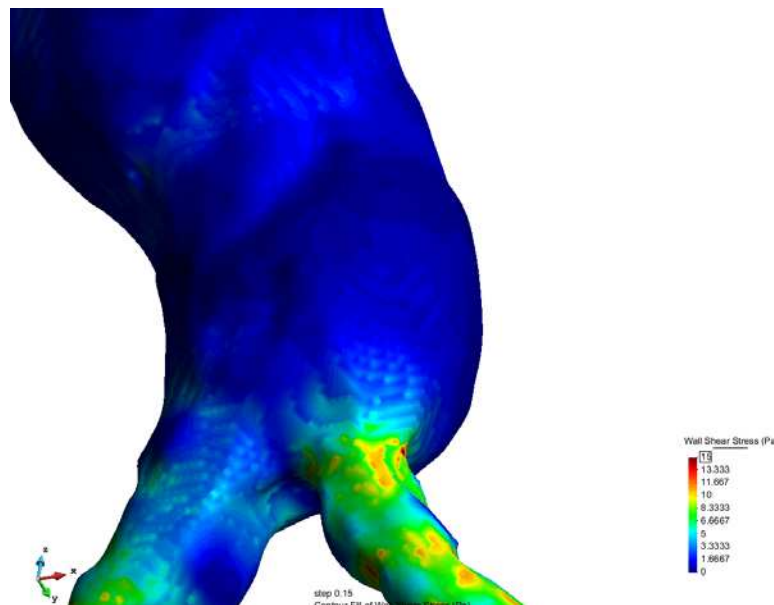


Figure 7. Mesh Surface: different layers are showed: lateral wall (dark blue), Inlet (purple) and outlet sections (light blue)

Next figure (figure 8) shows the WSS in the AAA sac. Risk zones are concentrated in the curved and twisted zones. This distribution of forces could improve the enhancement of the aneurysm due to the weaker characteristics of the vessel in the damaged zones subjected to the stress.

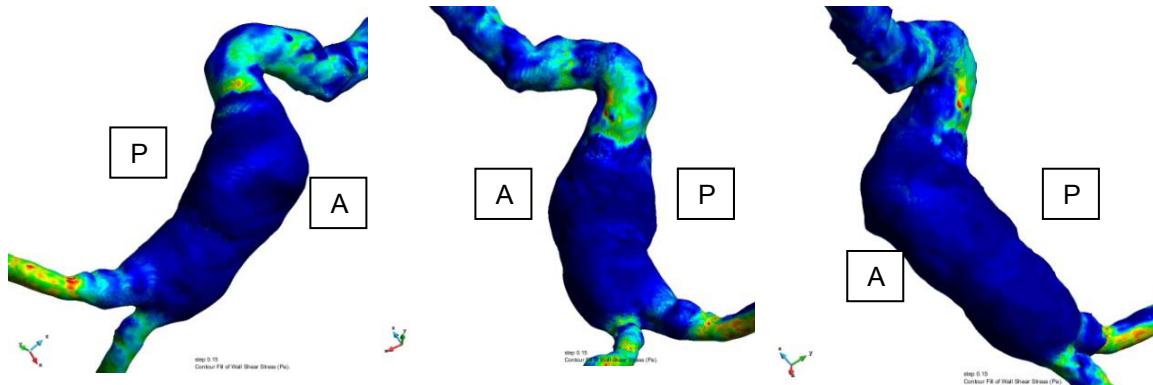


Figure 8. WSS in the AAA sac (A: Anterior, P: Posterior)

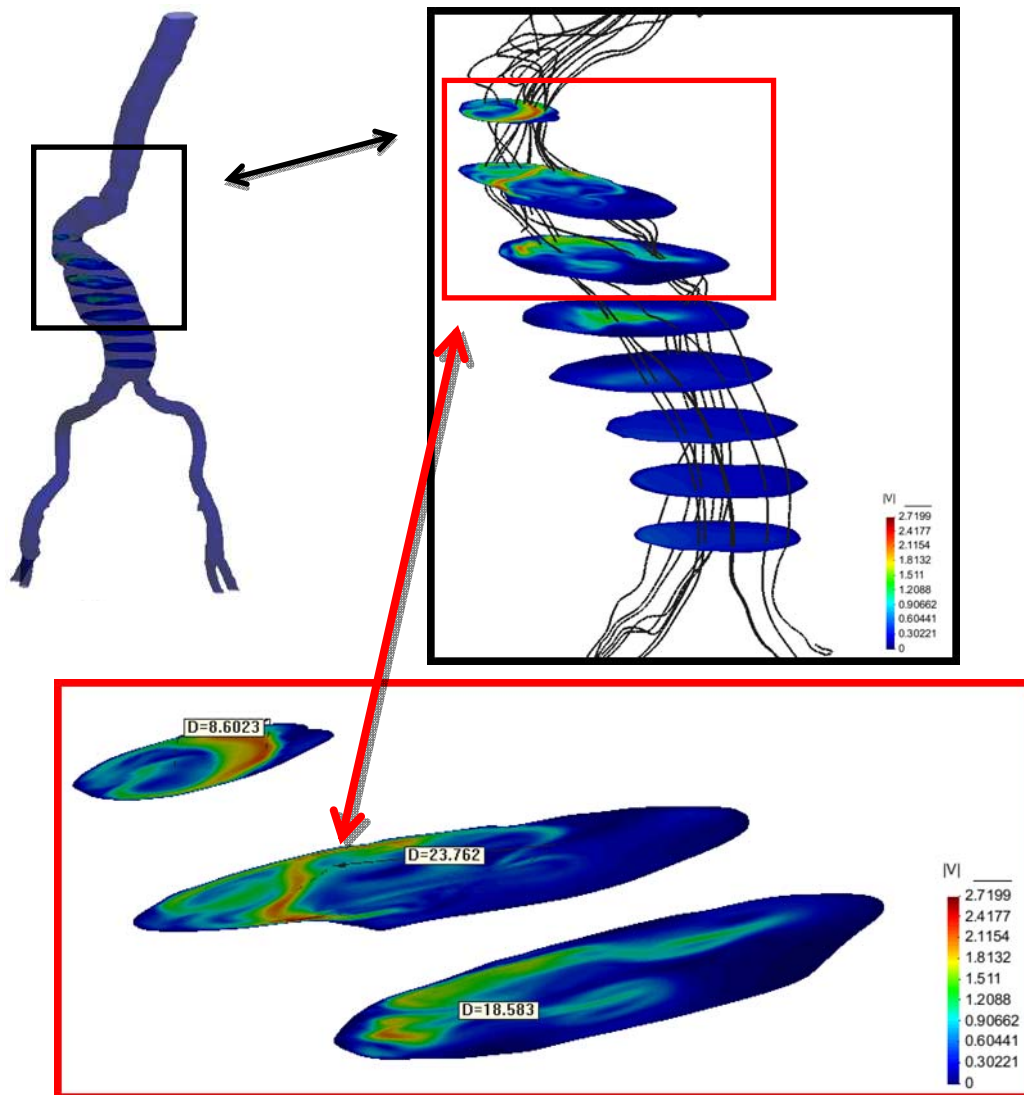


Figure 9. Velocity distribution in the aneurysm and stream lines vortices

Figure 9 shows eight parallel sections where are visualized the velocities results at the maximum flow (0.15s). Velocity field and stream lines remark the irregular shape of the eddies inside the AAA sac.

The torsion of the AAA can modify the blood flow inside the AAA, as it is showed in the bottom part of figure 9. In the first 3 planes the pick of velocity moves away progressively from the center of the sections studied from 8.6 mm (in the first section) to 23.7 mm (in the second section), after that the pick velocity recovers progressively the center of the Aorta. This distance can explain the effect of the torsion of the blood flow in the AAA.

b. Case S0953163G

i. Geometry and meshing

Second case is performed on a mesh of 1.795.787 tetrahedral elements. Segmentation was done on the abdominal aorta including femoral bifurcation because it is possible to note that also in femoral vessels is present an aneurysm deformation.

We segmented also two secondary abdominal vessels, in order to study more realistically the anatomy of the patient. Mesh quality is enough fine to perform shear stress analysis on the damaged surfaces. See Annex 1.

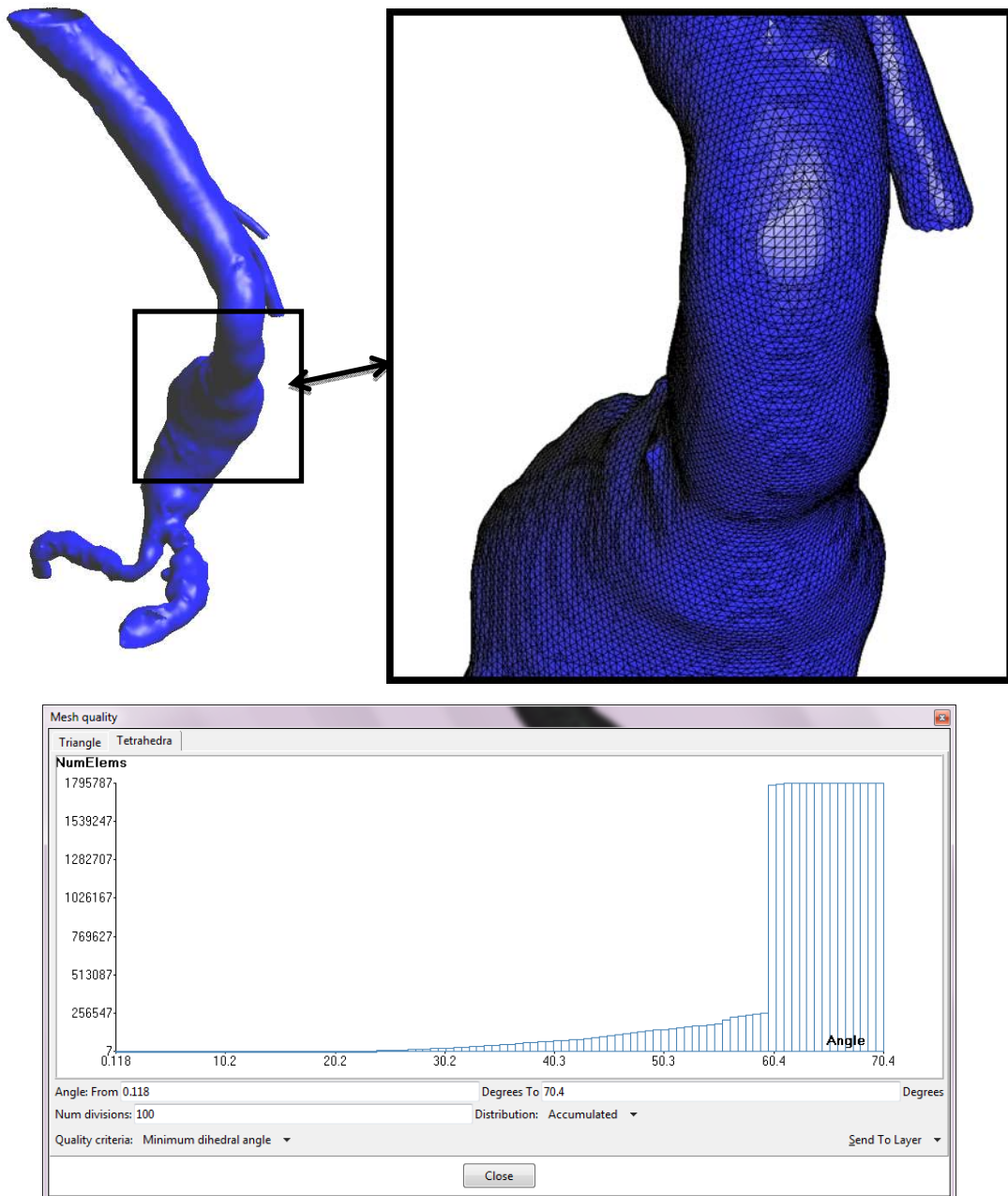


Figure 10. Mesh Volume appearance and detail of the upper part of the aneurysm, and mesh volume quality (good elements are with angle $>10^\circ$).

Next figure (figure 11) shows the geometry and the shape of the abdominal aortic aneurysm. The deformation due to the pathological condition of the vessel provokes an abnormal curvature.

For this case, we have tried to estimate the torsion of the Aorta provoked by the AAA. The angle α that describes the deviation from the right direction is 21° . To calculate this angle, we have taken two perpendicular points A and B (figure 11) between the upper Aorta neck and the distal femoral bifurcation, Point C is taken in the center of the section farthest to the line connecting A and B. the angle CAB is named α .

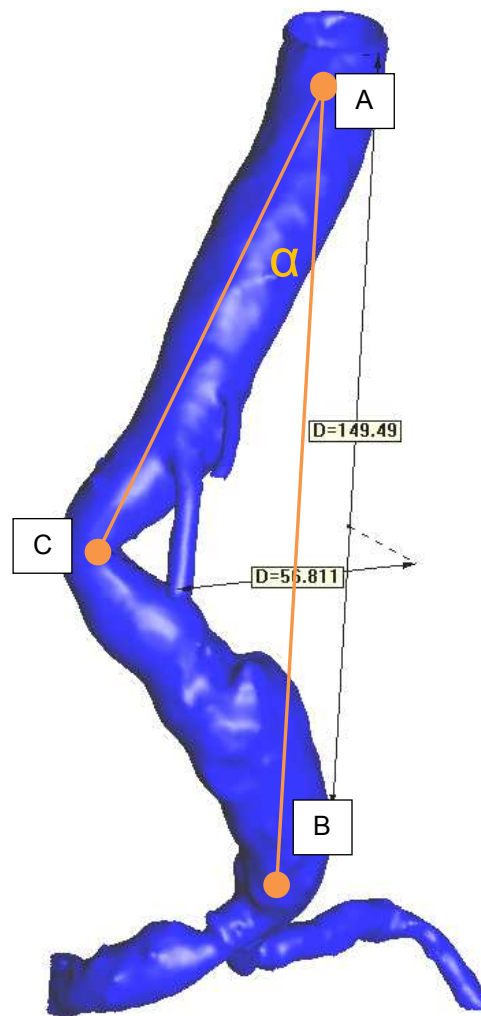


Figure 11. Geometrical deformation due to the aneurysm. α is the approximate angle of deviation from the physiological shape.

ii. Results

Aortic shape tortuosity[14] provokes huge changes in the flow pattern for this patient. Figure 10 shows different velocity situations along the time of heartbeat simulation (A: time = 0.025 sec, B: time = 0.1 sec, C: time = 0.15 sec and D: time = 0.25 sec)

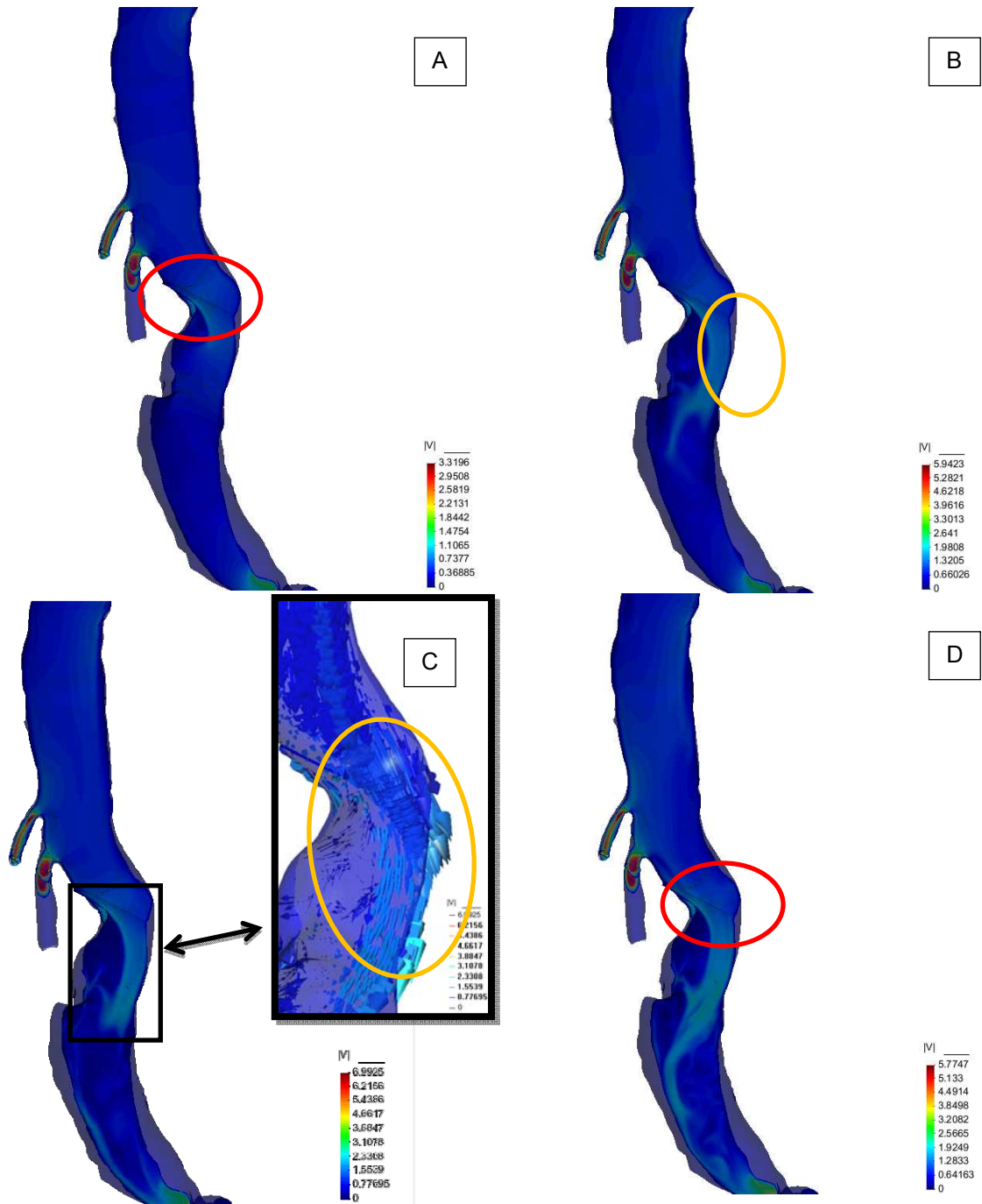


Figure 12. Velocity flow development along the simulation time.

For this particular case, there are two zones quite representative, the internal zone (red circle in figure 12) and the external zone (orange circle in figure 12). In figure 12, (B and C) it is possible to see how the flow pushes the external surface of the aneurysm sac. In C the velocity vectors direction show how blood particles collides the wall and this phenomena could provoke calcifications or develop the aneurysm sac.

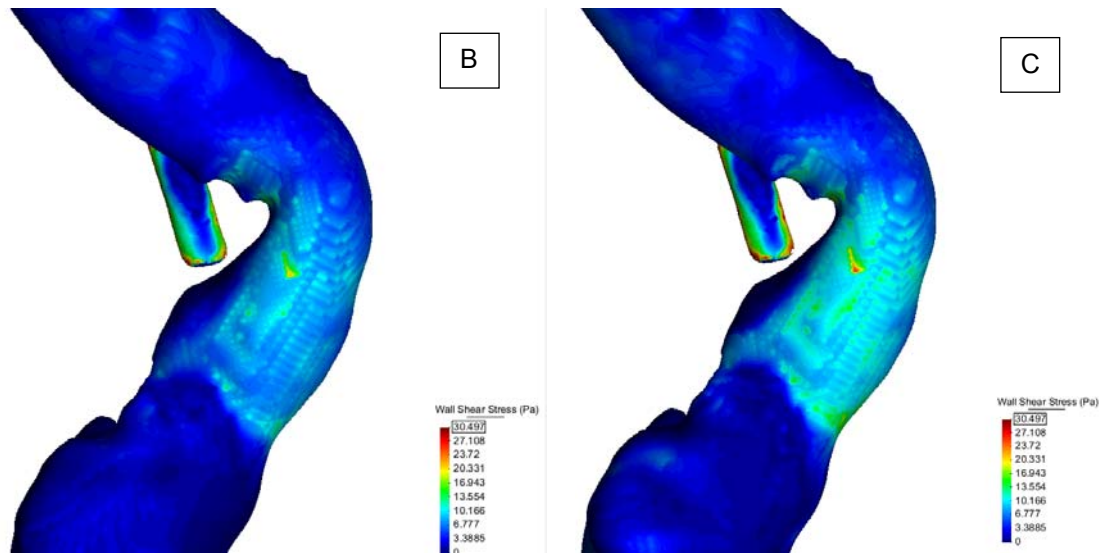


Figure 13. WSS distribution on deformed vessel curvature.

Figure 13 shows the WSS field caused by the deformation of the normal curvature of the aorta. The WSS is not uniform and high values of stresses are present in the zone where blood pushes the vessel wall.

c. Case S2530107B

i. Geometry and meshing

Third case presents an example of a reduced abdominal aorta aneurysm. The illness is localized just before femoral bifurcation. To simulate it a mesh of 854.743 tetrahedral elements was created.

Segmentation was performed until the next femoral / iliac bifurcation, in order to put farer the outlet conditions from the most important zone of study.

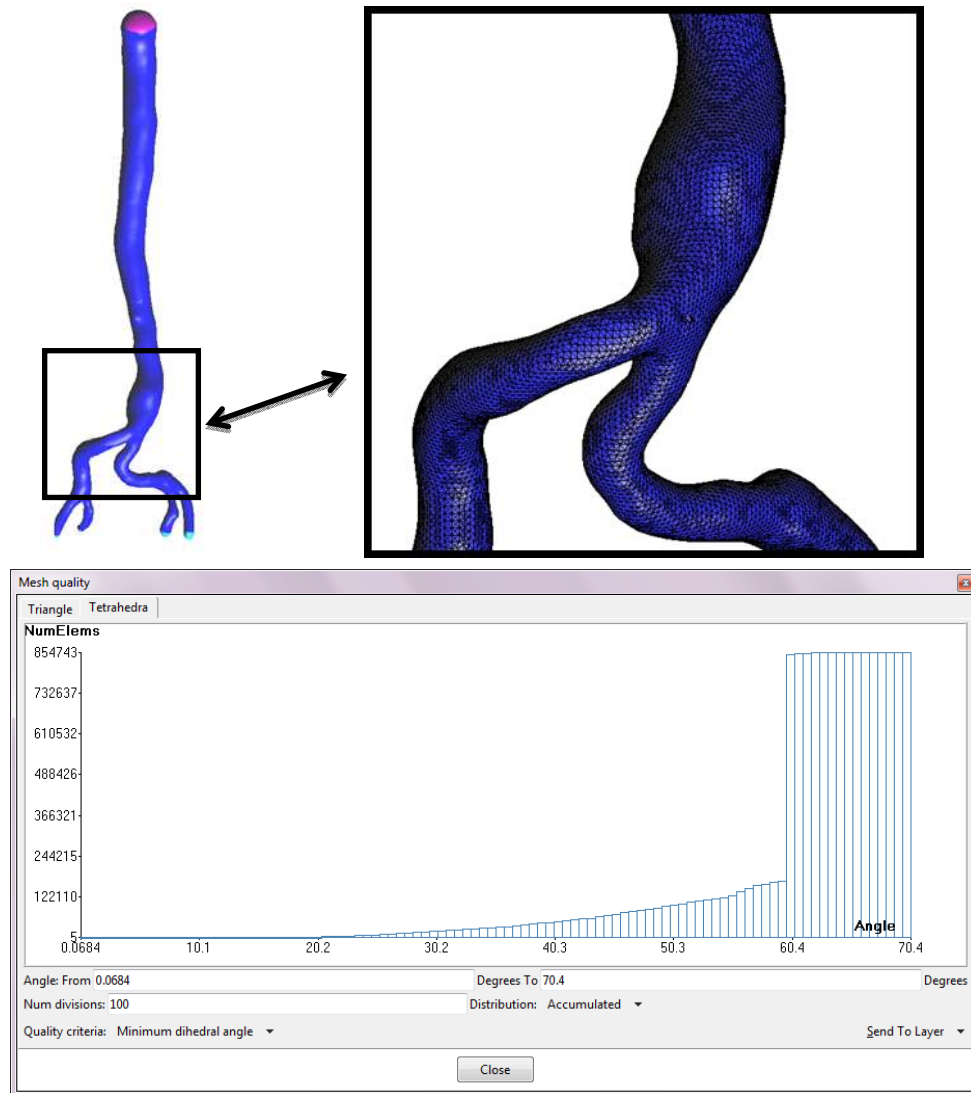


Figure 14. Mesh Volume appearance and detail of the upper part of the aneurysm, and mesh volume quality (good elements are with angle $>10^\circ$).

ii. Results

Figure 15 shows the velocities in a longitudinal cut section of the aorta for 3 different time steps. Maximum values of velocity are reached at 0.15s. Blood flow is deviated from the center line and its deviation could improve and generate ulterior deformation on vessel wall.

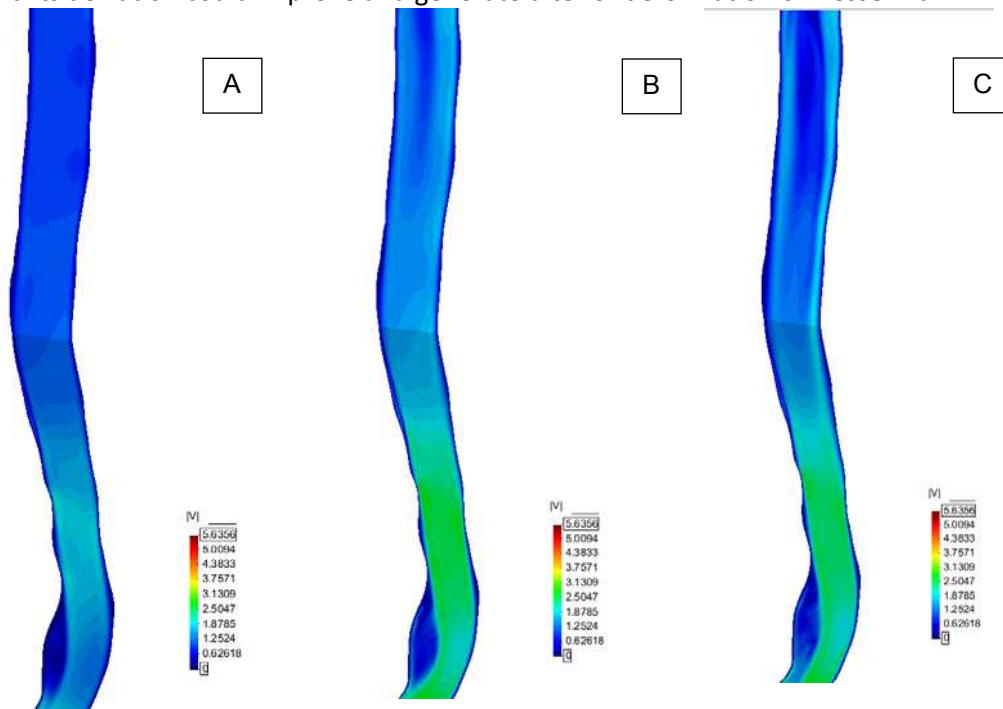


Figure 15. Velocity field at 0.075 sec, 0.1 sec and 0.15 sec

Figure 16 shows in detail how the flow is deviated from the first cut (upside) to the lower cuts, in the aneurysm sac. The screenshot is captured in 0.15 sec of the heartbeat cycle.

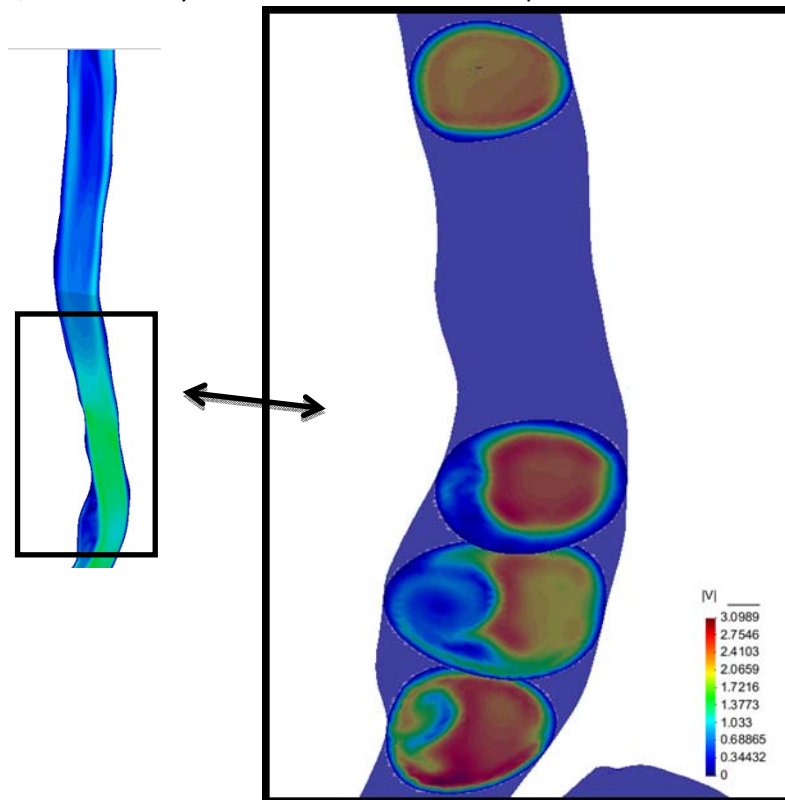


Figure 16. Velocity field at 1.5 sec transverse sections

Due to the reduced deviation and the little deformations showed with anatomical 3D reconstruction, WSS values are not huge. This could be reflecting a not severe condition of the patient analyzed. (See figure 17).

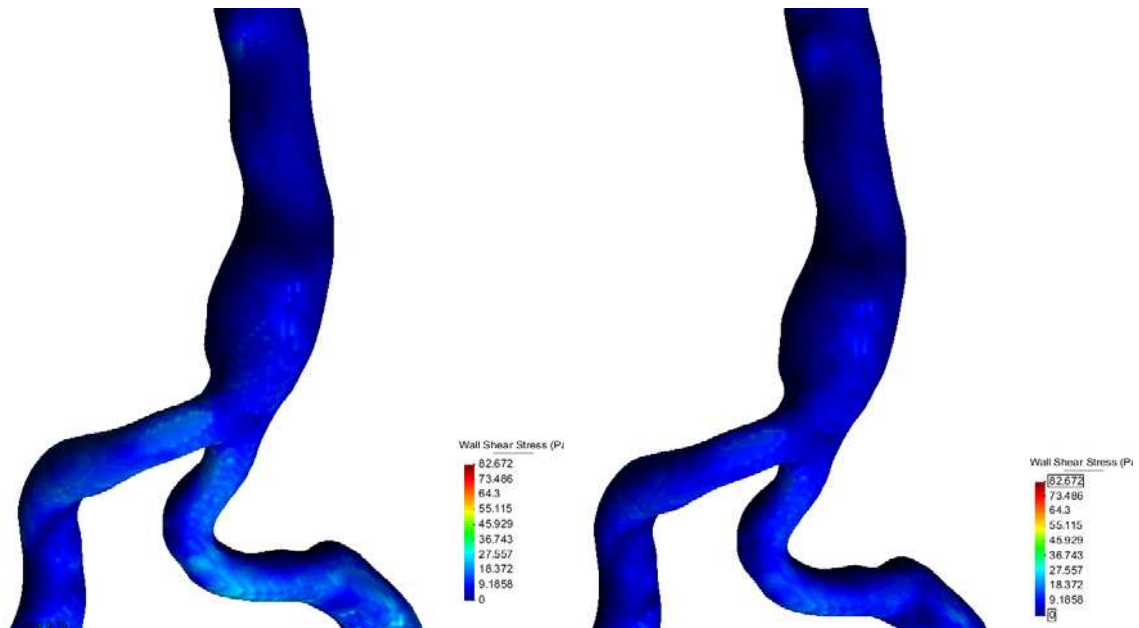


Figure 17. WSS values in aneurysm sac for 0.1 sec and 0.15 sec.

d. Case S2616541L

i. Geometry and meshing

This case is an example of healthy people, aorta dimension and shape show normal conditions and straight direction of development. Segmentation includes also five abdominal secondary vessels and a volume mesh of 830.716 elements was created. All the secondary vessels were considerate like outlet and for this they have pressure field condition imposed. See Annex 1.

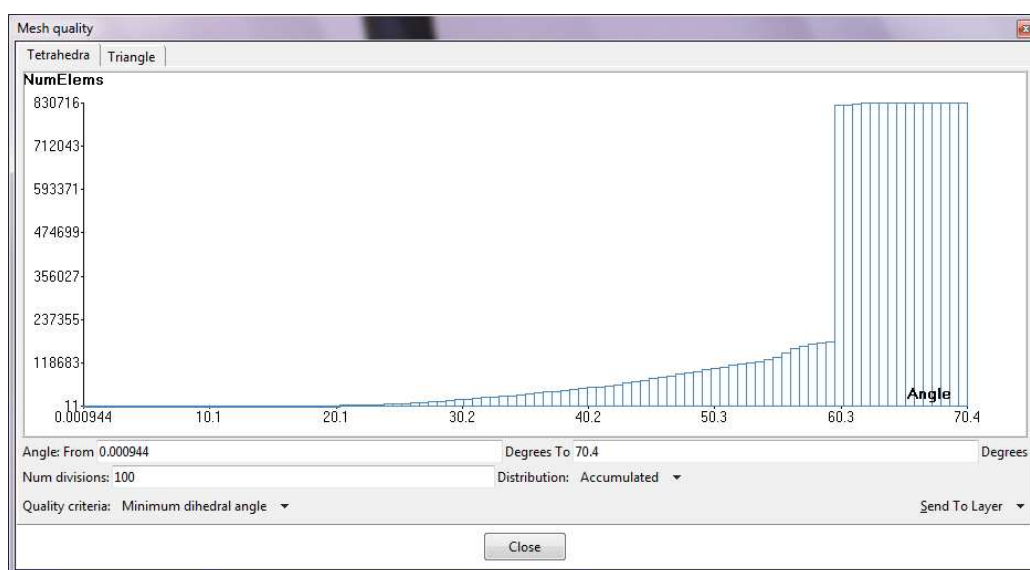
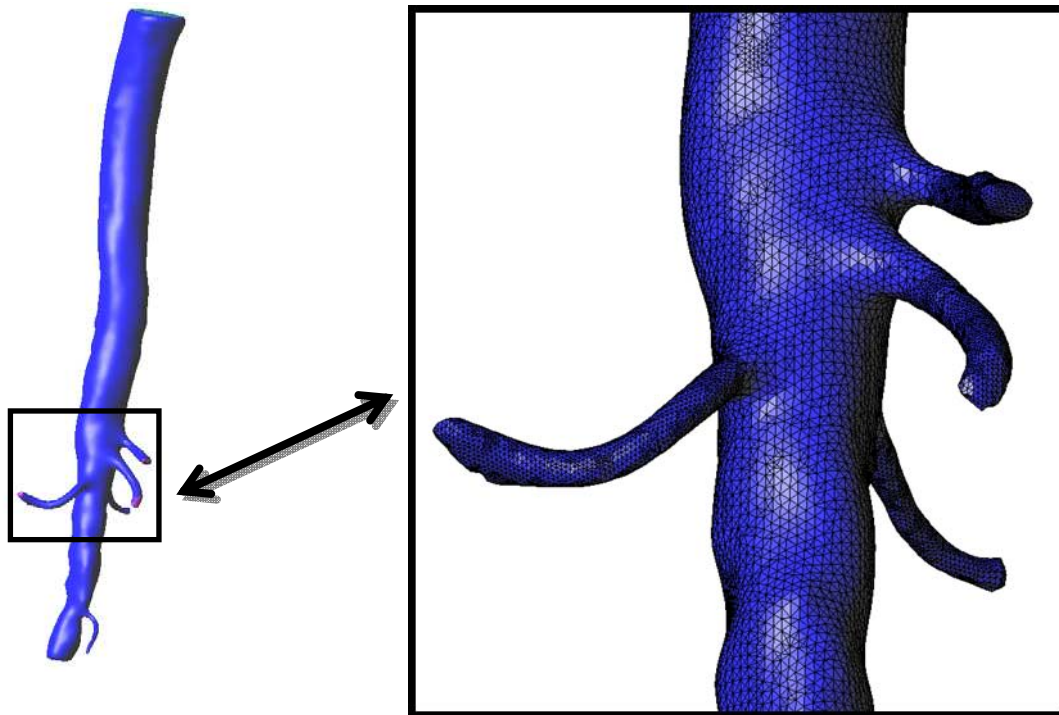


Figure 18. Mesh Volume appearance and detail of the upper part of the aneurysm, and mesh volume quality (good elements are with angle $>10^\circ$).

ii. Results

Firstly is possible to note that WSS does not reach high values in the aortic branch. Values calculated in the moment of maximum flow rate are lower than 15 Pa and present uniform distribution all around the vessel wall surface (fig 19).

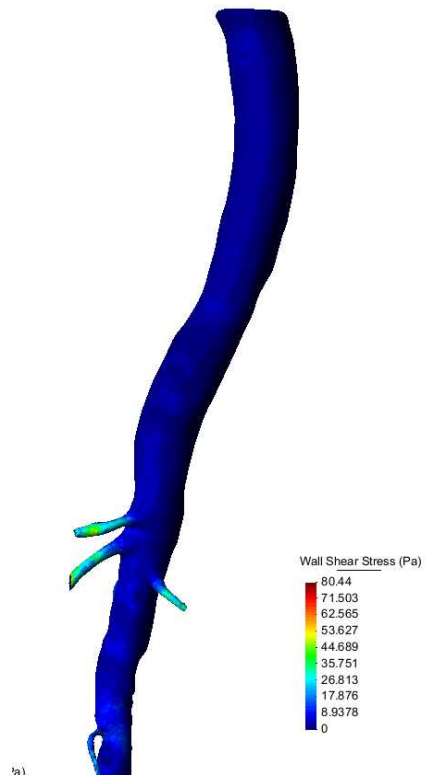


Figure 19. WSS distribution in maximum flow instant.

Analyzing velocity field in 3 different moments, simulation remark the uniformity of the flow and a good behavior of the flow. Figure 20 show velocity fields in moment 0.1, 0.15 (maximum flow rate) and 0.325 (initial part of steady solution). Velocity vectors also underline the lineal and absence of eddies and vortices.

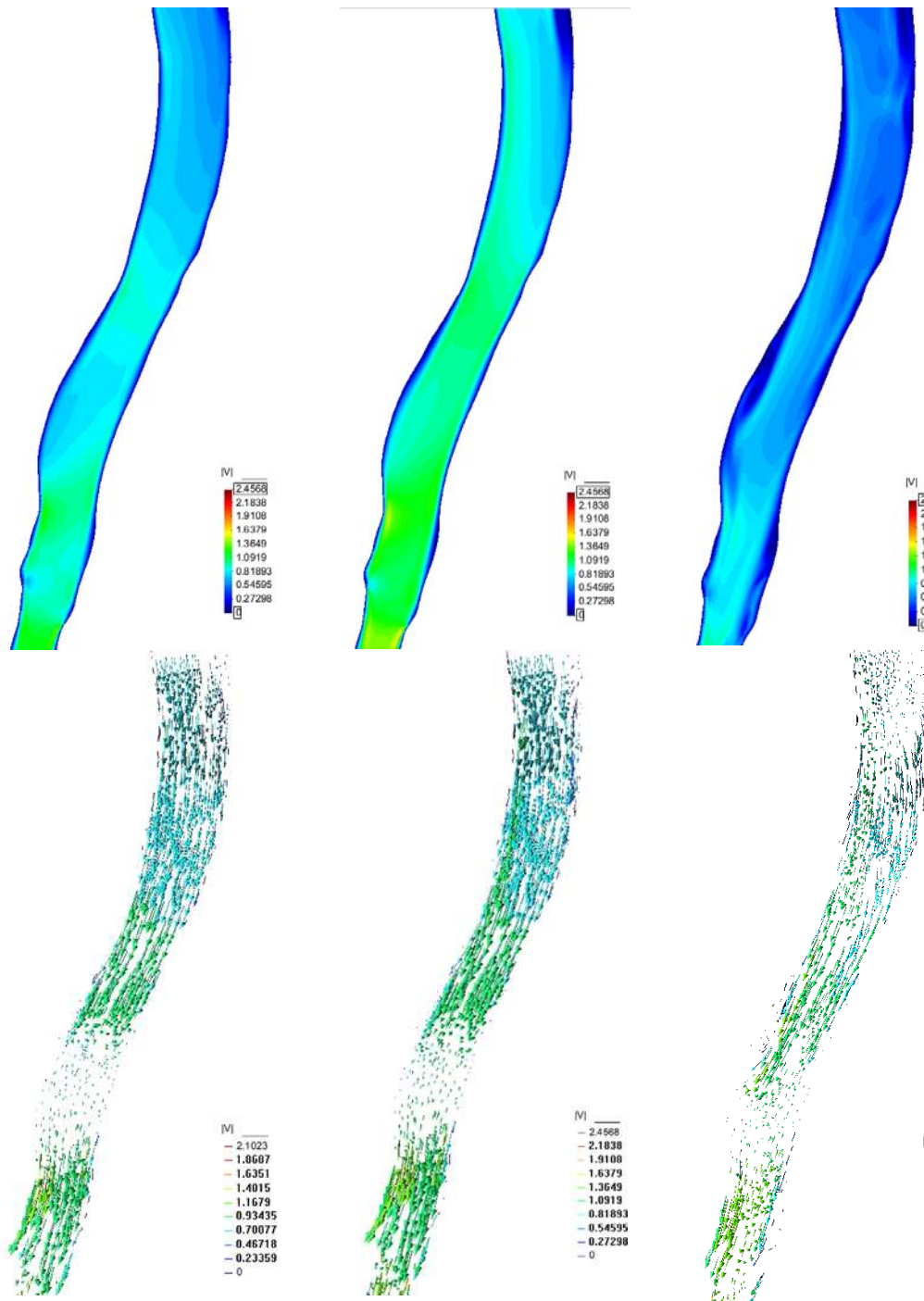


Figure 20. Velocity field and velocity vectors in 3 different moment of the cycle. 0.1 sec, 0.15 sec (maximum flow rate) and 0.325 sec.

Figure 21 shows 7 transversal cuts and the velocities on them, in the same instants of the simulation. Uniformity of solution is good in the three moments, confirming the low values of stresses on the wall vessel and the good shape of the aorta.

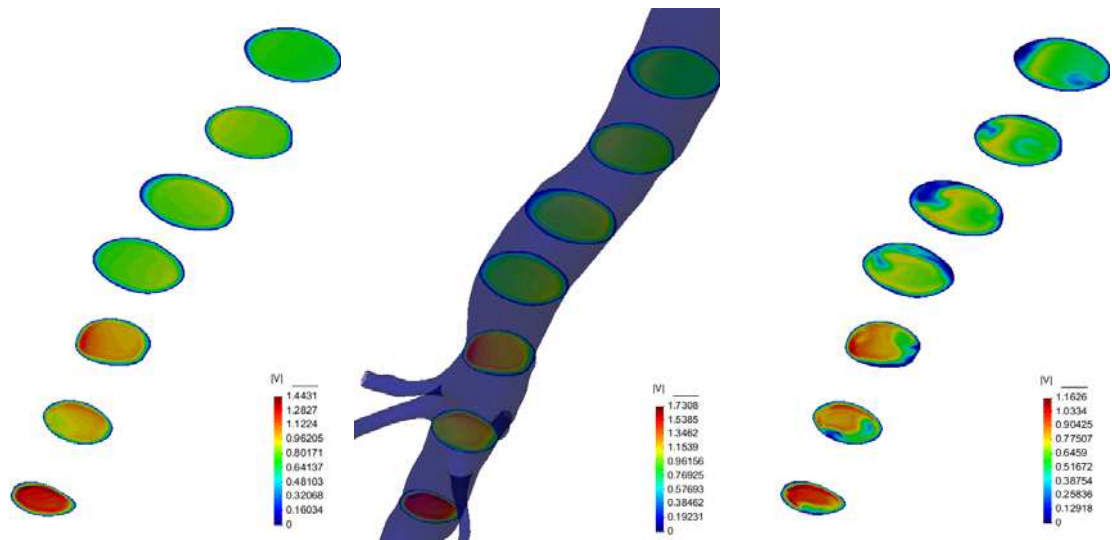


Figure 21. Velocity field in 3 different moment of the cycle in transversal sections. 0.1 sec, 0.15 sec (maximum flow rate) and 0.325 sec.

e. Case S0754065E

i. Geometry and meshing

Case S0754065E presents a little aneurysm just above the femoral bifurcation and some twists and torsion along the aorta. Aneurysm has a diameter of 4.5 cm. Geometry mesh was created with 1.074.672 elements. We considered 2 outlet sections in the initial part of femoral vessels (fig 22).

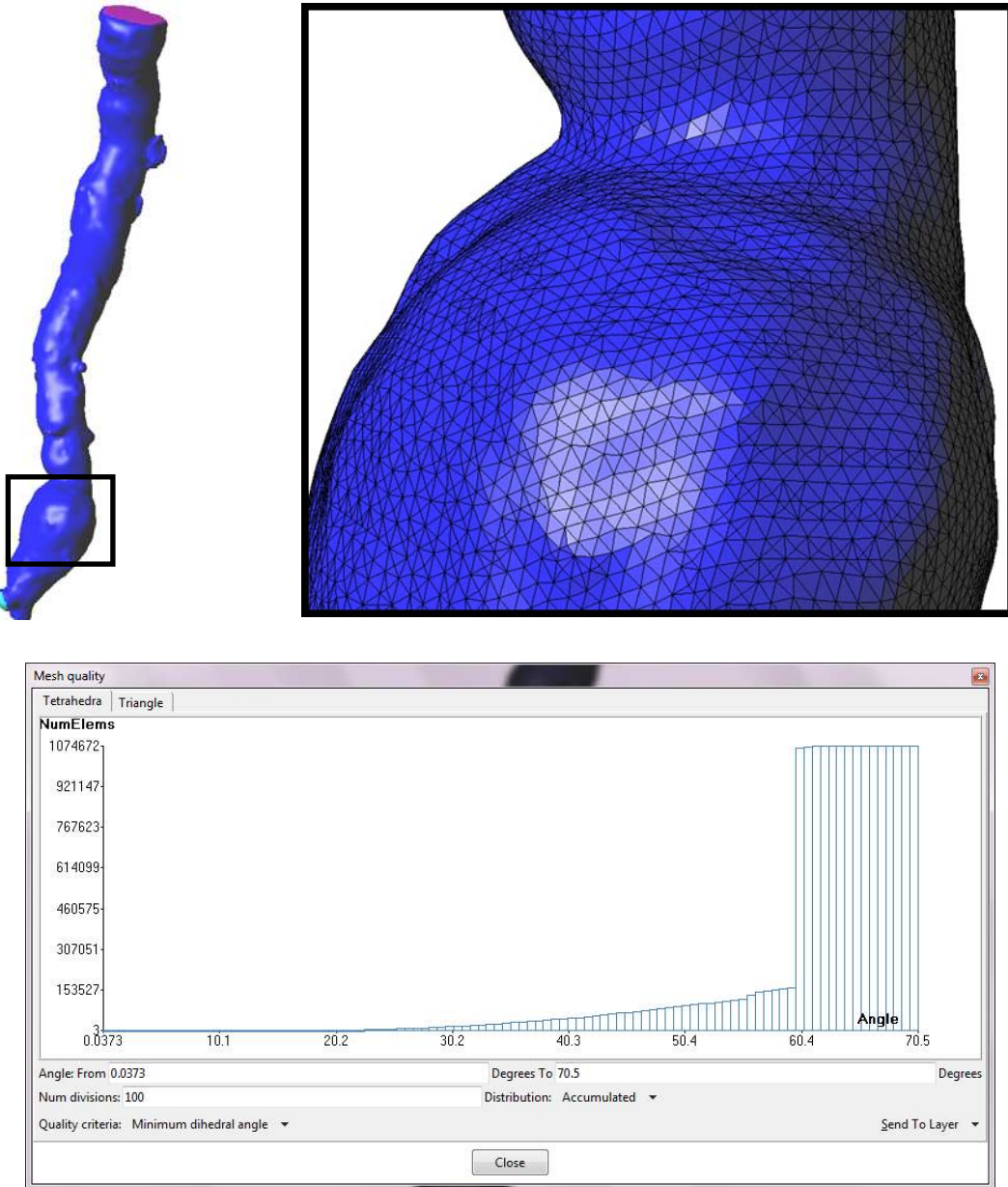


Figure 22. Mesh Volume appearance and detail of the upper part of the aneurysm, and mesh volume quality (good elements are with angle $>10^\circ$).

ii. Results

Analyzing velocity field in a longitudinal cut we could emphasize two different problematic zones, in figure 23 these zones are remarked in red and blue circles. These zones show irregular and asymmetric flow behavior. The asymmetric flow provokes concentration and localization of stresses on the vessel wall increasing the possibility to make worse the conditions of the aneurysm.

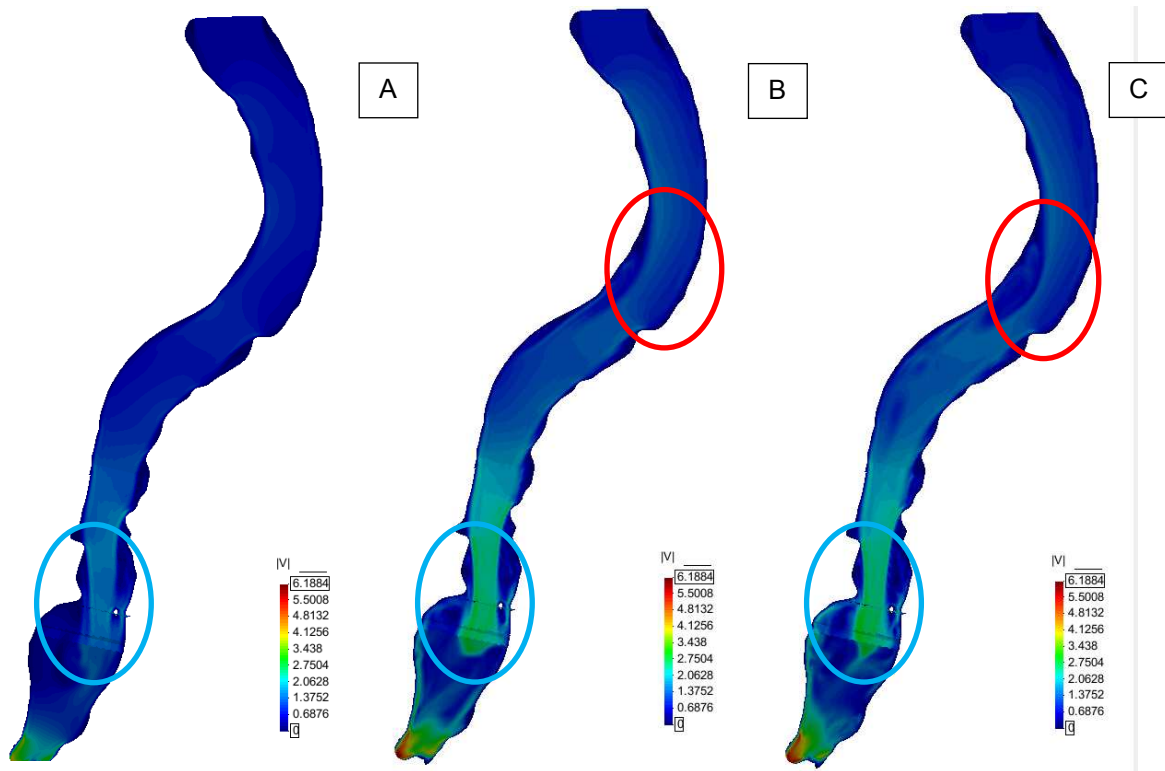


Figure 23. Velocity field in 3 different moment of the simulation A (0.075 sec), B (0.15 sec) and C (0.20 sec).

Figure 24 shows in transversal cuts the asymmetric flow along the upper zone of aortic vessel. From first cut until the last one the vessel produces a torsion and an accentuate curve, the inertia of the flow provokes that in the second cut the velocity reach high values near the interior part of the vessel. The concentration of the stress is displaced in the external zone in the last cut.

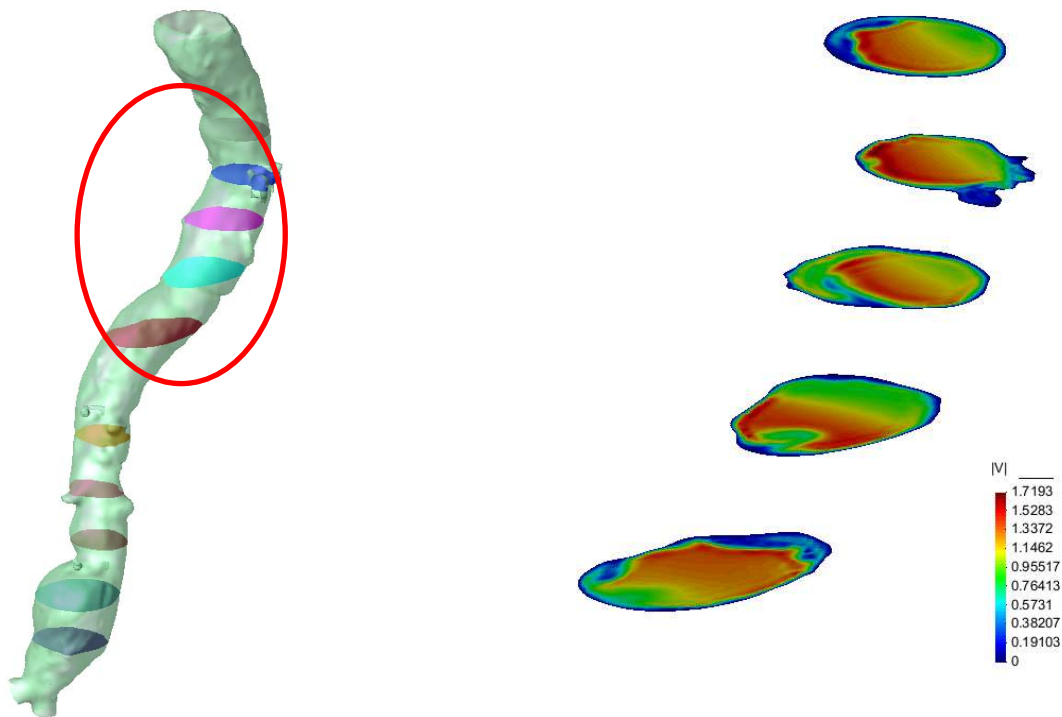


Figure 24. Velocity field in transversal cuts for the upper part of the aortic vessel.

In the lower zone is possible to see how a quasi-regular (cut A) flow changes and present asymmetries and in the last zones. High velocity zones are contiguous to low velocity zone in sections B, C and D. In this zone, the aneurysm presents also vortices that could increase calcification and enlargement (fig 25)

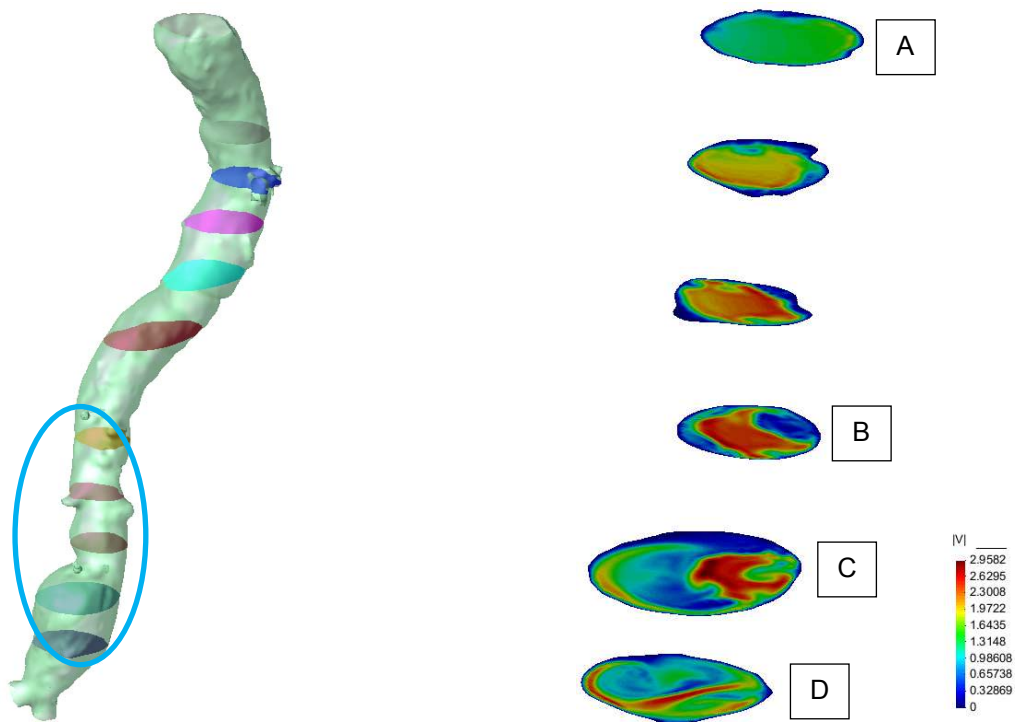


Figure 25. Velocity field in transversal cuts for the lower part of the aortic vessel.

In next figure 26 is possible to see the effects of the flow patterns irregularity on the WSS. In the bulge zone of the aneurysm stream lines denotes the eddies created by the aorta deformations.

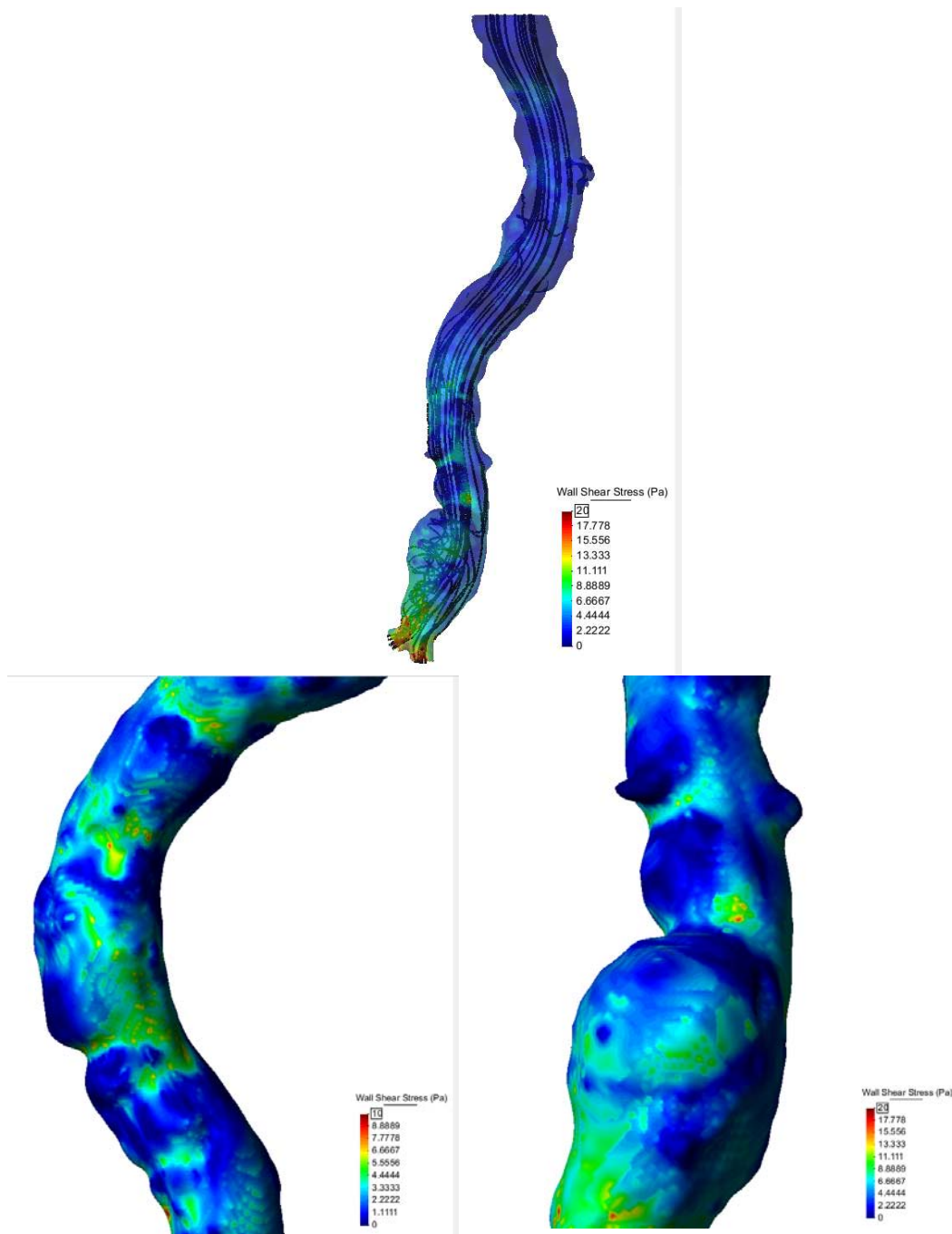


Figure 26. Wall Shear Stress in the upper and lower zones, these areas are related to the figure 24 and 25.

Irregular distribution of WSS (fig 26) is due by the asymmetric flow. Concentration of stresses may be an important factor of risk for patient. The stresses are higher in the damaged zone that generally present bad mechanical properties and are more prone to suffer rupture or ulterior deformations.

f. Case S0042268A

Next case presents a quite important aneurysm in abdominal sector of the aorta; the tortuosity of the segment studied is visible in the upper zone of the geometry analyzed. It is possible to note that also in the lower zone, where the femoral arteries start, the aneurysm is present. This fact leads to great changes in blood flow patterns as we could see forward.

i. Geometry and meshing

Mesh created was made up by 657.586 elements. The surface of the aneurysm was segmented with finer elements in order to compute with high precision the results of WSS.

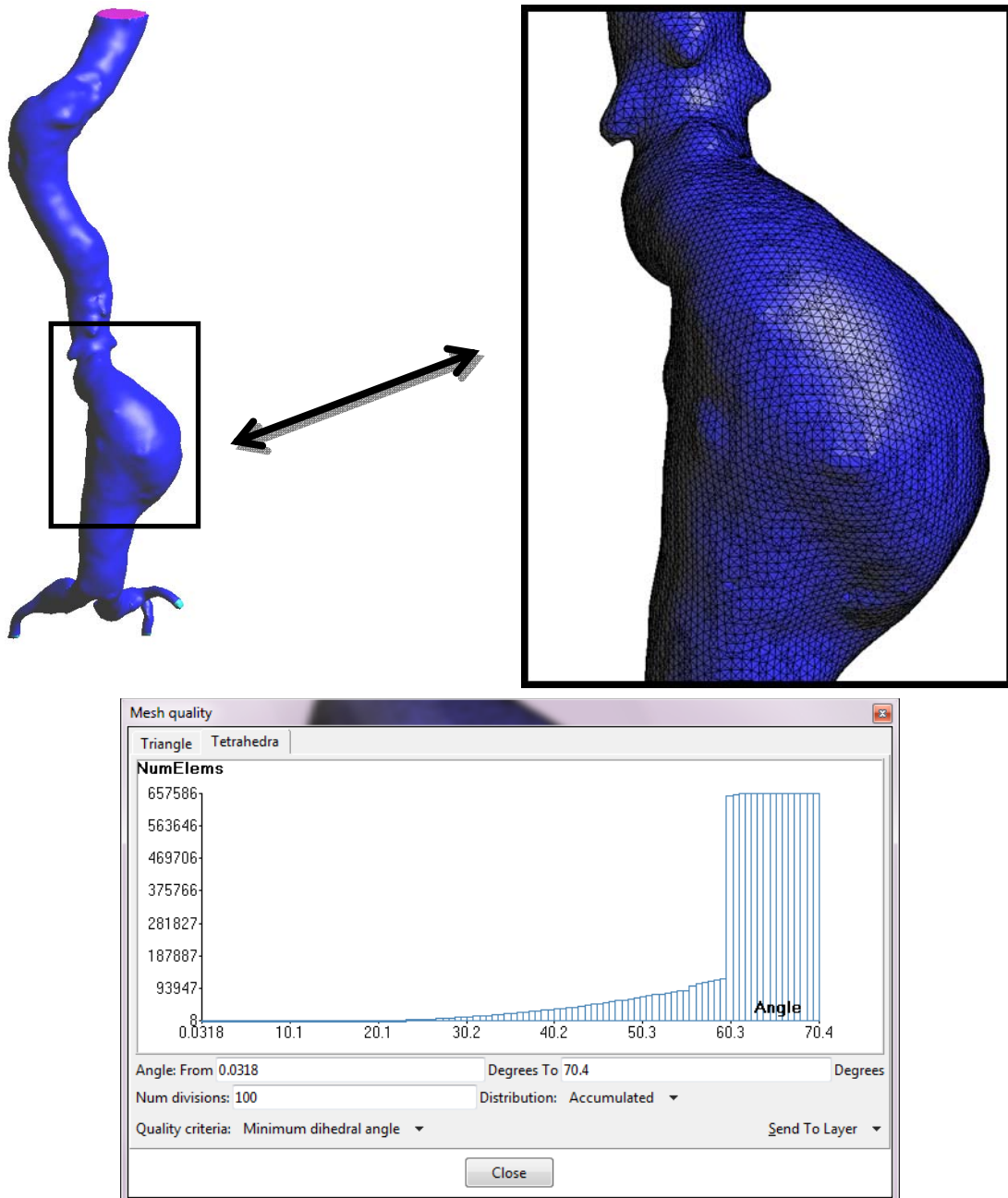


Figure 27. Mesh Volume appearance and detail of the upper part of the aneurysm, and mesh volume quality (good elements are with angle $>10^\circ$).

ii. Results

Analyzing velocity field in some composed longitudinal cuts we could a problematic zone, in figure 28 blue circle remarks the zone of interesting. The zone shows a very irregular and asymmetric flow behavior. The asymmetric flow provokes concentration and localization of stresses on the vessel wall increasing the possibility to make worse the conditions of the aneurysm. Blood flow is directed on the aneurysm enhanced zone, explaining the evolution and the modification of this part.

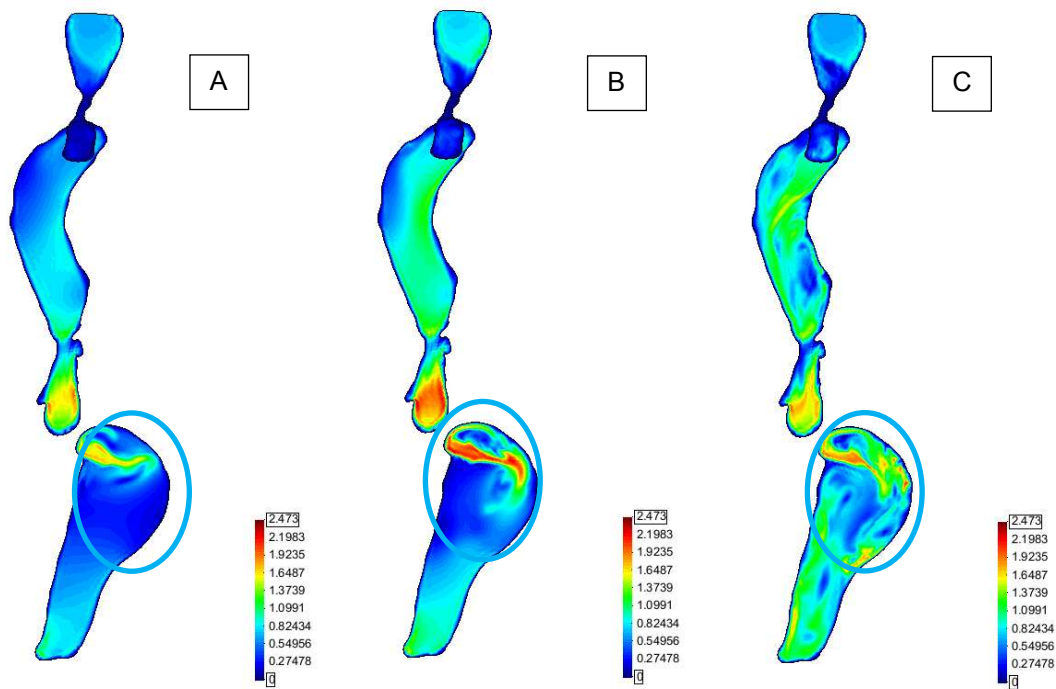


Figure 28. Velocity field in 3 different moment of the simulation A (0.1 sec), B (0.15 sec) and C (0.25 sec).

In next figures is possible to see how a quasi-regular (fig 29-30) flow changes and present asymmetries when pass through the curved zone and in the aneurysm sac the flow is concentrated in the external part of the same aneurysm.

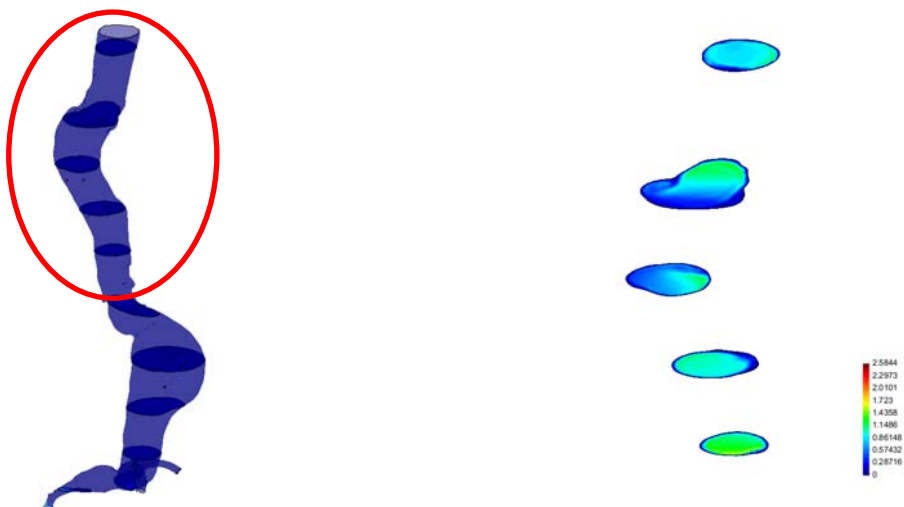


Figure 29. Velocity field in transversal cuts for the upper part of the aortic vessel.

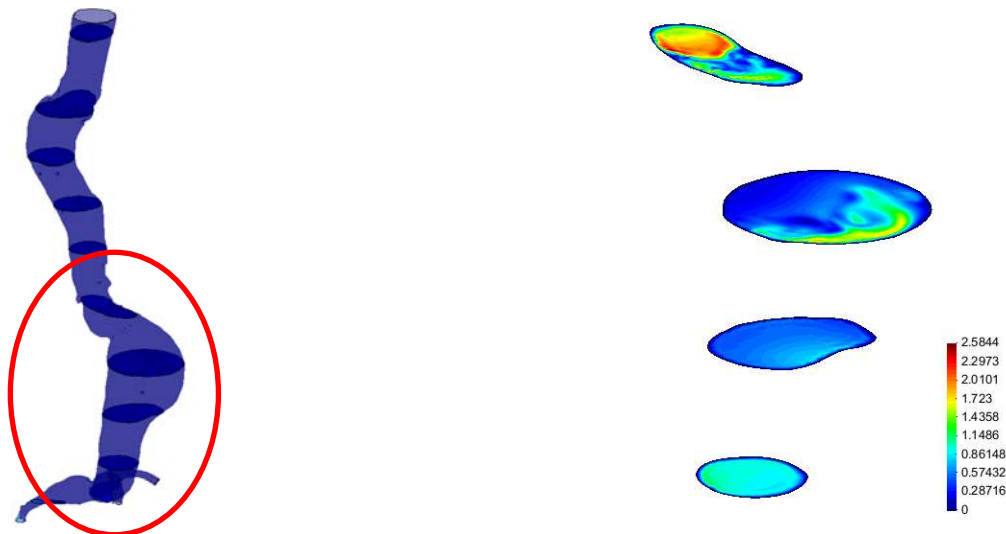


Figure 30. Velocity field in transversal cuts for the lower part of the aortic vessel.

In next figure 31 is possible to see the effects of the flow concentration on the wall vessel. WSS reaches higher values where the flow impact on the wall in bulge zone.

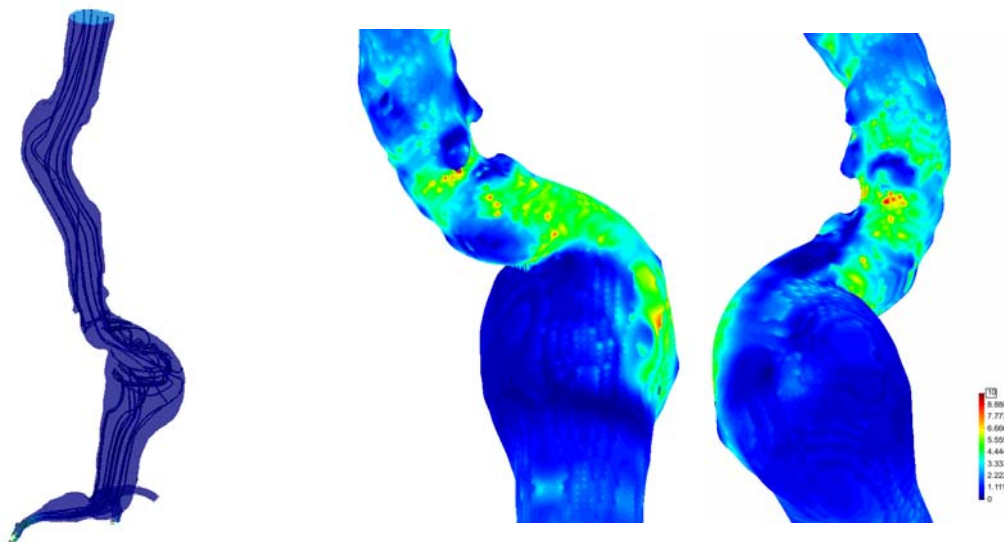


Figure 31. Wall Shear Stress in the aneurysm zone in two opposite views.

g. Case S0638600H

This case is performed on a mesh of 887.753 tetrahedral elements. Segmentation included the abdominal aorta and the initial portion of femoral bifurcation, in addition to other secondary vessel in the upper part of abdominal aorta in order to study more realistically the anatomy of the patient.

Mesh quality is enough fine to perform an exhaustive shear stress analysis on the damaged aneurysm surfaces.

i. Geometry and meshing

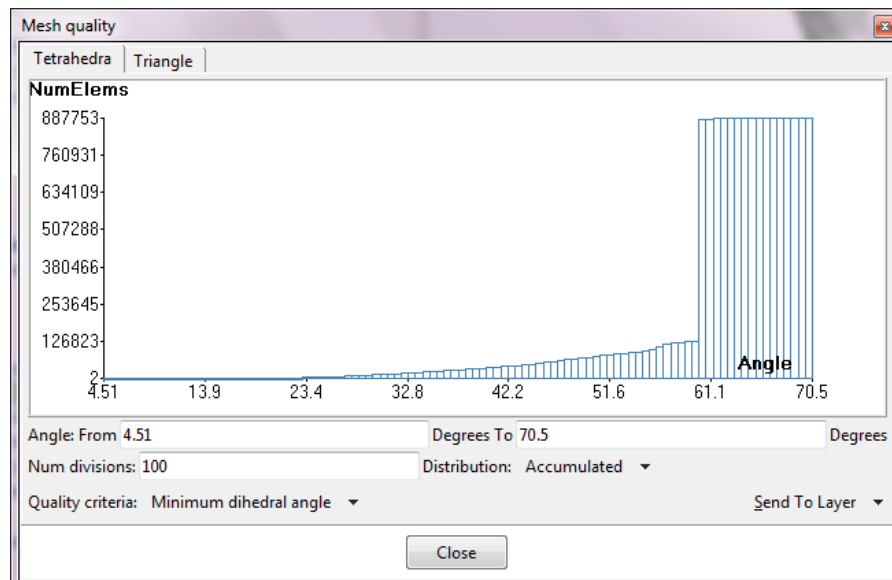
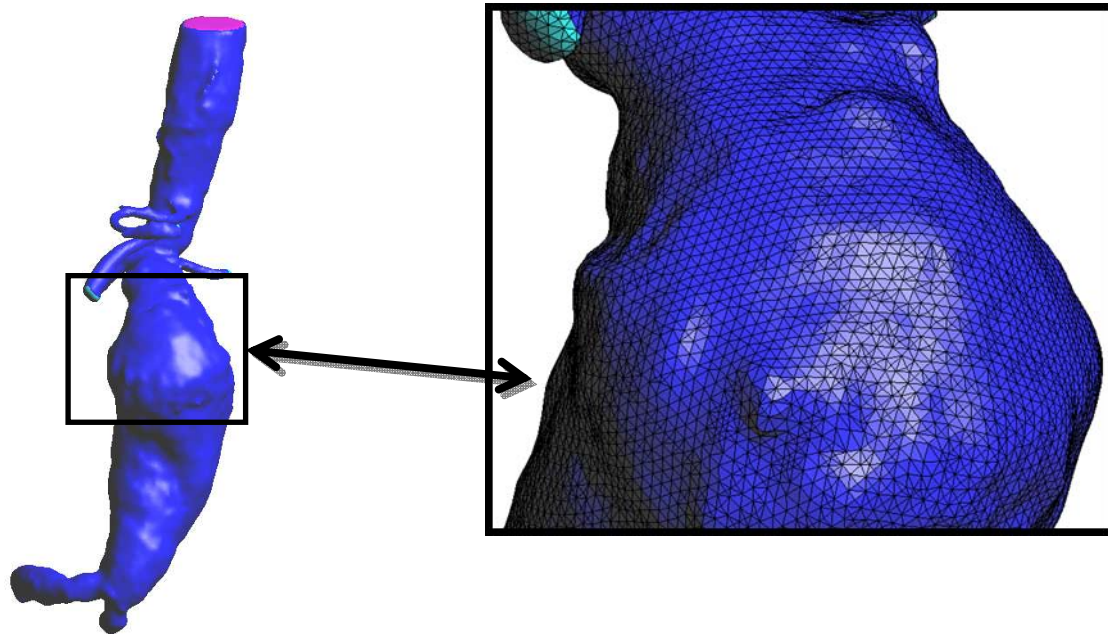


Figure 32. Mesh Volume appearance and detail of the upper part of the aneurysm, and mesh volume quality (good elements are with angle $>10^\circ$).

ii. Results

Figure 33 shows the velocities in a longitudinal central cut section of the aorta for 3 different time steps. Maximum values of velocity are reached at 0.15s as the velocity boundary condition imposes. Blood flow is deviated from the center line and its deviation could improve deformation on vessel wall. Red circle remark the zone where the blood jet impacts to the wall vessel. This zone coincides with the enhanced zone of the aneurysm. It is possible that in the next future the vessel will suffer ulterior deformation.

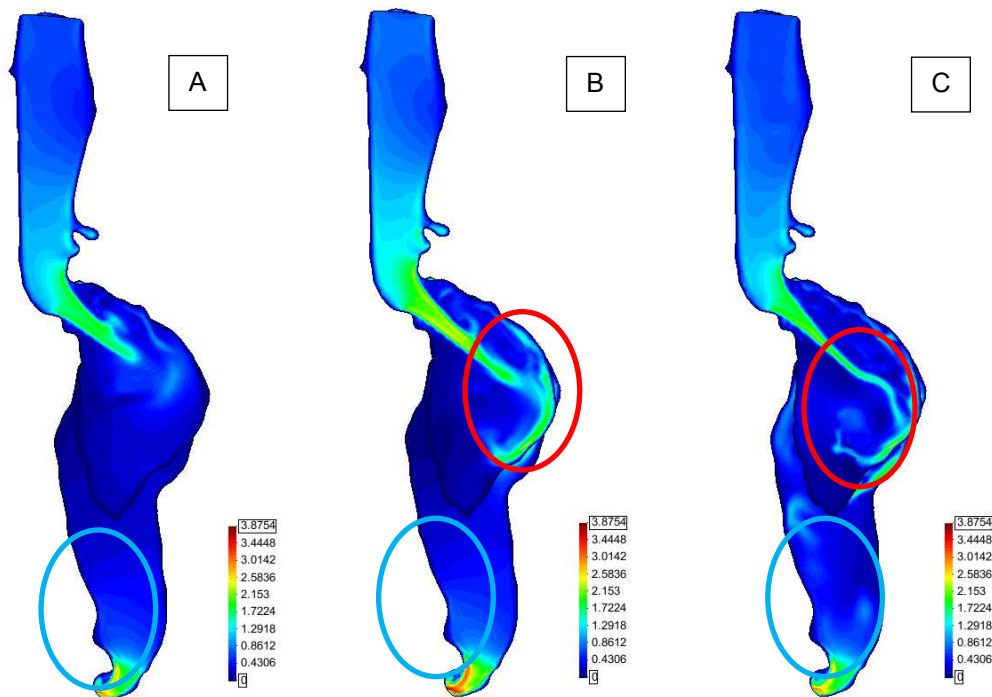


Figure 33. Velocity field in 3 different moment of the simulation A (0.1 sec), B (0.15 sec) and C (0.25 sec).

Next figures (34 and 35) show the flow is deviated to the periferical zone after the curved zone, this deviation will provoke effect also on WSS distribution as we will see in next illustrations.

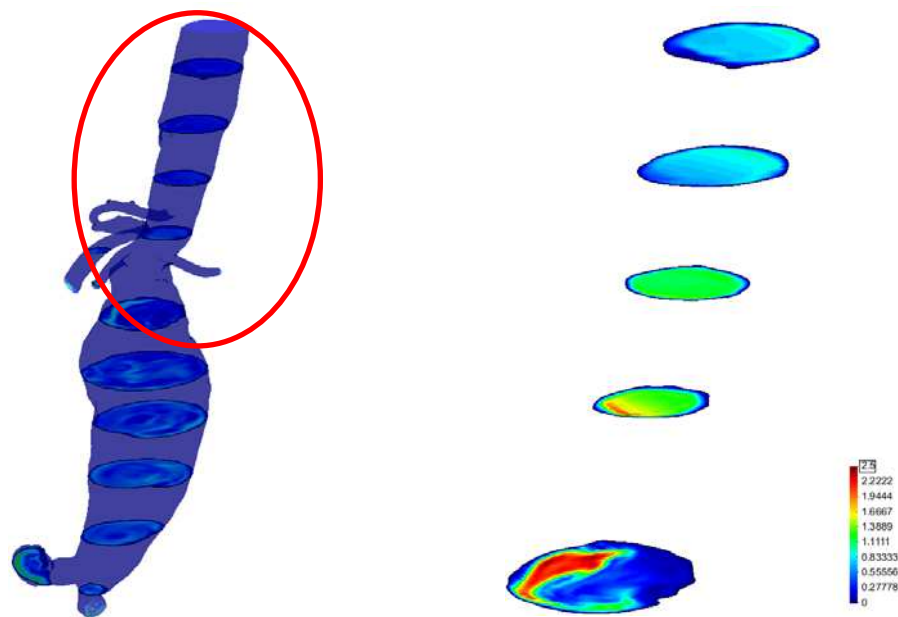


Figure 34. Velocity field in transversal cuts for the upper part of the aortic vessel.

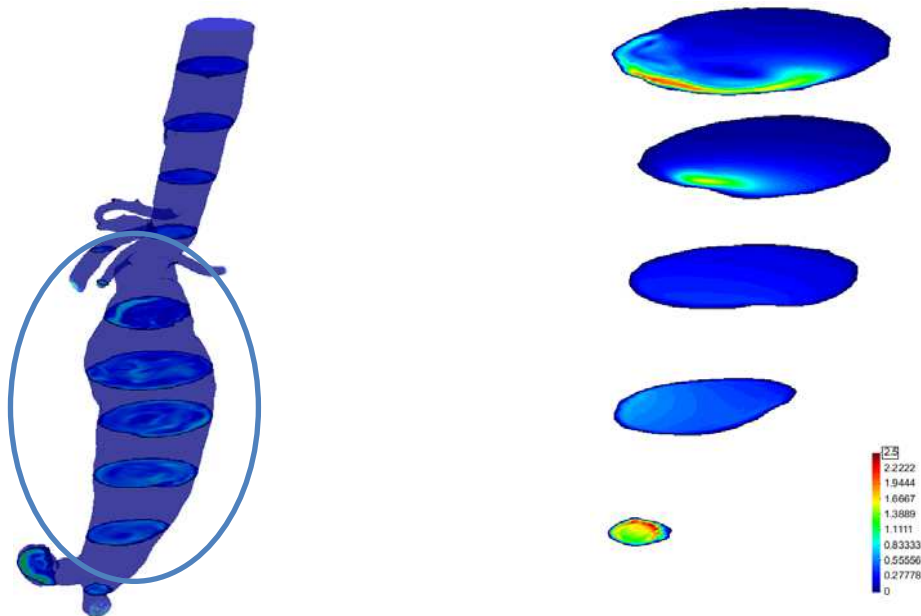


Figure 35. Velocity field in transversal cuts for the lower part of the aortic vessel.

Figure 36 show WSS distribution caused by the deformation of the normal curvature of the aorta. The WSS is not uniform and high values of stresses are present in the zone where blood pushes the vessel wall.

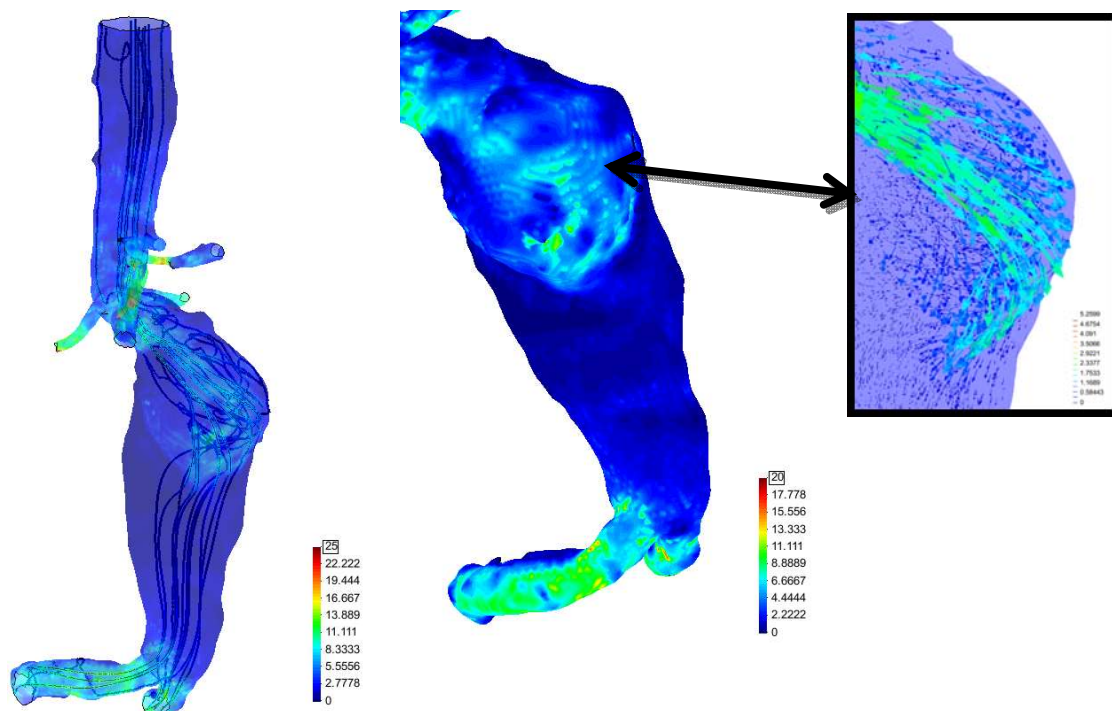


Figure 36. Wall Shear Stress in the saccular zone.

h. Case S1184041H

The mesh created of 456.462 elements reconstructs the geometry of a healthy abdominal aorta. This geometry will clarify the differences between normal and abnormal geometries. The quality of the mesh can permit a good analysis of WSS distribution along the vessel surface.

i. Geometry and meshing

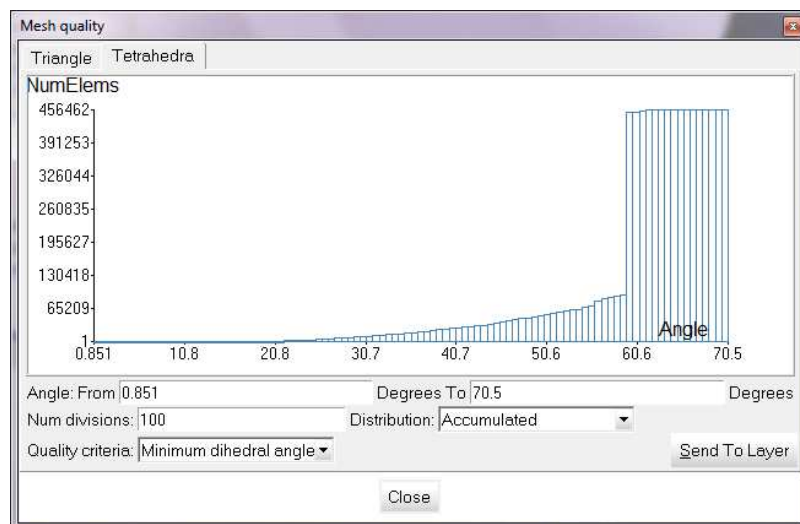
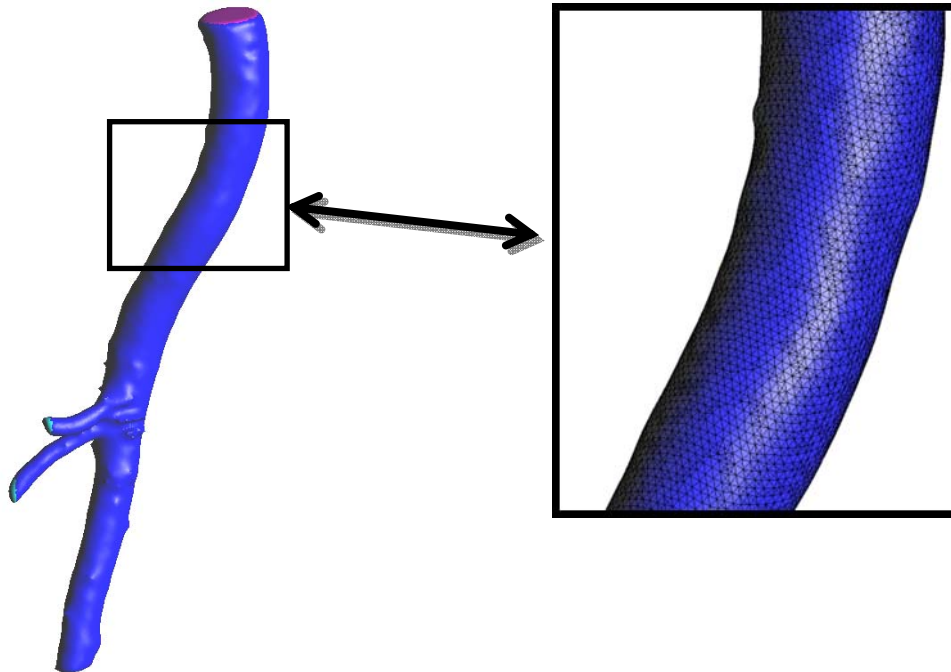


Figure 37. Mesh Volume appearance and detail of the upper part of the aneurysm, and mesh volume quality (good elements are with angle $>10^\circ$).

ii. Results

Analyzing velocity field in 3 different moments, simulation remarks the uniformity of the flow and a good its behavior along the vessel. Figure 38 shows velocity fields in moment 0.1, 0.15 (maximum flow rate) and 0.25 (initial part of steady solution).

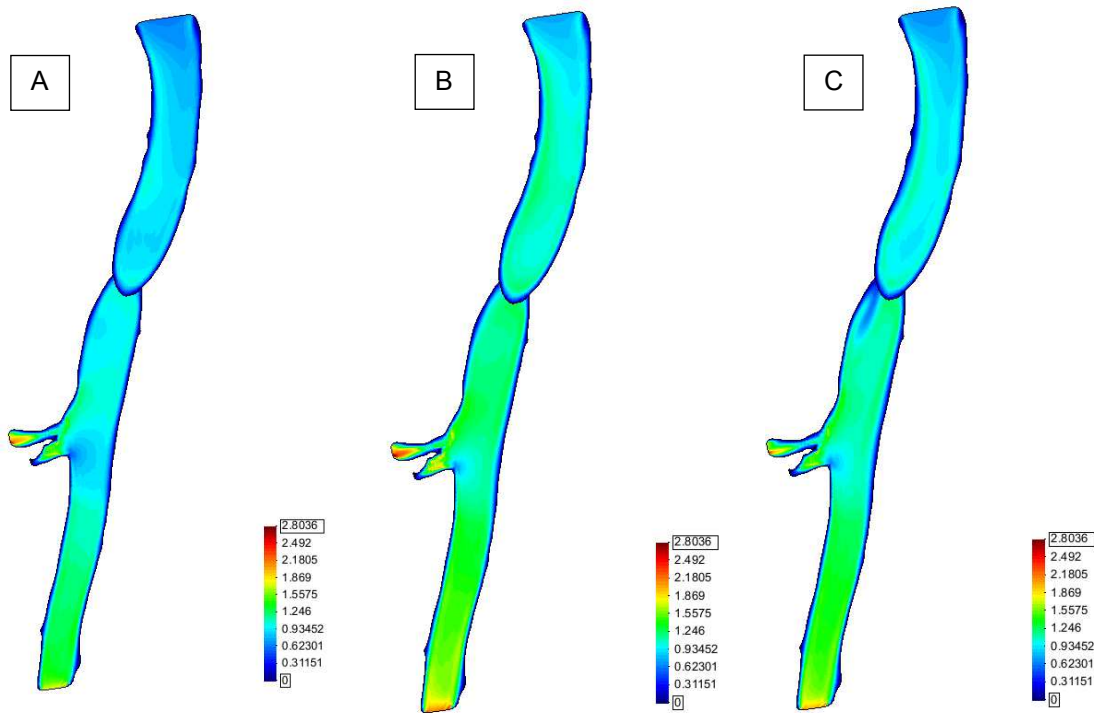


Figure 38. Velocity field in 3 different moment of the simulation A (0.1 sec), B (0.15 sec) and C (0.25 sec).

It is possible to note that WSS does not reach high values in the aortic branch. Values calculated in hyperemia moment flow rate are lower than 5 Pa in all the vessel wall, presenting uniform distribution all around the surface (fig 39 and 40). Stream lines in figure 41 also underline the lineal and absence of eddies and vortices.

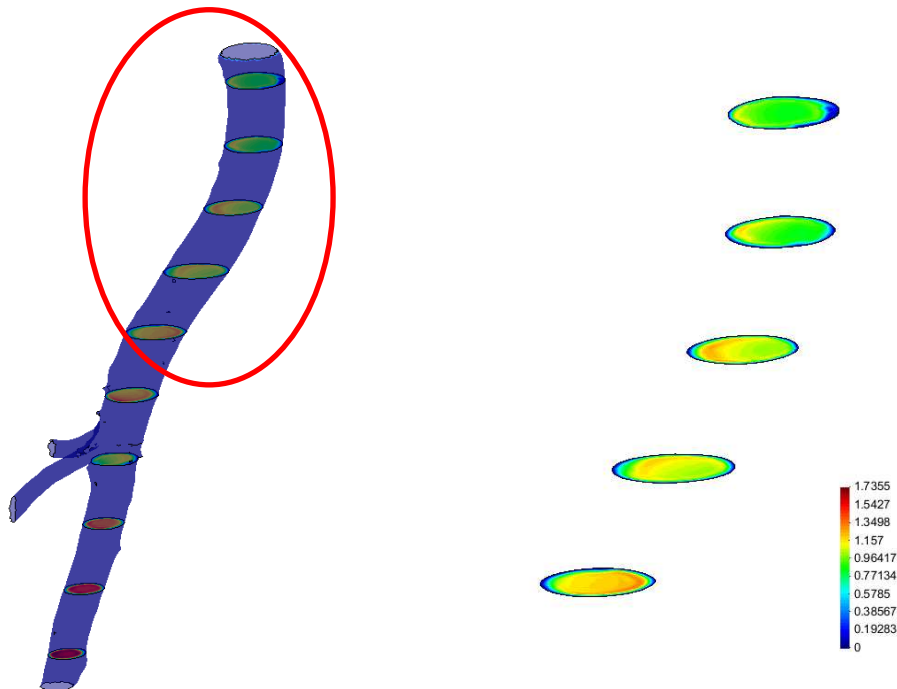


Figure 39. Velocity field in transversal cuts for the upper part of the aortic vessel.

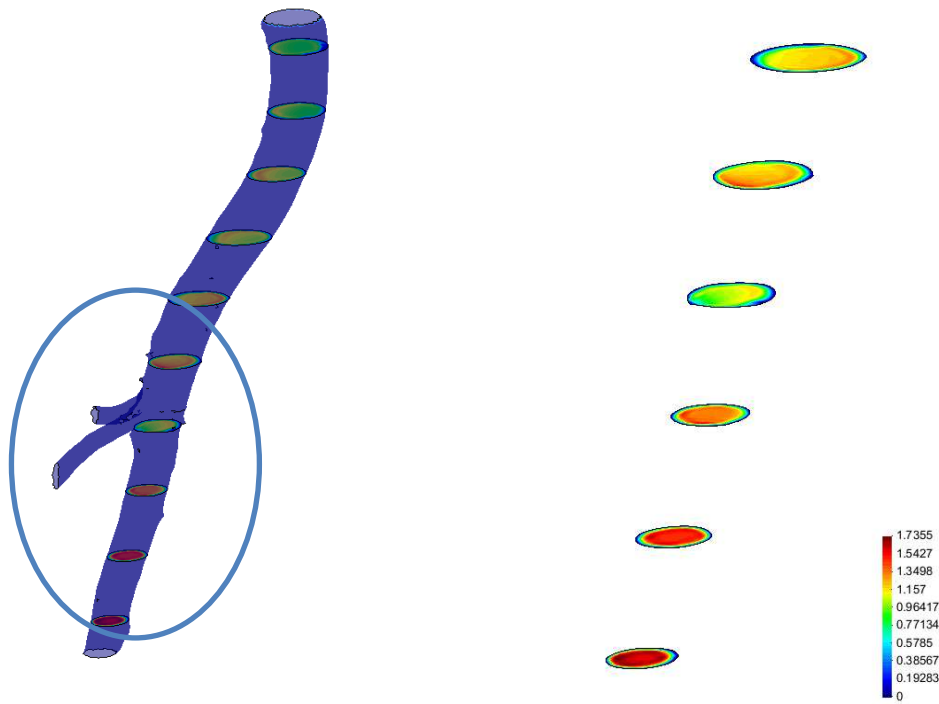


Figure 40. Velocity field in transversal cuts for the lower part of the aortic vessel.

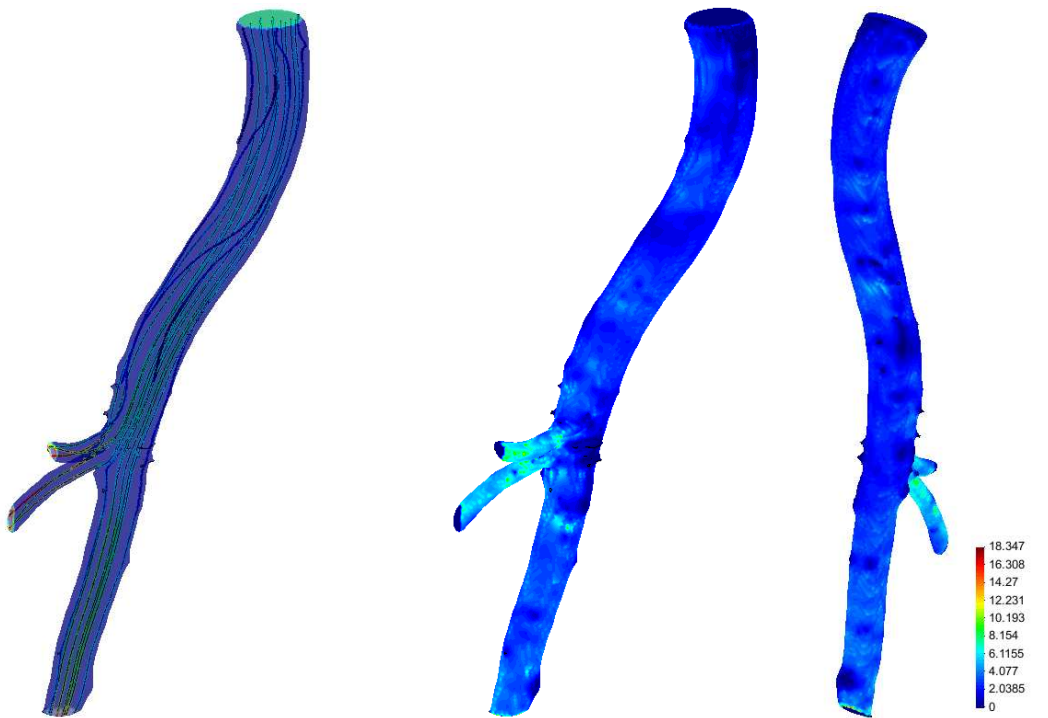


Figure 41. Wall Shear Stress in the two opposite views.

i. Case S1168446G

Next case identified as S1168446G shows an aneurysm in the bottom zone in concomitance of an accentuation of the curvature of the vessel, just before the bifurcation of the femoral vessels. The quality of the mesh, composed by 506.019 is enough for WSS analysis in the damaged zones. The segmentation included the initial part of femoral vessels, due to the enhanced geometry of one of them.

i. Geometry and meshing

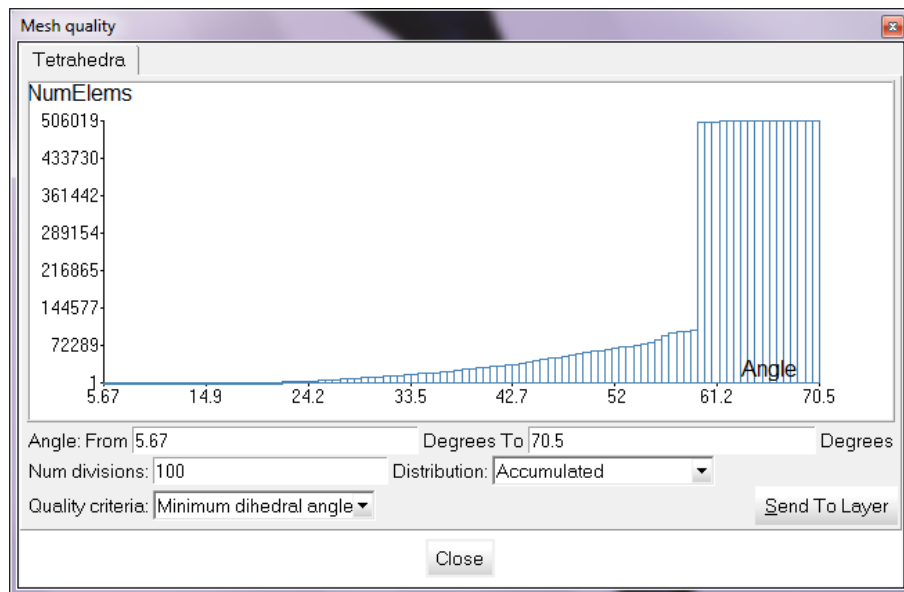
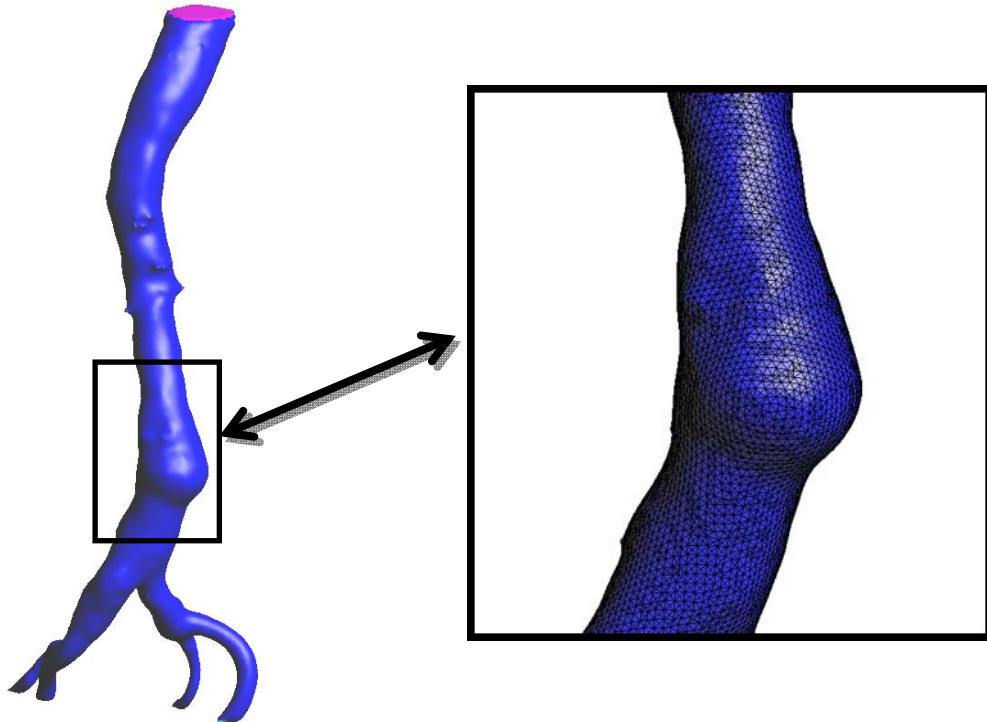


Figure 42. Mesh Volume appearance and detail of the upper part of the aneurysm, and mesh volume quality (good elements are with angle $>10^\circ$).

ii. Results

Velocity analysis is also in this case interesting when we want to study the behavior of the blood in the diseased zone. Blood flow produces abnormal pattern and irregular velocity field. Flow is moved to the external zone, impacting to the vessel wall, increasing the stress on the tissue yet interested to the illness.

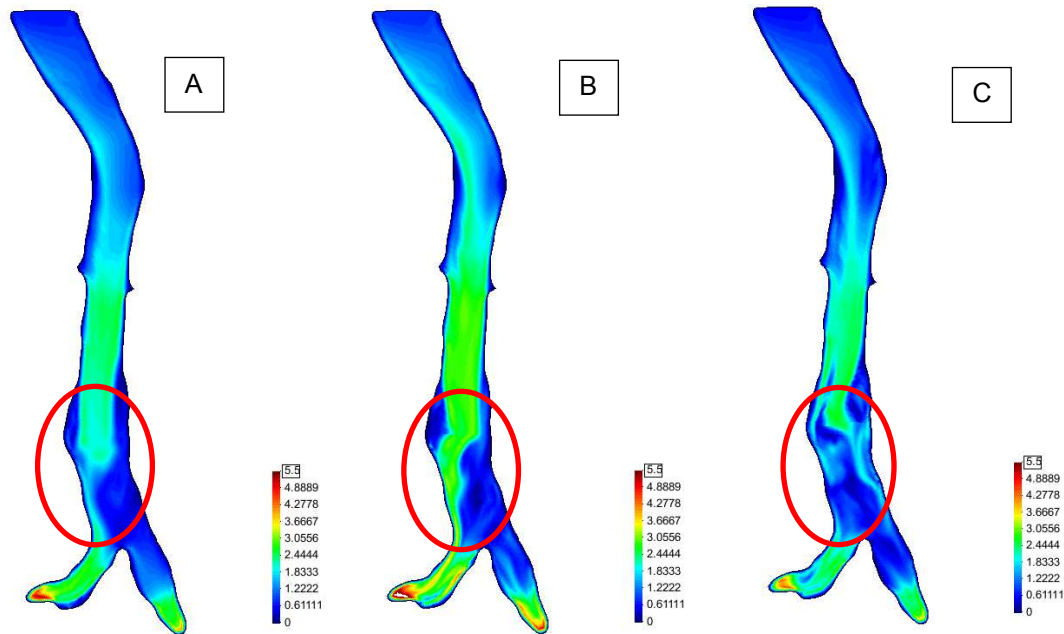


Figure 43. Velocity field in 3 different moment of the simulation A (0.1 sec), B (0.15 sec) and C (0.25 sec).

Next pictures (44 and 45) confirm with transversal cuts the trend of the flow to increase near the enhanced zone. It is easy to see how the normal and ordinated flow (fig. 44) changes along the tube and reach not regular distribution in the bottom part affected to the aneurysm (fig. 45)

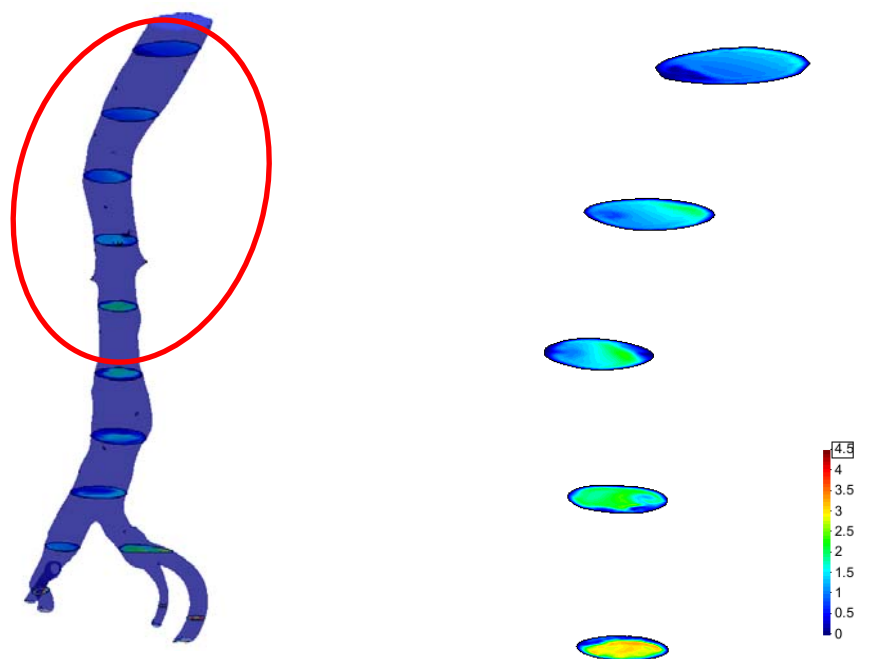


Figure 44. Velocity field in transversal cuts for the upper part of the aortic vessel.

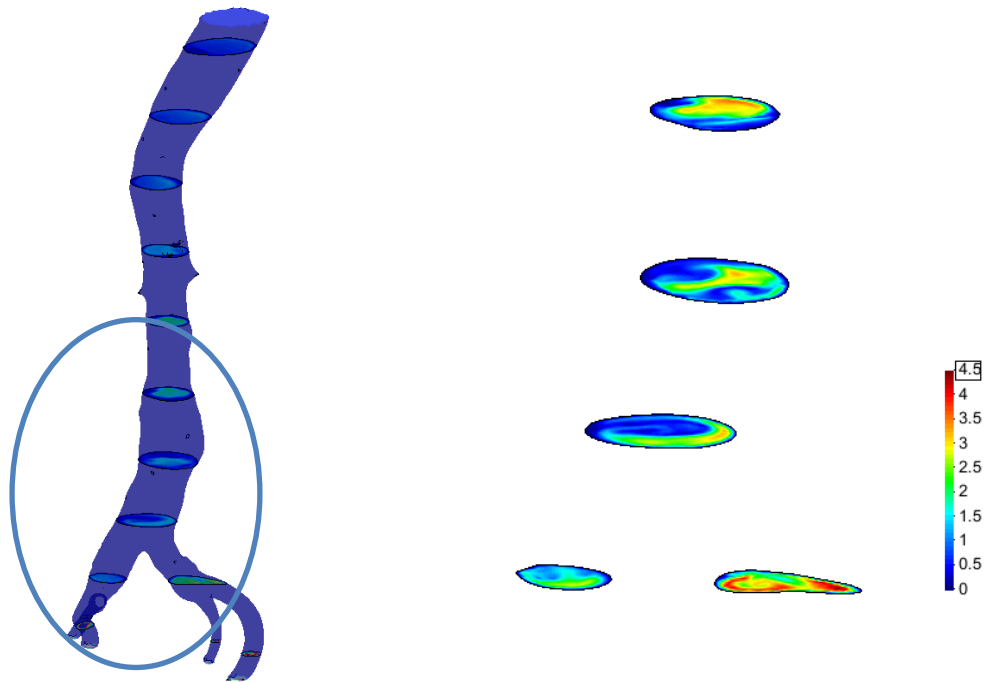


Figure 45. Velocity field in transversal cuts for the lower part of the aortic vessel.

Figure 46 remarks the conclusion done before studying the velocity fields. The lower zone of the aneurysm presents high values of WSS, inducing a future enhancement of the saccular zone.

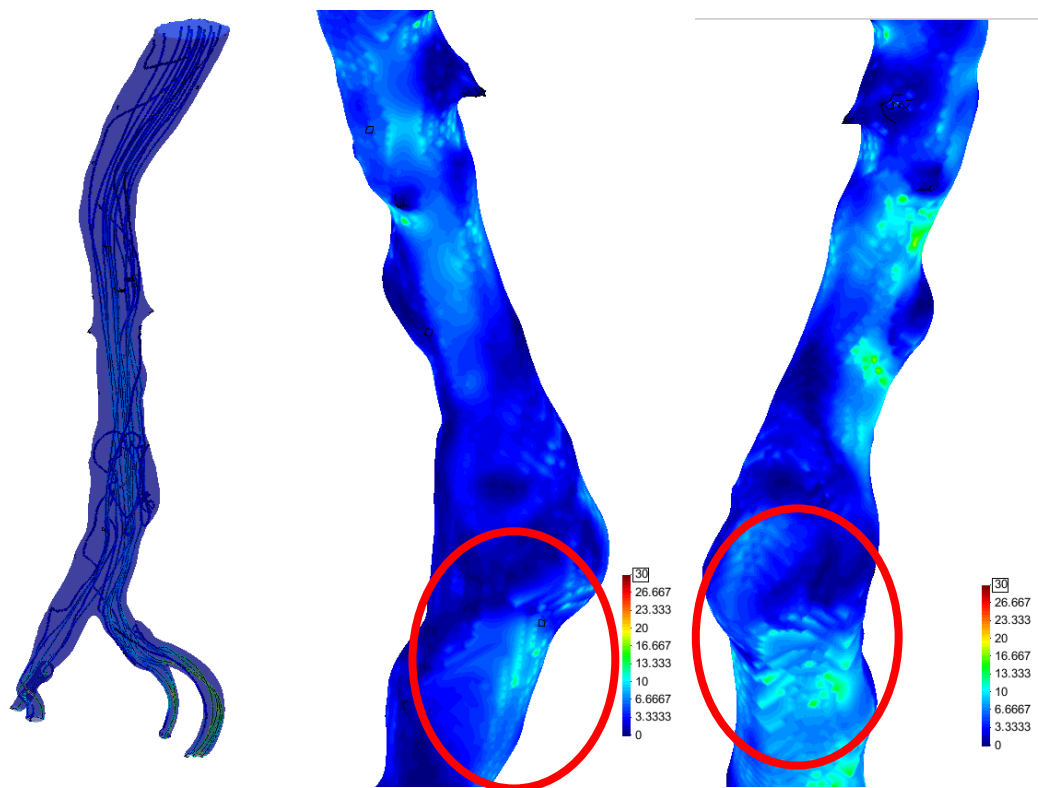


Figure 46. Wall Shear Stress in the saccular zone.

j. Case S0722132J

Also in this case results analysis is focused on the study of the relationship between wall shear stress (WSS) and flow behavior inside the aneurysm.

i. Geometry and meshing

Mesh created present 431.268 volume elements. In some zone that need a more precise values computation are meshed with finer elements, like the little branch in upper zone and the saccular zone, due to the intention of study of WSS values. See Annex 1.

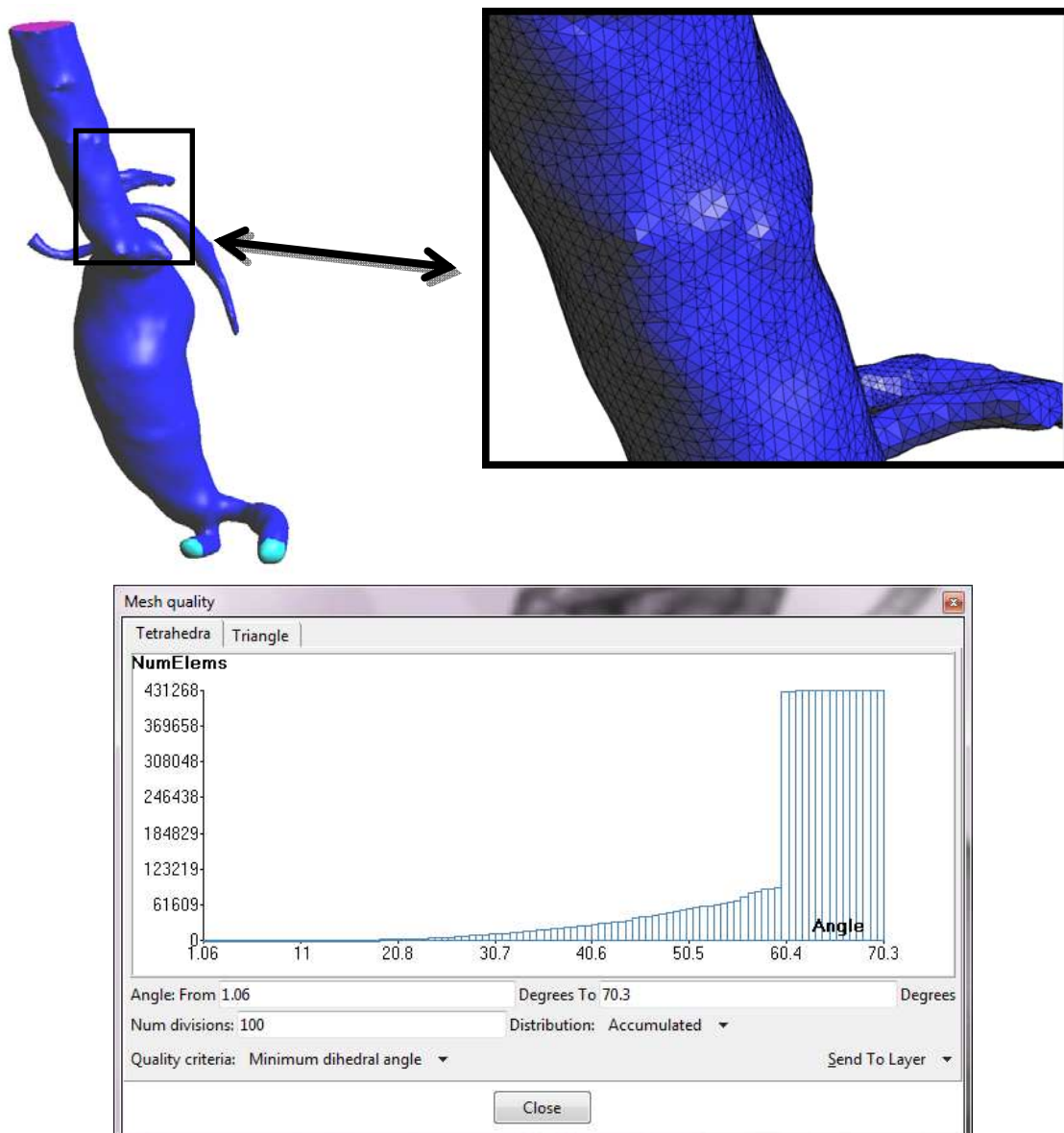


Figure 47. Mesh Volume appearance and detail of the upper part of the aneurysm, and mesh volume quality (good elements are with angle $>10^\circ$).

ii. Results

As noted we could see in other cases the blood jet is accelerated and concentrated by the tortuous and narrow segments that precede the aneurysm. This fact leads that the jet impact strongly to the wall of the aneurysm provoking more stresses on the artery wall that, due to its modified mechanical properties, will follow its enhancement. (fig 48).

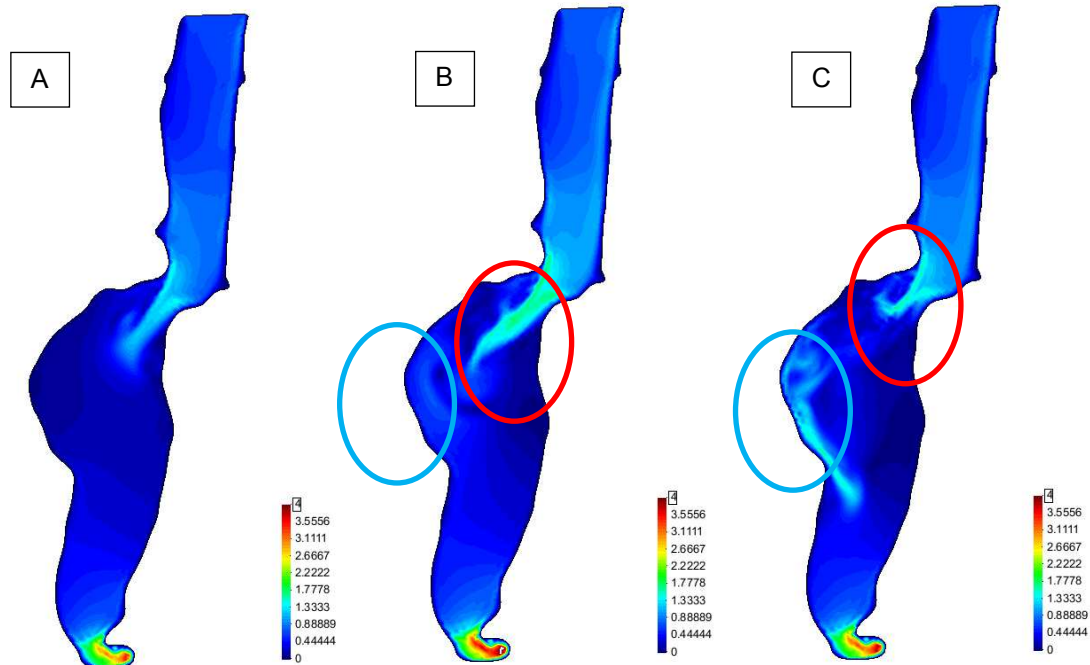


Figure 48. Velocity field in 3 different moment of the simulation A (0.1 sec), B (0.15 sec) and C (0.25 sec).

Transversal section shown in figure 49 and 50 remarks the vortices created inside the curved zone and the aneurysm, in the highlighted zone (green circle)

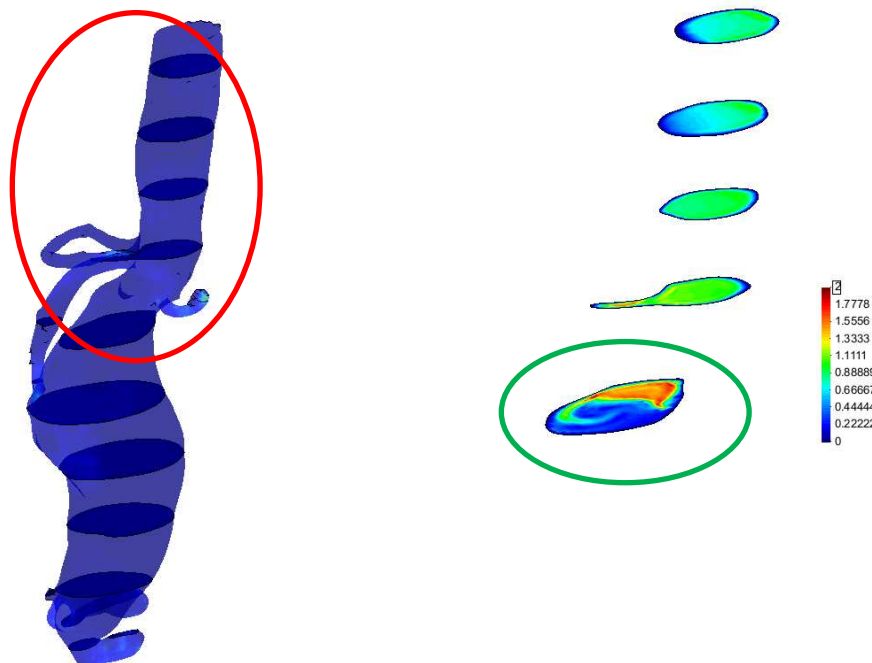


Figure 49. Velocity field in transversal cuts for the upper part of the aortic vessel.

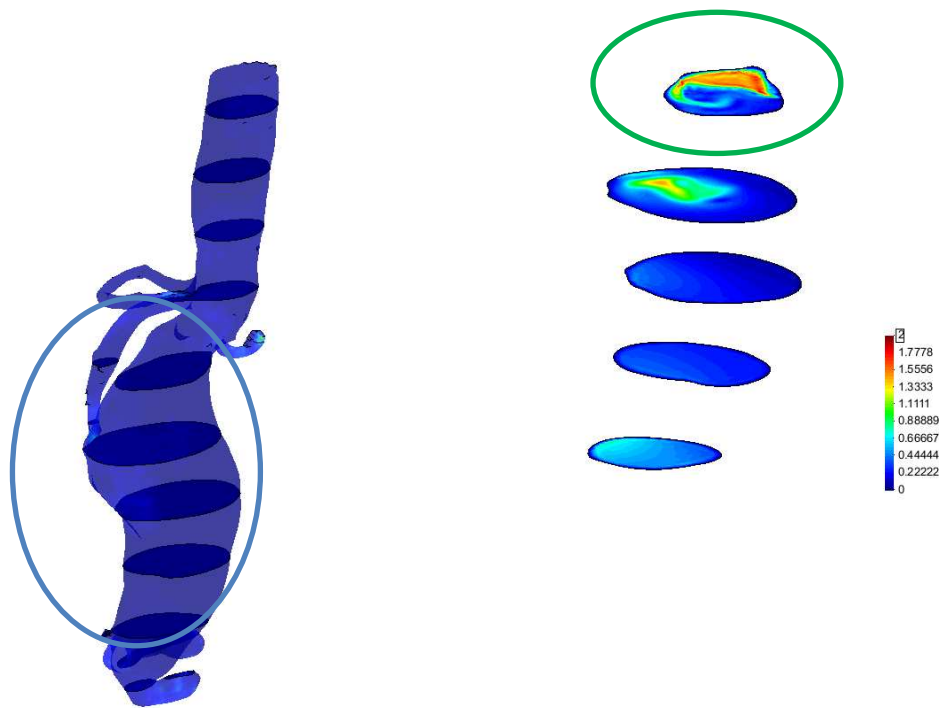


Figure 50. Velocity field in transversal cuts for the lower part of the aortic vessel.

In the figure 51, WSS on the surface in the moment of maximum velocity of the heartbeat cycle (0.15 sec) are shown. It is easy to remark that in the elbow of the aneurysm the WSS is incremented.

It is also possible to see that the increment of the WSS is due to an increased velocity field: blood jet hits the vessel wall. This situation increase mechanical stress on the arterial wall, inducing more deformation respect normal and physiological shape of the aorta.

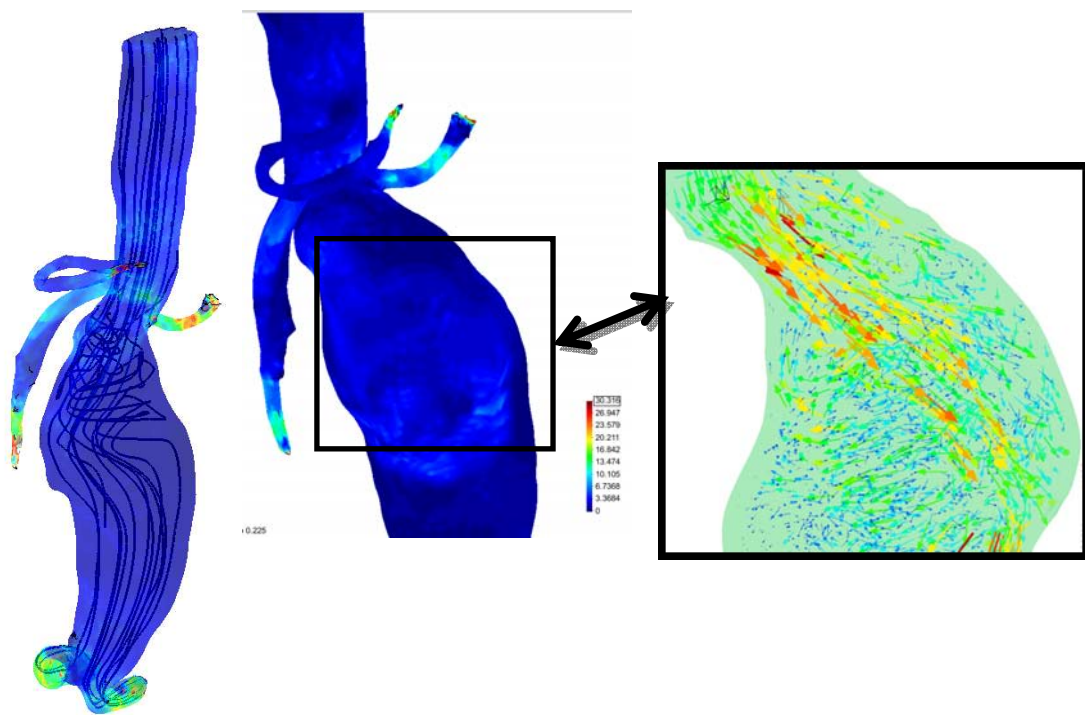


Figure 51. Wall Shear Stress in the saccular zone.

k. Case S0942654Z

Last case analyzed presents a big aneurysm just before the bifurcation of the femoral arteries. Geometry mesh was optimized in order to use only 390.866 elements, but the superficial zones were meshed with finer elements in order to improve the quality of WSS results.

i. Geometry and meshing

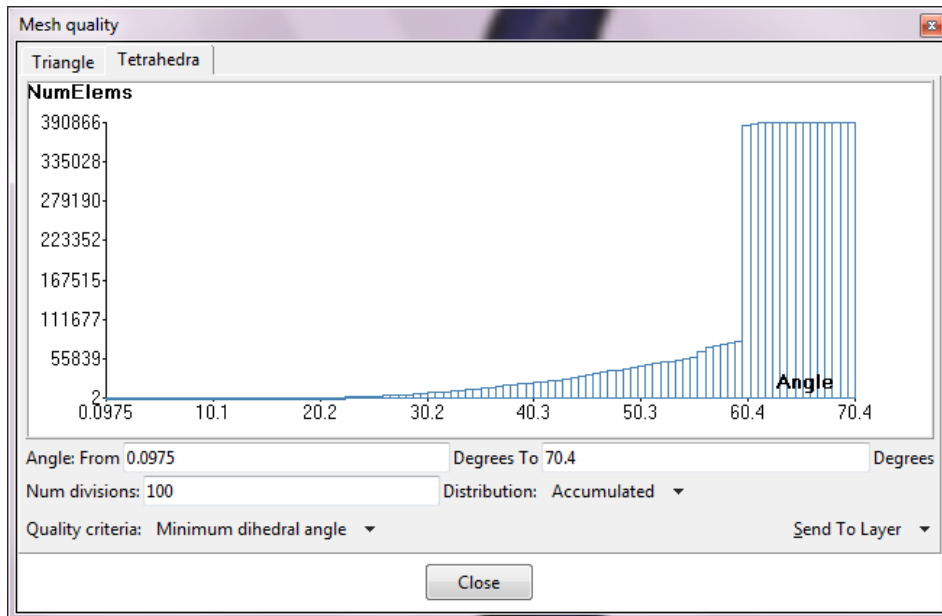
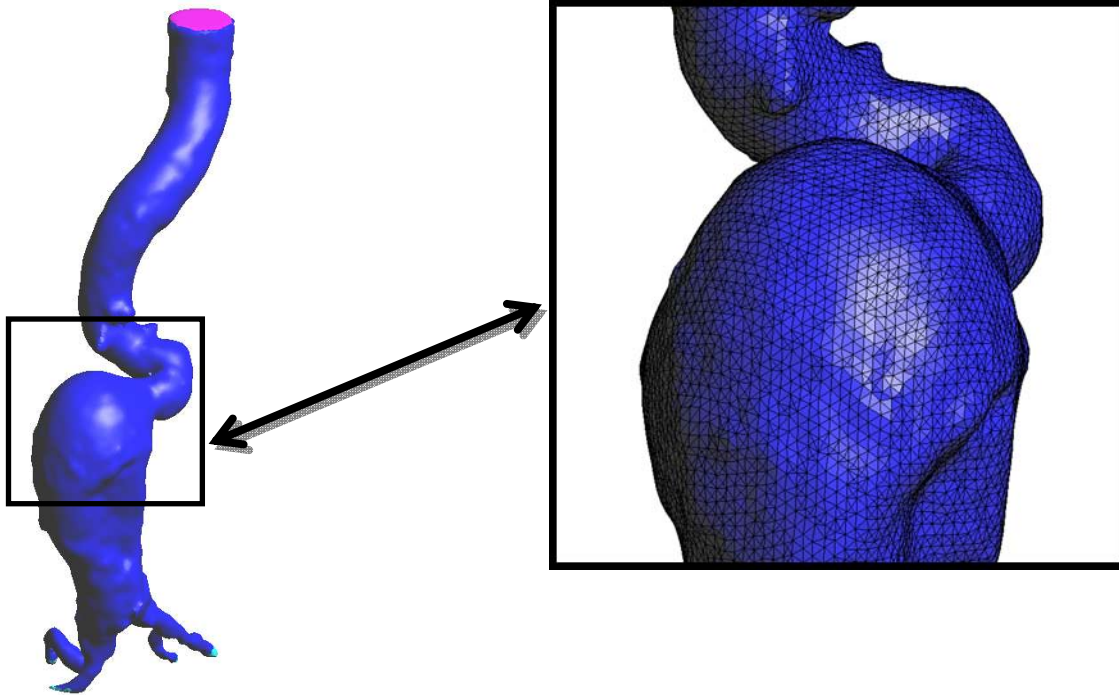


Figure 52. Mesh Volume appearance and detail of the upper part of the aneurysm, and mesh volume quality (good elements are with angle $>10^\circ$).

ii. Results

Velocity results show the typical behavior of the flow in the saccular zone. Figure 53 show, in the blue marker how the jet flow impact along the time on the vessel wall. Red circle also highlight some zone of vortices with high velocity and irregular flow patterns.

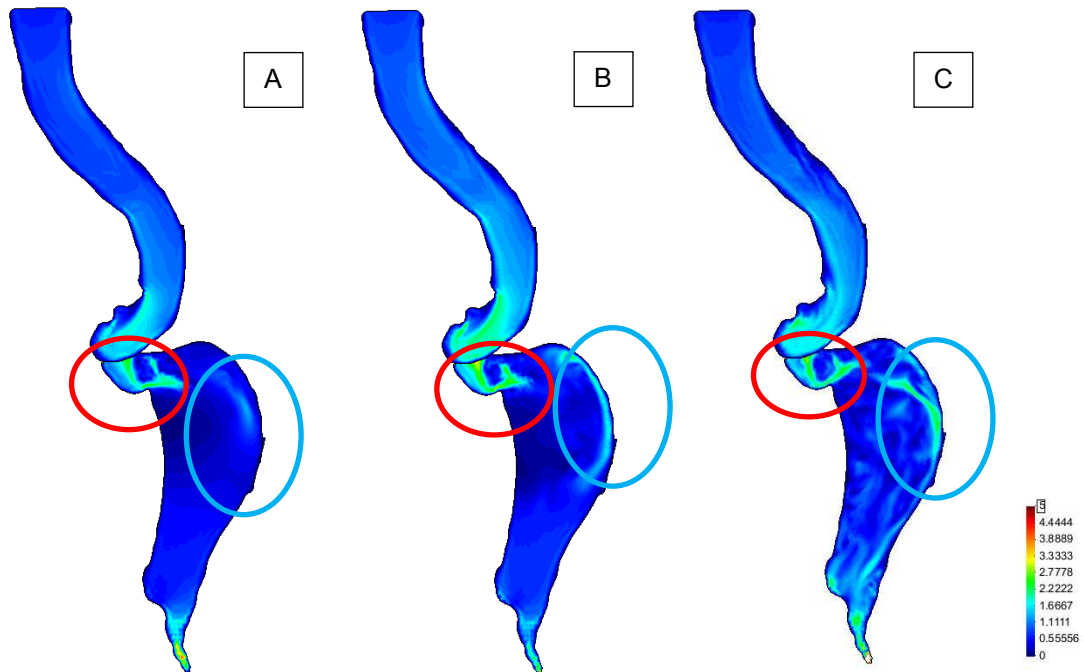


Figure 53. Velocity field in 3 different moment of the simulation A (0.1 sec), B (0.15 sec) and C (0.22 sec).

It is interesting to see how the regular flow show in figure 54 change after pass to the tortuous zone (fig 55) where the flow reach irregular morphology causing problems to the blood flow circulation.

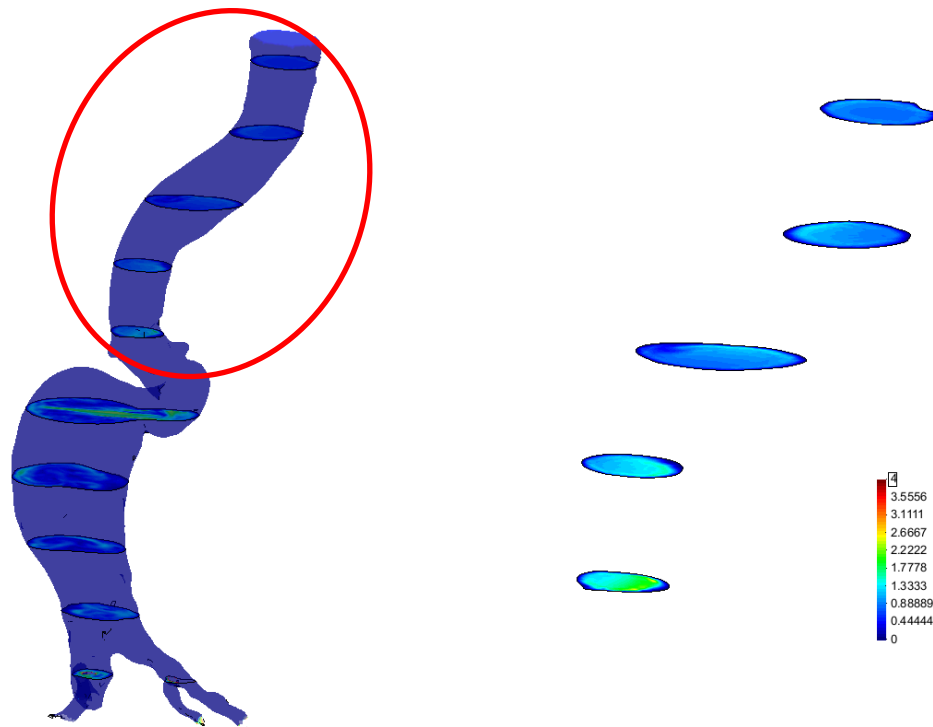


Figure 54. Velocity field in transversal cuts for the upper part of the aortic vessel.

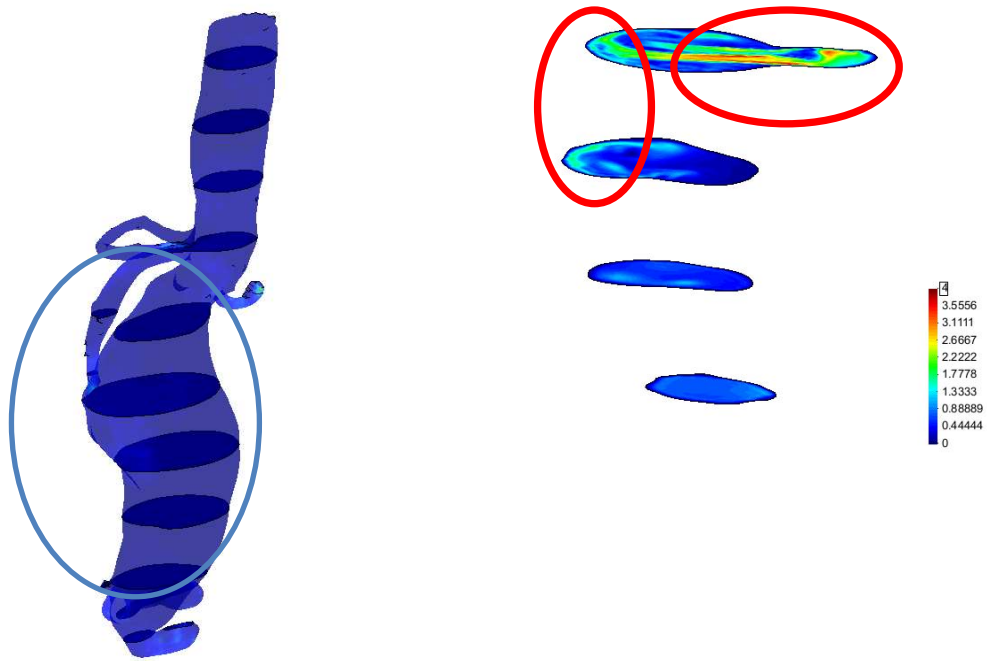


Figure 55. Velocity field in transversal cuts for the lower part of the aortic vessel.

WSS analysis confirms that the zones with higher stresses are the same where the flow jet impacts. Figure 56 show the 2 important zone with high WSS value.

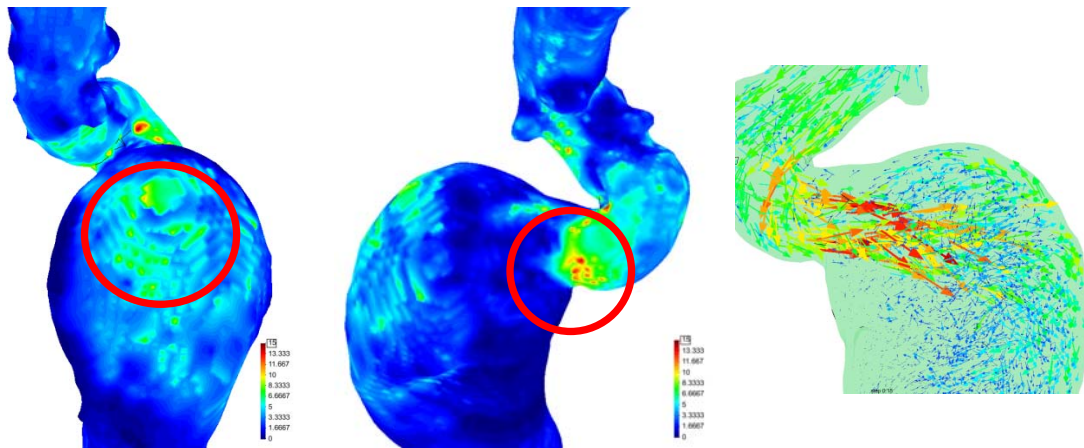


Figure 56. Wall Shear Stress in the aneurysm zone.

4. Conclusions

Most of abdominal aneurysms (AAA) (about 90%) are located below the level of the renal arteries, the vessels that leave the aorta to go to the kidneys. These abdominal aneurysms are known as Infrarenal aneurysm. Infrarenal aneurysm is a pathology involving the enlargement of the aorta in the inferior thoracic area taking a fusiform shape and may extend into the iliac arteries. This mortality of this pathology is high (15% for ruptured aneurysms), for this reason, in this study eleven infrarenal aneurysms were analysed in order to understand the geometrical features and the hemodynamic loads with a possible AAA rupture. The current standard of determining rupture risk is based on maximum diameter, it is known that smaller AAAs that fall below this threshold (diameter < 5.5 cm) may also rupture, and larger AAAs (diameter > 5.5 cm) may remain stable [1], but not all the cases would have succumbed to rupture prior to surgical intervention as the diameter was less than 5 cm, suggesting that other biomechanics or geometrical factors come into play in the rupture of the aneurysm. Several authors have proposed several criteria for the collapse of the aneurysms based on the clinical empirical evidence, if the asymmetry index factor, $\beta < 0.4$ the AAA rupture is high [18], in [21] the AAA collapse is when the Deformation diameter ratio [20] is $\chi > 3.3$ or in [19][22] if the saccular index is < 0.6 . But depending of the index that is analyzed the surgical criteria is different. Therefore, alternative methods of AAA rupture assessment are needed. The majority of these new approaches involve the numerical analysis of AAAs using computational fluid dynamics (CFD) to determine the wall shear stress (WSS) distributions. From a mechanical point of view, stress is the amount of force exerted on a surface per unit area of the wall. The peak of the WWS refers to the mechanical load sustained by the AAA wall, during maximal systolic pressurization. It is also known that wall stress alone does not completely govern failure as an AAA will usually rupture when the wall stress exceeds the wall strength. Its value depends on arterial systolic pressure, the mechanical properties and the geometric configuration of the material under study. More recently proposed AAA rupture-risk is related with the presence of intraluminal thrombus (ILT) [23], and perhaps, one of the most ambiguous issues in the computational evaluation of rupture risk is the integration of ILT and perivascular tissues in the models. It has been suggested that the intraluminal thrombus layer plays an important role in expansion and rupture of advanced aneurysms through direct mechanical as well as indirect chemomechanical effects [18]. Therefore, the AAA dilatation (and a possible rupture) is not only depending of geometrical factor or the hemodynamic load is depending on the correlation of the geometrical indexes and the hemodynamic loads or new indexes as the tortuosity. In some cases, the highest shear stress values are depending especially of the tortuosity of the AAA.

This study concentrated on the wall stress using a computational simulation to demonstrate the stress distributions within the patient-specific AAA. From a mechanical point of view, stress is the amount of force exerted on a surface per unit area of the wall. The simulations were carried out for two cardiac cycles, but the results of both stress and flow patterns were found to be periodic after the second cardiac cycle. The figures show the flow patterns inside the infrarenal Aneurysms sac models for whole patients to examine the link between abnormal flow patterns and the anatomical geometrical. As shown in refs. [8,14,15,17], the asymmetric flow patterns can provide an insight into the mechanism that promotes the thrombus renewal (ILT) and possibly enlargement inside the aneurysm. Rapid decrease in the velocity and regions of very high (or low) hemodynamic stresses gradients, may all contribute in various ways to the vascular disease, primarily via their effects on the endothelium. For example, platelets trapped in recirculating zones tend to be deposited in areas of low shear stress (stenosis), since this and the presence of vortices cause prolonged contact of the platelets with the surface in the layer of slow fluid motion [16].

In the future will be interesting to plan a protocol in order to run many simulations on the geometries of different patients of interest and perform standard studies in order that the physician could read the result with minimal efforts and clearly. If it will be possible, it would be interesting to use real input and output data (PATIENT-SPECIFIC DATA). Measuring the pressure and the velocity inside the aorta will improve the results and the fidelity of the simulation.

5. References

- [1] Vorp D.A. Biomechanics of abdominal aortic aneurysm. *J. Biomech.*, 40(2007), 1887–1902.
- [2] Soudah E., Pennecot J, Perez J.S, Bordone M., Oñate E. Chapter 10: “Medical-GiD: 381 From medical images to simulations, MRI Flow Analysis”. Book: Computational Vision and Medical Image Processing: Recent Trends. ISSN 1871-3033 383 Ed.Springer.
- [3] Soudah E., Bordone M., Perez J.S, “Gmed: a platform for images treatment inside gid system. 5th Conference On Advances And Applications Of GiD. Barcelona 2010. www.gidhome.com GiD - The personal pre and postprocessor.
- [4] A. Paul, P.A. Yushkevich, J. Piven, H.C. Hazlett, R.G. Smith, S. Ho, et al., User- 413 guided 3D active contour segmentation of anatomical structures: Significantly 414 improved efficiency and reliability, *Neuroimage* 31 (2006) 1116–1128.
- [5] Lorensen, W.E., Cline, H.E. Marching cubes: A high resolution 3d surface construction algorithm. In *Proceedings of SIGGRAPH*, pages 163–169 (1987).
- [6] M.Bordone, C.García, J.García, E.Soudah, *Biodyn User Manual .TDYN: theoretical Background: www.compassis.com/compassis. COMPASSIS (2012)*
- [7] E. A. Finol, K. Keyhani, C. H. Amon. The Effect of Asymmetry in Abdominal Aortic Aneurysms Under Physiologically Realistic Pulsatile Flow Conditions. *Journal of Biomechanical Engineering* APRIL 2003, Vol. 125, 207- 217. DOI: 10.1115/1.1543991
- [8] Biasetti J, Hussain F, Gasser TC: Blood flow and coherent vortices in the normal and aneurysmatic aortas: a fluid dynamical approach to intra-luminal thrombus formation. *J.R. Soc. Interface*, Doi:10.1098/rsif.2011.0041.
- [9] E. Oñate, S. Idelsohn, O.C. Zienkiewicz, R.L. Taylor, A finite point method in computational mechanics. Applications to convective transport and fluid flow, *Int, Journal for Numerical Methods in Engineering* 39 (1996) 3839–3866.
- [10] García, J., Oñate, E., Sierra, H., Sacco, C. and Idelsohn, S. “A Stabilised Numerical Method for Analysis of Ship Hydrodynamics”. *Proceedings Eccomas Conference on CFD*, 7-11 September 1998, Athens, John Wiley, 1998.
- [11] Y. Papaharilaou, J.A Ekaterinaris, E. Manousaki, et al: A decoupled fluid structure approach for estimating wall stress in abdominal aortic aneurysm. *J. Biomech.* 40 (2007), 464-475.
- [12] A. Borghia, N.B. Wooda, R.H. Mohiaddinb, X.Y. Xua. Fluid–solid interaction simulation of flow and stress pattern in thoracoabdominal aneurysms: A patient-specific study. *Journal of Fluids and Structures* 24 (2008) 270–280.
- [13] R. Barrett et al., *Templates for the Solution of Linear Systems: Building Blocks for Iterative Methods*, 2nd Edition, Philadelphia, PA: SIAM, 1994.
- [14] Scotti CM, Fino EA: Compliant biomechanics of abdominal aortic aneurysm: A fluid-structural interaction study. *Computer and Structures*, 85 (2007), 1097-1113.
- [15] Salsac AV, Sparks SR, Chomaz JM, Lasheras JC: Evolution of the wall shear stresses during the progressive enlargement of symmetric abdominal aortic aneurysms. *J. Fluid Mech*, 560 (2006), 19-51.
- [16] Bluestein, D., Rambod, E., Gharib, M. Vortex shedding as a mechanism for free emboli formation in mechanical heart valves. *ASME Journal of Biomechanical Engineering* 122,2 (2000), 125–134.

- [17] A. Sheidaei, S.C. Hunley, S. Zeinali-Davarani, L.G. Raguin, S. Baek, Simulation of abdominal aortic aneurysm growth with updating hemodynamic loads using a realistic geometry. *Medical Engineering & Physics* 33 (2011) 80–88.
- [18] Vorp DA, Lee PC, Wang DHJ, Makaroun MS, Nemoto EM, Ogawa S, et al. Association of intraluminal thrombus in abdominal aortic aneurysm with local hypoxia and wall weakening. *Journal of Vascular Surgery* 2001;34:291–9.
- [19] Clement Kleinstreuer and Zhonghua Li “Analysis and computer program for rupture-risk prediction of abdominal aortic aneurysms” .*BioMedical Engineering OnLine* 2006, 5:19.
- [20] Judy Shum, Giampaolo Martufi, Elena Di Martino, Christopher B. Washington, Joseph Grisafi, Satish C. Muluk, and Ender A. Finol. Quantitative Assessment of Abdominal Aortic Aneurysm Geometry. *Ann Biomed Eng.* 2011 January; 39(1): 277–286.
- [21] Cappeller WA, Engelmann H, Blechschmidt S, Wild M, Lauterjung L: Possible objectification of a critical maximum diameter for elective surgery in abdominal aortic aneurysms based on one-and three-dimensional ratios. *Journal of Cardiovascular Surgery* 1997, 38:623-628.
- [22] Ouriel K, Green RM, Donayre C, Shortell CK, Elliott J, Dewese JA: An evaluation of new methods of expressing aortic aneurysm size: Relationship to rupture. *Journal of Vascular Surgery* 1992, 15:12-20.
- [23] Vorp DA, Raghavan ML, Webster MW (April 1998). "Mechanical wall stress in abdominal aortic aneurysm: influence of diameter and asymmetry". *Journal of Vascular Surgery* 27 (4): 632–9. doi:10.1016/S0741-5214(98)70227-7.
- [24] GiD (<http://gid.cimne.upc.es/>). CIMNE 2012.

ANNEX: Mesh Quality

The objective of generate a good quality volume grid is needed because:

- Designates the cells or elements on which the flow is solved.
- Is a discrete representation of the geometry of the problem.
- Has cells grouped into boundary zones where b.c.'s are applied.

Indeed, the grid has a significant impact on:

- Rate of convergence (or even lack of convergence).
- Solution accuracy.
- CPU time required.

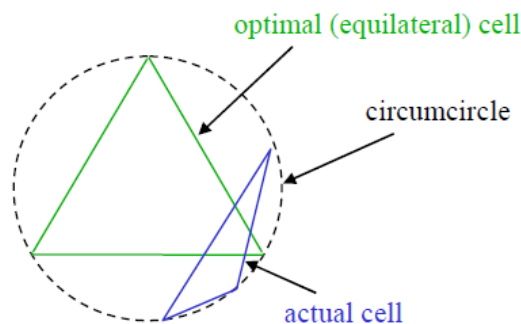
And it is importance of mesh quality for good solutions.

- Grid density.
- Adjacent cell length/volume ratios.
- Skewness.
- Mesh refinement through adaption.

For determinate a good quality mesh we have calculated the aspect ratio of the triangles and tetrahedral elements based on the equilateral volume:

- Skewness = optimal cell size cell size / optimal cell size

Next figure shows the skewness of the triangle element.

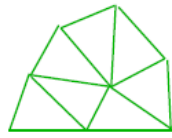


In order to generate a good volume meshes, the process consists of:

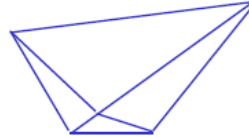
1. Import volume mesh from the AAA
2. Check if the mesh is properly closed (requirement needed for the isostuffing algorithm).
 - a. If NOT CLOSED: smoothing and collapse is applied.
3. Set the Isostuffing algorithm parameters.
4. Volume mesh. Check the quality of tetrahedral elements.

All the algorithms used in this process are integrated in GiD [24]. In order to check the quality of the mesh the two parameters have been considered:

- Change in size should be gradual (smooth),



smooth change
in cell size



large jump in
cell size

- Aspect ratio is ratio of longest edge length to shortest edge length. Equal to 1 (ideal) for an equilateral triangle.



aspect ratio = 1



high-aspect-ratio triangle

Using the isostuffing algorithm we have obtain a smooth element and an aspect radio for whole of the meshes is upper than 0.9. The overall mesh generation procedure of the 3D volume mesh to the AAA was quite satisfactory.

CFD Modelling of Abdominal Aortic Aneurysm on Hemodynamic Loads using a Realistic Geometry with CT

Eduardo Soudah¹, E.Y.K. Ng², T.H. LOONG³, Maurizio Bordone¹, Pua Uei³ and Narayanan Sriram³

¹ Biomedical Engineering Department. Centre Internacional de Mètodes Numèrics en Enginyeria. c/ Gran Capità, s/n, 08034 Barcelona.

² School of Mechanical and Aerospace Engineering, Nanyang Technological University, 50 Nanyang Avenue, Singapore 639798

³ Department of General Surgery, Tan Tock Seng Hospital, 11 Jalan Tan Tock Seng, Singapore 308433

Abstract

The objective of this study is to find a correlation between the abdominal aorta aneurysm (AAA) geometric parameters, wall stress shear (WSS), abdominal flow patterns, intra-luminal thrombus (ILT) and AAA arterial wall rupture using computational fluid dynamics (CFD). Real AAA 3D models were created by three-dimensional (3D) reconstruction of in vivo acquired computed tomography (CT) images from 5 patients. Based on 3D AAA models, a high quality volume meshes were created using an optimal tetrahedral aspect ratio for whole domain. In order to quantify the WSS and the recirculation inside the AAA, a 3D CFD using finite elements analysis was used. The CFD computation was performed assuming that the arterial wall is rigid and the blood is considered an homogeneous Newtonian fluid with density 1050 kg/m^3 and a kinematic viscosity of $4 \times 10^{-3} \text{ Pa.s}$. Parallelization procedures were used in order to increase the performance of the CFD calculations. A relation between AAA geometric parameters (Asymmetry index (β), Saccular index (γ), Deformation diameter ratio (χ) and tortuosity index (ϵ)) and hemodynamic loads were observed, and it could be used as potential predictors of AAA arterial wall rupture and the possible ILT formation.

1. Introduction

Nowadays, it is recognized that current clinical criteria for assessment of the abdominal aortic aneurysm rupture risk can be considered insufficient because they have not a physically theoretical basis [1]; despite they are based on a wide empirical evidence. Hence, in last many years, researchers and physicians have had the challenge to identify a more reliable criterion associated with the actual rupture risk of the patient-specific aneurysm. The literature begins to reflect the existence of a consensus that, rather than empirical criteria, the biomechanical approach, based on the material failure, could facilitate a better method to assess the AAA rupture risk. One of these AAA rupture criteria are based on the evaluation of the hemodynamic stresses inside the AAA.

To estimate the AAA rupture risk, from biomechanical point of view (material failure), an aneurysm ruptures when the stresses acting on the arterial wall exceed its failure strength. According to the Laplace's law, the wall stress on an ideal cylinder is directly proportional to its radius and intraluminal pressure. Even though, the AAA is not ideal cylinder, Laplace's law said that with a large diameter, the internal pressure increases, and therefore increases the risk of rupture. Due to the increasing of the internal pressure, against the aortic walls, the AAA diameter grows progressively, and eventually, it could be able to overcome the resistance of the aortic wall with its breakup. In turn, further increase of the AAA diameters produces internal flow recirculation producing ILT formation in the AAA sac. This phenomenon provokes AAA stabilization and starting a vicious circle inside the AAA. It is well documented [1], that the aneurysm shape has a strong influence on flow patterns and consequently on wall stress distribution (peak values and locations). It is reflected by the interaction between the arterial wall structural remodeling and the forces generated by blood flow within the AAA. Therefore, the AAA morphology has a significant influence in its potential rupture. The aim of this study is to analyze real geometries obtained directly from the computed tomography and to characterize the relation of the main geometric parameters (maximum diameter D_{AMAX} , the length L_{AAA} , tortuosity ϵ and the asymmetry β) of the AAA with the hemodynamic stresses acting on intimal layer.

2. Material and Methods

Five patients with infrarenal aneurysms of the Tan Tock Seng Hospital (Singapore) were included in this study. The patients chosen for this study were selected with different AAAs, in order to cover the different stages of this pathology. All the patient participated in this trial analysis were volunteered and provided written informed consent of the study. This study was reviewed and approved by the Ethics Committee of the Tan Tock Seng Hospital, Singapore. For the medical image acquisition, a Computed Tomography (CT) Somatom Plus Scanner(AS+) (Siemens Medical Solutions) was used with the following parameters: 512x512x110, pixel spacing: 0.785/0.785 with a resolution of 1.274 pixels per mm and 5-mm slice thickness. CT Scanning was conducted while the volunteer was awake in the head first-supine position using an Endo_leak protocol. The CT covering the entire volume of the abdomen and pelvis and it was performed after the administration of intravenous Omnipaque 350 as IV contrast medium. The main AAA geometrical characteristics for each patient are shown in table 1. Table 2 shows how the indexes have been calculated.

Case	Sex	Thoracic Aorta length (L)	Hypothetic Thorac. Aorta Length (τ)	AAA Neck diameter (dneck)	r	R	AAA Max Diameter (D_{AMAX})	AAA length (L_{AAA})	χ	β	γ	ϵ
1	Male	359,94	320,44	2,8	1,49	2,45	3,945	6,7	0,709	0,608	0,588	0,123
2	Male	319,5	310,2	1,7	0,67	1,74	2,416	4,1	0,703	0,388	0,589	0,029
3	Male	216,28	176,8	2,6	1,02	2,03	3,056	8,98	0,850	0,508	0,340	0,223
4	Male	293,55	255,26	2,6	0,95	3,07	4,031	15,6	0,644	0,309	0,258	0,150
5	Male	310,34	296,24	2,5	1,25	1,25	2,5	-	1	1	-	0,047

Table 1: Patient and aneurysm characteristics (Thoracic Aorta length (L), Hypothetic Thoracic .Aorta Length (τ), AAA neck Diameter (dneck), r (see figure 1) , R(see figure 1), AAA Max Diameter (D_{AMAX}), AAA length(L_{AAA})). All the measurements are expressed in centimeter. The Asymmetry index (β), Saccular index (γ), Deformation diameter ratio(χ) and tortuosity index (ϵ) are the indexes determinate the shape of the AAA.

$$\beta = \frac{r}{R} \quad \gamma = \frac{D_{AMAX}}{L_{AAA}} \quad \chi = \frac{D_{AMAX}}{d_{neck}} \quad \epsilon = \frac{L}{\tau} - 1$$

Table 2: Asymmetry index (β)[18], Saccular index (γ)[19], Deformation diameter rate (χ)[20] and tortuosity index (ϵ)[14].

The main geometrical AAA parameters are the aneurysm length L_{AAA} and the maximum diameter of the aneurysm, D_{AMAX} . The factor which assesses the length (L_{AAA}) and the diameter (D_{AMAX}) of the AAA sac is known as Saccular index (γ). If the saccular index is close to 1, means saccular(spherical) aneurysm, meanwhile is close to 0 means fusiform aneurysm. The deformation diameter rate (χ) characterizes the non-deformed abdominal aorta diameter (d_{neck}) with the maximum diameter of the aneurysm sac, D_{AMAX} . A non-aneurysmal aorta is defined as ($D_{AMAX} = d_{neck}$). To evaluate the axisymmetric (β) of the aneurysm, r and R are defined as the radii measured at the midsection of the AAA sac from the longitudinal z-axis to the posterior and anterior walls, respectively, as shown in the inset of Figure 1 (right). Thus, $\beta=1.0$ yields an azimuthal symmetry and $\beta = 0.2$ is an AAA for which only the anterior wall is dilated while the posterior wall is nearly flat. The tortuosity index (ϵ) is the relation between the actual lengths of the centerline of the AAA with the length of a hypothetical healthy aorta Figure 1 (Left).



Figure 1: Schematic visualization of tortuosity (ϵ) (absolute number) and the axisymmetric (β) of the aneurysm.

Based on these indexes and the wide clinical empirical evidence there are several criteria of the AAA grade. However, at the present, there is not a clinical consensus to use it.

To create the computational model, the medical data were sent directly to a personal computer and stored in digital imaging and communications in medicine format (DICOM format). The region of interest (ROI) analyzed was segmented using the three-dimensional computer-aided design system DIPPO software [2]. The segmented area for each patient started at the abdominal aorta (approximately in the infra renal arteries) and extended down to the common iliac arteries. The abdominal images were segmented from CT DICOM images combining two different segmentation procedures thresholding and level set method (based on snakes). Thresholding is a non-linear operation that converts a gray-scale image into a binary image where the two levels are assigned to pixels that are below or above the specified threshold value. The image snake operation creates or modifies an active contour/snake in a grayscale image. The operation iterates to minimize the snake's energy which consists of multiple components including the length of the snake, its curvature and image gradient [3].

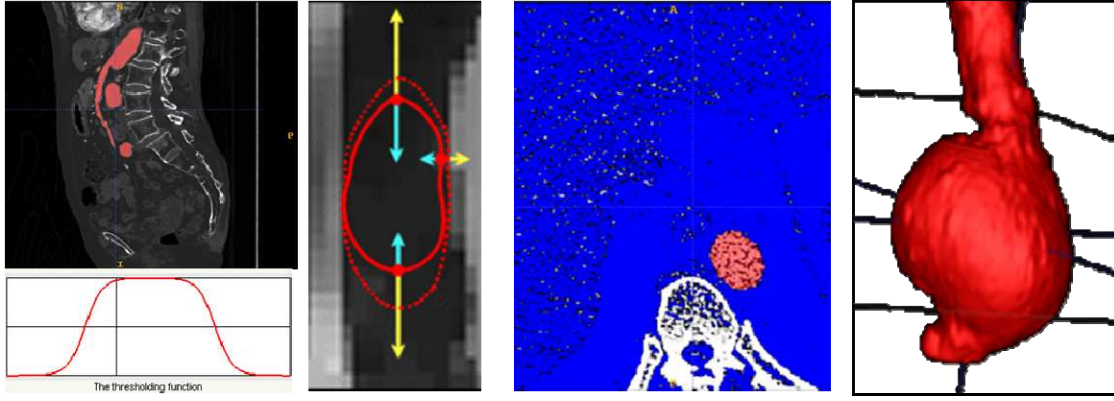


Figure 2: AAA Segmentation Process

After AAA abdominal segmentation, we get a 3D volume image useful to create a 3D computational model to analyze the blood flow behavior inside the AAA using computational fluid dynamics (CFD). Figure 2 shows an AAA workflow segmentation process. A mesh sensitivity analysis was performed to ensure the accuracy of the simulations using steady test. Depending on the complexity of the AAA model a 3D mesh consisted of 2.000.000–2.500.000 tetrahedral elements. Using the isostuffing algorithm we have obtained a smooth element and an aspect ratio for whole of the meshes upper than 0.9 (ideal ratio=1 for an equilateral triangle). For the 5 acquisitions the same medical image protocol, image processing and volume mesh reconstruction were used. Figure 3 shows the 3D segmentation image, 3D computational model and a detail of the elements generated.

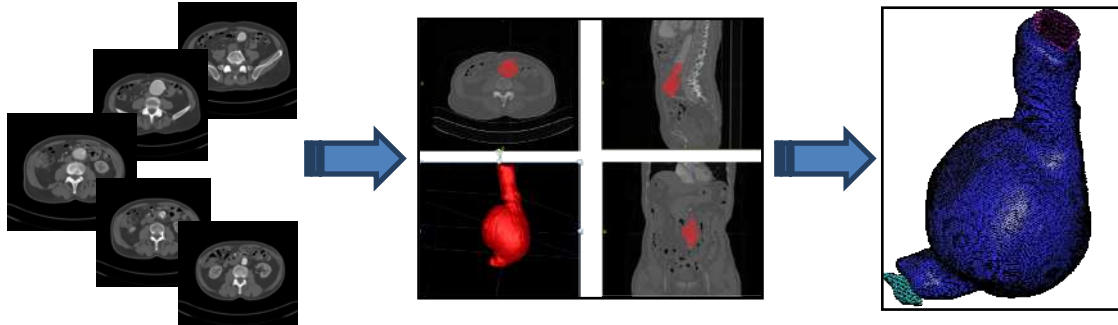


Figure 3: Workflow of the 3D AAA model. Obtaining the CT image of the abdominal aorta, segmentation of the vessel lumen using level set method and 3D model of the AAA.

3. Computational Fluid Mechanics Solver

CFD analysis was performed using BioDyn, a friendly user-interface based on the commercial software Tdyn [6]. Tdyn is a fluid dynamics and multi-physics simulation environment based on the stabilized Finite Element Method that solved the Navier–Stokes equations. To characterize accurately the blood flow in the AAA, a Reynolds number was calculated for whole cases. Reynolds number is a dimensionless number that determinate the dynamic of the fluid. Reynolds number is defined as $Re = UD/\nu$, where U is the mean velocity, ν is the kinematic viscosity of air and D is the characteristic length given as the hydraulic diameter $D=4A/P$ for the inlet velocity, here A is the cross-sectional area and P is the perimeter of the aorta. Due to the Reynolds numbers in inlet is low (< 1000); we decided to use a CFD solver for laminar flow considering steady, homogeneous, incompressible, adiabatic and Newtonian. Although, three-dimensional flow features such as flow separation and recirculation might trigger a transition to turbulence at lower Reynolds numbers [7]. Based on a preliminary study [8], the effect of the turbulence has been considered to be negligible. Following, we show the Navier-Stokes equations (Equation 1).

$$\left. \begin{aligned} \rho \left(\frac{\partial u}{\partial t} + (u \cdot \nabla) u \right) + \nabla p - \nabla \cdot (\mu \nabla u) &= \rho f & \text{in } \Omega \times (0, t) \\ \nabla \cdot u &= 0 & \text{in } \Omega \times (0, t) \end{aligned} \right\}$$

Equation 3. Navier-Stokes Equation for CFD analysis

where $u=u(x,t)$ denotes the velocity vector, $p=p(x,t)$ the pressure field, the density (ρ) is considered constant with a value of 1050 Kg.m^{-3} and dynamic viscosity (ν), fixed at 0.004 Pa.s and f the volumetric acceleration. The spatial discretization of the Navier-Stokes equations has been done by means of the finite element method (FEM), while for the time discretization an iterative algorithm that can be considered as an implicit two steps "Fractional Step Method" has been used. A new stabilisation method, known as finite increment calculus, has recently been developed [9, 10]. By considering the balance of flux over a finite sized domain, higher order terms naturally appear in the governing equations, which supply the necessary stability for a classical Galerkin finite element discretisation to be used with equal order velocity and pressure interpolations.

The inlet velocity waveform was taken from the literature [11], Figure 4 shows the pulsatile waveforms used. For inlet condition, a transient blood flow was imposed in the abdominal aorta (approximately above the infra renal arteries). The velocity U was calculated for each patient in order to obtain a total fluid volumetric flow rate of 500 ml for an entire cardiac cycle. The outlet boundaries were located at the common iliac arteries where the pressure follows pulsatile waveforms as defined in Figure 4(b). It is important to remark that these profiles are not patient-specific data (MR velocity mapping was not performed on these subjects), which can be a limitation of this study. In further studies a patient-specific velocity and pressure profile will be used as boundary conditions

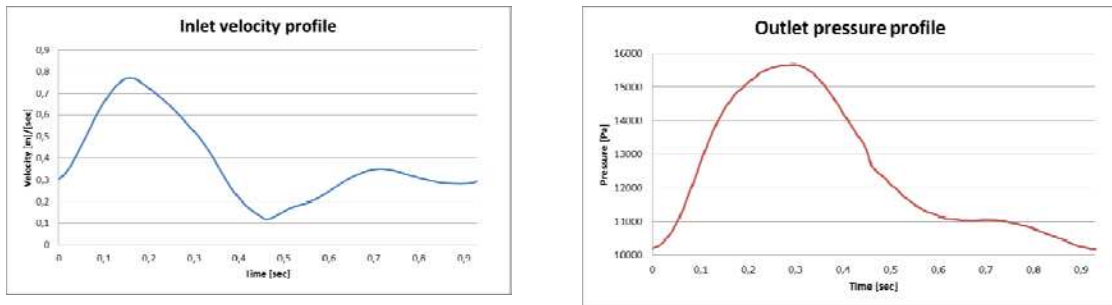


Figure 4. Boundary conditions for the hemodynamic simulations, adapted from [11]

Mathematically the boundary conditions can be expressed as in equations 2. No-slip condition (vessel rigid wall) was imposed on the surface of the arteries, equation 2a. This choice is motivated by the fact that the physiological parameters characterizing the arterial mechanical behaviour of the AAA wall are not well determined. This approach however reduces the discretization effort considerably, in particular boundary layer gridding and the computational cost although other approaches consider Fluid Structure Interaction (FSI) models [12]. The inlet velocity is assuming fully developed parabolic profile at the inlet (2b), and time dependent normal traction due to luminal pressure at the outlet (2c).

$$\mathbf{V} = 0|_{\text{wall}} \quad (2a)$$

$$u_z = 2(u(t)) \left(1 - \left(\frac{2r}{d_r} \right)^2 \right); u_r = 0|_{z=0} \quad (2b)$$

$$\tau_{nn} = \hat{n} \cdot p(t) I \cdot \hat{n} \quad (2c)$$

where d_r is the inner radius of the abdominal aorta, u_r is the Cartesian components of the velocity vector in the 'z' direction, $u(t)$ and $p(t)$ are the time-dependent velocity and pressure waveforms designate in Figure 3. The pressure boundary conditions are given by equation 2c, where τ_{nn} is the normal traction designates at the outlet; I is the standard identity matrix and \hat{n} designates the normal of the respective boundary. Figure 5 shows an example of the AAA reconstructed models and the layers in which our domain is divided in order to impose the boundary conditions.

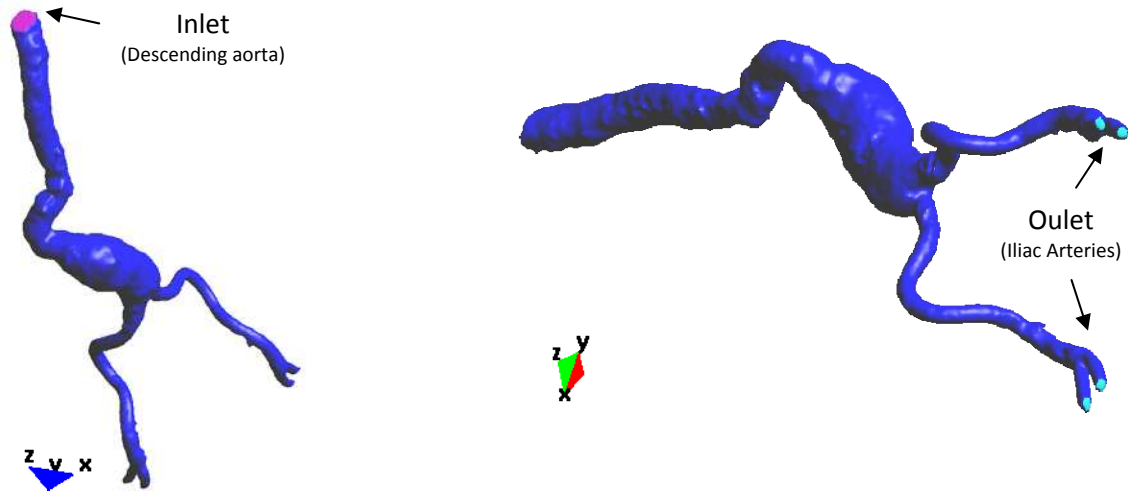


Figure 5. Mesh Surface: different layers are showed: lateral wall (dark blue), Inlet (purple) and outlet sections (light blue)

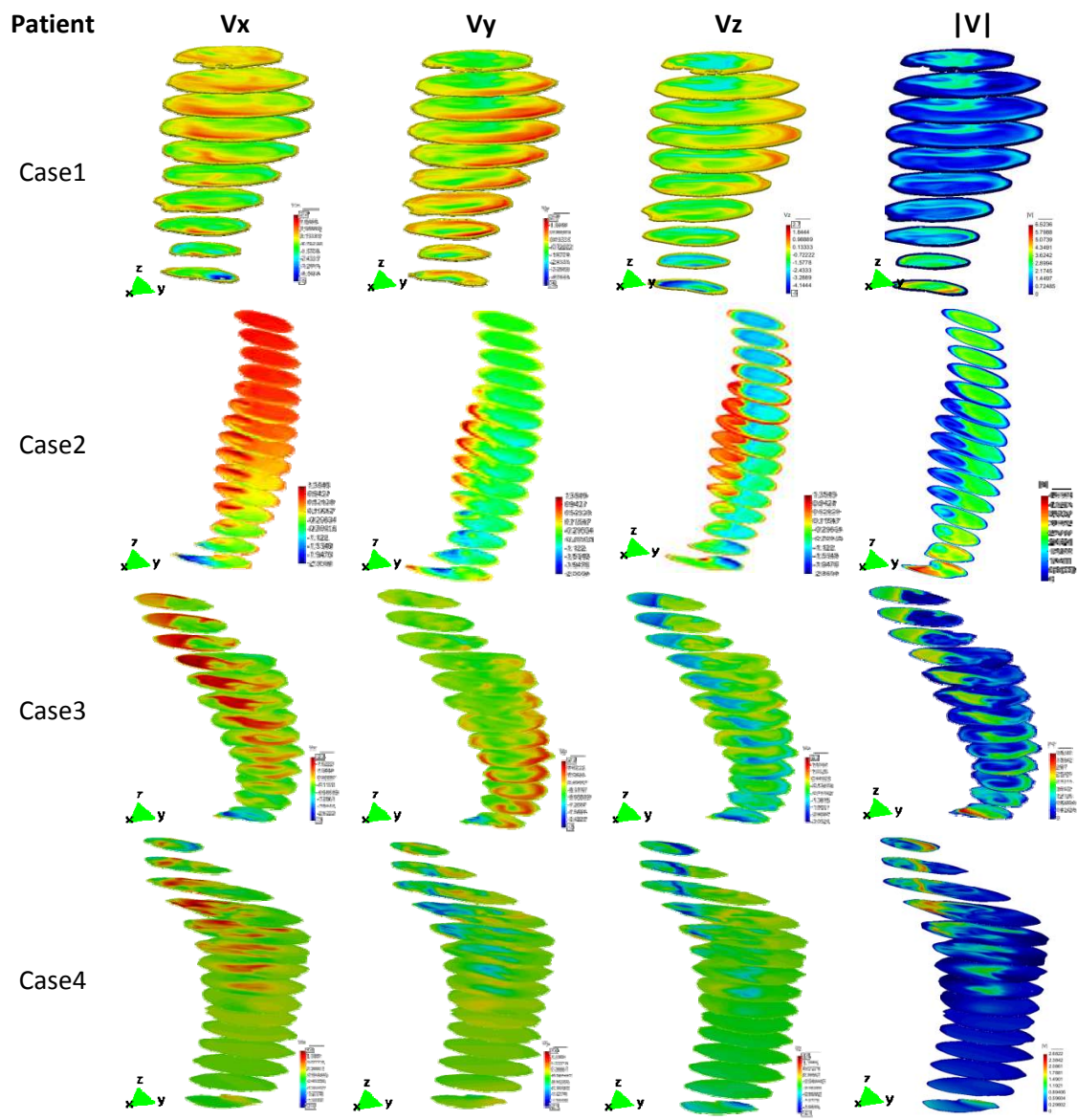
We start the simulation with 50 initial steps in order to stabilize the initial condition solution. Time integration method chosen was a Backward Euler, using a Bi Conjugate Gradient Non-symmetric solver in order to accelerate the calculation time performance. We used a pressure stabilization of 4th order and automatic velocity advection stabilization [13]. The total CPU time in a Microsoft Windows XP 32-bit PC with 3 GB-RAM using 2 CPU was between 4-6 hours depending of the case.

4. Results

Five models of infrarenal aneurysm with patient-specific geometry were analyzed using computational fluid dynamics in order to evaluate the flow patterns, WSS and pressure over the Aneurysms sac and its correlation with the AAA geometrical parameters. Patients 1 to 4 suffer infrarenal aneurysm and patient 5 is the control case. ILT was not found in any case. The simulations were carried out for two cardiac cycles, but the results of both stress and flow patterns were found to be periodic after the second cardiac cycle.

Figure 6 shows the flow patterns (V_x, V_y, V_z and $|V|$) inside the infrarenal Aneurysms sac models for whole patients to examine the link between abnormal flow patterns and the geometrical parameters. Note that forward flow points downwards and has a negative value in the adopted coordinate system. The direction of the flow is from top to bottom (direction Z

negative). As shown in refs. [8,14,15,17], the asymmetric flow patterns can provide an insight into the mechanism that promotes the thrombus renewal (ILT) and possibly enlargement inside the aneurysm. Rapid decrease in the velocity and regions of very high (or low) hemodynamic stresses gradients, may all contribute in various ways to the vascular disease, primarily via their effects on the endothelium. For example, platelets trapped in recirculating zones tend to be deposited in areas of low shear stress (stenosis), since this and the presence of vortices cause prolonged contact of the platelets with the surface in the layer of slow fluid motion [16]. According to these, as more asymmetry and fusiform shape is the AAA (lower β and lower γ), higher is the possibility of blood recirculating and ILT formation. As well as, the tortuosity index of the AAA is a factor to be also in account, for example in case 4, the tortuosity of the AAA provokes some areas inside the AAA sac with low velocities.



Case5

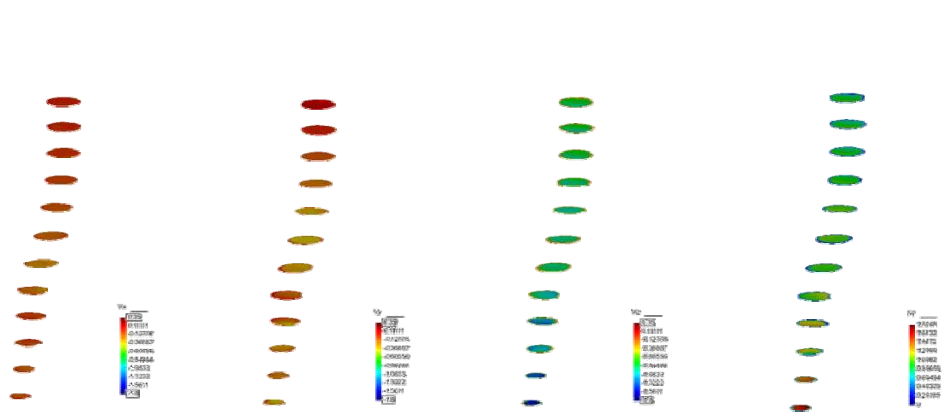
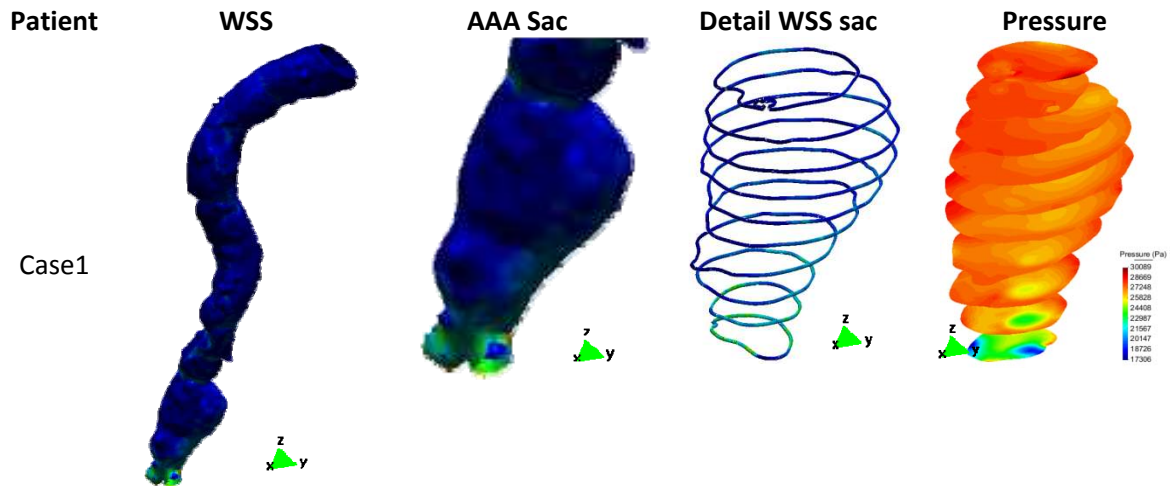


Figure 6: Flow patterns at systole at peak flow.

In Figure 7, the wall shear stress patterns in different sections on the aneurysm wall are shown. The WSS calculated are based on [1] and is directly linked with velocity profiles shown in figure 5 and the AAA tortuosity. It is interesting to note that stress levels in all infrarenal aneurysms models are higher than those in the normal aorta which has a fairly uniform stress distribution. The maximum wall shear stress during the pulsatile cycle is obtained at peak flow, where the velocities and their spatial gradients are greatest. As more tortuosity is the area of the AAA, the peaks of WSS are higher due to the abrupt changes of the blood flow motivated by the angles in the aorta. This WSS peak areas are not so much important in aneurysm growth but it's are a potential areas of arterial wall failure because of the blood flow jet effort in the arterial wall. In Figure 7, pressure distribution for different sections is shown. High pressure areas inside the sac may indicate the growth directions of AAA sac, according to Laplace Law. Due to the increasing of the internal pressure, against the aortic walls, the AAA diameter grows progressively, and eventually, it could be able to overcome the resistance of the aortic wall with its breakup. The way of arterial wall failure due to the tortuosity and to the pressure distribution are physically different, first is because of a punctual force over a point, and the second is as a consequence of a pressure distribution over the AAA sac.



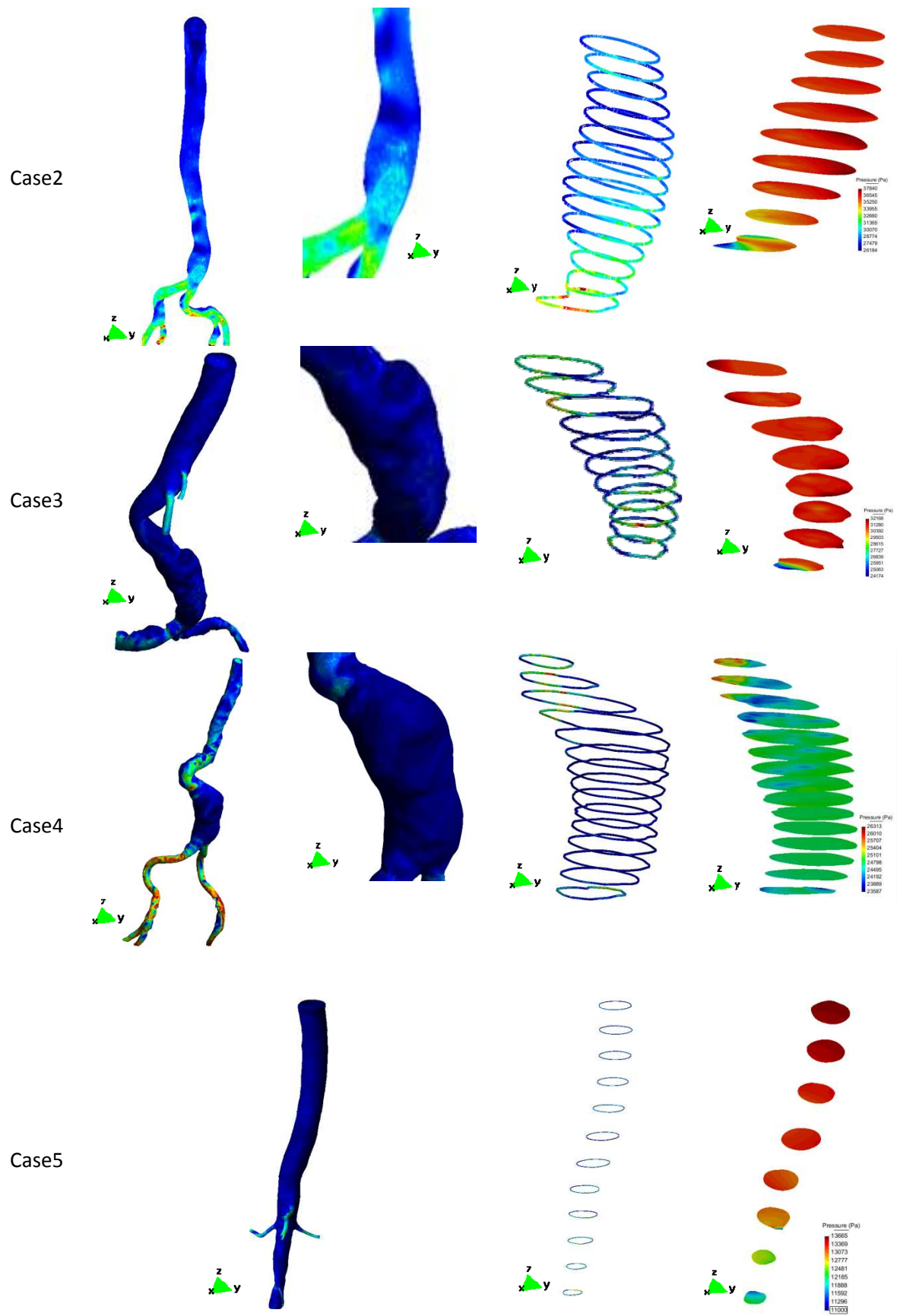


Figure 7: Pressure and WSS at systole at peak flow.

5. Discussions

Most of abdominal aneurysms (AAA) (about 90%) are located below the level of the renal arteries, the vessels that leave the aorta to go to the kidneys. These abdominal aneurysms are known as Infrarenal aneurysm. Infrarenal aneurysm is a pathology involving the enlargement of the aorta in the inferior thoracic area taking a fusiform shape and may extend into the iliac arteries. This mortality of this pathology is high (15% for ruptured aneurysms), for this reason, in this study five infrarenal aneurysms were analyzed in order to understand the geometrical features and the hemodynamic loads with a possible AAA rupture. The current standard of determining rupture risk is based on maximum diameter, it is known that smaller AAAs that fall below this threshold (diameter < 5.5 cm) may also rupture, and larger AAAs (diameter > 5.5 cm) may remain stable [1], but not all the cases would have succumbed to rupture prior to surgical intervention as the diameter was less than 5 cm, suggesting that other biomechanics or geometrical factors come into play in the rupture of the aneurysm. Several authors have proposed several criteria for the collapse of the aneurysms based on the clinical empirical evidence, if the asymmetry index factor, $\beta < 0.4$ the AAA rupture is high [18], in [21] the AAA collapse is when the Deformation diameter ratio is $\chi > 3.3$ or in [22] if the saccular index is < 0.6 . But depending of the index that is analyzed the surgical criteria is different. Therefore, alternative methods of AAA rupture assessment are needed. The majority of these new approaches involve the numerical analysis of AAAs using computational fluid dynamics (CFD) to determine the wall shear stress (WSS) distributions. From a mechanical point of view, stress is the amount of force exerted on a surface per unit area of the wall. The peak of the WWS refers to the mechanical load sustained by the AAA wall, during maximal systolic pressurization. It is also known that wall stress alone does not completely govern failure as an AAA will usually rupture when the wall stress exceeds the wall strength. Its value depends on arterial systolic pressure, the mechanical properties and the geometric configuration of the material under study. More recently proposed AAA rupture-risk is related with the presence of intraluminal thrombus (ILT) [23], and perhaps, one of the most ambiguous issues in the computational evaluation of rupture risk is the integration of ILT and perivascular tissues in the models. It has been suggested that the intraluminal thrombus layer plays an important role in expansion and rupture of advanced aneurysms through direct mechanical as well as indirect chemomechanical effects [18]. Therefore, the AAA dilatation (and a possible rupture) is not only depending of geometrical factor or the hemodynamic load is depending on the correlation of the geometrical indexes and the hemodynamic loads or new indexes as the tortuosity. In the Figure 7, the highest shear stress values are depending especially of the tortuosity of the AAA.

The current study, in spite of the limitations of do not considered the patient-specific wall strength and the intraluminal thrombus, the AAA cases analyzed provides useful information to understanding who the aneurysm growth and its possible rupture. The pathological cases (case 1 to 4) always present irregular flow, no uniform distribution of WSS and great deformations in the curvatures of the aortic vessel. These anomalies are proportional to the shape of the aneurysm and the angles of twist that the aorta has. Asymmetric flow is always correlated to the modified curvature of the vessel or when some enlargement in the aneurysm is present. The AAA tortuosity could initiate the ILT formation and at the same time could provoke arterial wall failure. In case that the tortuosity is high and low saccular index, the WSS has more effects than the pressure distribution in a possible AAA failure, nevertheless, in the case that AAA is not twisted and a high saccular index, the pressure effect takes more importance. These phenomena can be observed thanks to the velocity domain decomposition inside the AAA (figure 6), and the WSS calculated due to stress caused by the blood flow jet on the arterial wall (figure 7). Based on these two indexes possible areas of the ILT formation could be proposed.

6. Conclusions

To conclude, in this work the wall shear stress, internal pressure and flow patterns of five patients with infrarenal aneurysm have been analyzed using finite element method with patient-specific AAA models. Results from the patient-specific infrarenal aneurysm models (case 1-4) were compared with those of a normal aorta (case5) and it has been found that the normal aorta has a much more uniformly distributed wall shear stress and pressure. Maximum wall shear stresses in all infrarenal aneurysm models are higher than in the normal aorta and these values are not directly related to the maximum aneurysm diameter, but are directly related with the tortuosity and the saccular index of the aorta, providing further evidence that a patient-specific aorta shape analysis is necessary for a more reliable assessment of the rupture risk of aortic aneurysms. In a future would be interesting to define a protocol for using patient-specific boundary conditions and wall strength.

Acknowledgments

This project was supported by the NTU-NHG innovation seed grant project no. ISG/11007.

References

- [1] D.A. Vorp, "Biomechanics of abdominal aortic aneurysm". J. Biomech., 40(2007), 1887–1902.
- [2] E. Soudah, J. Pennecot, J.S. Perez, M. Bordone, E. Oñate, Chapter 10: "Medical-GiD: 381 From medical images to simulations, MRI Flow Analysis". Book: Computational Vision and Medical Image Processing: Recent Trends. ISSN 1871-3033 383 Ed. Springer.
- [3] E. Soudah, M. Bordone, J.S. Perez, "Gmed: a platform for images treatment inside GiD system". 5th Conference On Advances And Applications Of GiD. Barcelona 2010. www.gidhome.com GiD - The personal pre and postprocessor.
- [4] A. Paul, P.A. Yushkevich, J. Piven, H.C. Hazlett, R.G. Smith, S. Ho, et al., "User- 413 guided 3D active contour segmentation of anatomical structures: Significantly 414 improved efficiency and reliability", Neuroimage 31 (2006) 1116–1128.
- [5] W.E. Lorensen, H. E. Cline, Marching cubes: A high resolution 3d surface construction algorithm. In Proceedings of SIGGRAPH, pages 163–169 (1987).
- [6] M. Bordone, C.García, J.García, E.Soudah, Biodyn User Manual. TDYN: theoretical Background: www.compassis.com/compassis. COMPASSIS (2012)
- [7] E. A. Finol, K. Keyhani, C. H. Amon. "The Effect of Asymmetry in Abdominal Aortic Aneurysms Under Physiologically Realistic Pulsatile Flow Conditions". Journal of Biomechanical Engineering APRIL 2003, Vol. 125, 207- 217. DOI: 10.1115/1.1543991
- [8] J. Biasetti, F. Hussain, T.C. Gasser, "Blood flow and coherent vortices in the normal and aneurysmatic aortas: a fluid dynamical approach to intra-luminal thrombus formation". J.R. Soc. Interface, Doi:10.1098/rsif.2011.0041.
- [9] E. Oñate, S. Idelsohn, O.C. Zienkiewicz, R.L. Taylor, "A finite point method in computational mechanics. Applications to convective transport and fluid flow", Int. Journal for Numerical Methods in Engineering 39 (1996) 3839–3866.
- [10] J. García, E. Oñate, H. Sierra, C. Sacco, and S. Idelsohn, "A Stabilised Numerical Method for Analysis of Ship Hydrodynamics". Proceedings Eccomas Conference on CFD, 7-11 September 1998, Athens, John Wiley, 1998.
- [11] Y. Papaharilaou, J.A Ekaterinaris, E. Manousaki, et al: "A decoupled fluid structure approach for estimating wall stress in abdominal aortic aneurysm". J. Biomech. 40 (2007), 464-475.
- [12] A. Borghia, N.B. Wooda, R.H. Mohiaddinb, X.Y. Xua. "Fluid–solid interaction simulation of flow and stress pattern in thoraco abdominal aneurysms: A patient-specific study". Journal of Fluids and Structures 24 (2008) 270–280.

- [13] R. Barrett et al., *Templates for the Solution of Linear Systems: Building Blocks for Iterative Methods*, 2nd Edition, Philadelphia, PA: SIAM, 1994.
- [14] C.M. Scotti, E.A. Fino, "Compliant biomechanics of abdominal aortic aneurysm: A fluid-structural interaction study". *Computer and Structures*, 85 (2007), 1097-1113.
- [15] A.V. Salsac, S.R. Sparks, J.M. Chomaz, J.C. Lasheras, "Evolution of the wall shear stresses during the progressive enlargement of symmetric abdominal aortic aneurysms". *J. Fluid Mech*, 560 (2006), 19-51.
- [16] D. Bluestein, E. Rambod, M. Gharib, "Vortex shedding as a mechanism for free emboli formation in mechanical heart valves". *ASME Journal of Biomechanical Engineering* 122,2 (2000), 125–134.
- [17] A. Sheidaei, S.C. Hunley, S. Zeinali-Davarani, L.G. Raguin, S. Baek, "Simulation of abdominal aortic aneurysm growth with updating hemodynamic loads using a realistic geometry". *Medical Engineering & Physics* 33 (2011) 80–88.
- [18] D.A. Vorp, P.C. Lee, D.H.J. Wang, M.S. Makaroun, E.M. Nemoto, S. Ogawa, et al. "Association of intraluminal thrombus in abdominal aortic aneurysm with local hypoxia and wall weakening". *Journal of Vascular Surgery* 2001; 34: 291–9.
- [19] C. Kleinstreuer and Z. Li, "Analysis and computer program for rupture-risk prediction of abdominal aortic aneurysms". *BioMedical Engineering OnLine* 2006, 5:19.
- [20] Judy Shum, Giampaolo Martufi, Elena Di Martino, Christopher B. Washington, Joseph Grisafi, Satish C. Muluk, and Ender A. Finol. Quantitative Assessment of Abdominal Aortic Aneurysm Geometry. *Ann Biomed Eng.* 2011 January; 39(1): 277–286.
- [21] W.A. Cappeller, H. Engelmann, S. Blechschmidt, M. Wild, L. Lauterjung, "Possible objectification of a critical maximum diameter for elective surgery in abdominal aortic aneurysms based on one-and three-dimensional ratios". *Journal of Cardiovascular Surgery* 1997, 38:623-628.
- [22] K. Ouriel, R.M. Green, C. Donayre, C.K. Shortell, J. Elliott, J.A. Deweese, "An evaluation of new methods of expressing aortic aneurysm size: Relationship to rupture". *Journal of Vascular Surgery* 1992, 15:12-20.
- [23] D.A. Vorp, M.L. Raghavan, M.W. Webster (April 1998). "Mechanical wall stress in abdominal aortic aneurysm: influence of diameter and asymmetry". *Journal of Vascular Surgery* 27 (4): 632–9. doi:10.1016/S0741-5214(98)70227-7.